Enclosure 33 to TN E-29128

Transnuclear Calculation MP197HB-0402, Revision 2
associated with RAI 3-21

DCR NO (if applicable) : NUH09-006	**PROJECT NAME:** MP197HB Transport Packaging Design
PROJECT NO: 61003	**CLIENT:** Transnuclear, Inc.

CALCULATION TITLE:

Thermal Analysis of Baskets for Normal Conditions of Transport in MP197HB Transport Cask

SUMMARY DESCRIPTION:

1) Calculation Summary

This calculation determines the maximum fuel cladding temperature and the maximum basket component temperatures for DSCs in MP197HB transport cask under normal conditions of transport (NCT) and under loading/unloading conditions.

The effective thermal properties are also calculated for 69BTH and 37PTH baskets to be used in the transient analysis.

2) Storage Media Description

Secure network server initially, then redundant tape backup

If original issue, is licensing review per TIP 3.5 required?

Yes ☐ **No** ☒ **(explain below)** **Licensing Review No.:**_______

This calculation is performed to support a 10CFR71 transport license application that will be reviewed and approved by the NRC. Therefore, review of proposed activities for conformance with a 10CFR71 transport packaging Certificate of Compliance per TIP 3.5 is not applicable.

Software Utilized (subject to test requirements of TIP 3.3):	Version:
ANSYS	8.1 and 10.0
Calculation is complete: Originator Name and Signature: Davy Qi	Date: 02/18/10
Calculation has been checked for consistency, completeness and correctness: Checker Name and Signature: Venkata Venigalla	Date: 02/18/10
Calculation is approved for use: Project Engineer Name and Signature: Steven Streutker	Date: 4/9/10

REVISION SUMMARY

REV.	DATE	DESCRIPTION	AFFECTED PAGES	AFFECTED Computational I/O
0	3/27/09	Initial Issue	All	All
1	4/29/09	Changes resulting from internal review	14, 16, 25-27, 33, 65, 91, 116	None
2	4/8/10	Add Appendix F to justify the methodology by applying the DSC types previously evaluated for storage conditions for transportation application (RAI 3-6). Add Appendix G to justify the assumed gaps used in thermal evaluation of the MP197HB transportation cask (RAI 3-7). Add Appendix H to address the effect of high burnup damaged fuel assemblies under NCT (RAI-2-7). Add Appendix I to justify poison material density and specific heat (RAI 3-5).	1-5, 8-11, 17, 19, 22, 27, 44-45, 48, 62, 80-81, 84, 92-93, 106,120-128	Additional runs/ spreadsheets: Table F-2, Table G-2, Table H-3, Poison_Cp.xls

TABLE OF CONTENTS

LIST OF TABLES

LIST OF FIGURES

1.0 PURPOSE

The purpose of this calculation is to determine the maximum fuel cladding temperature and the maximum component temperatures for baskets in MP197HB transport cask (TC) for normal conditions of transport (NCT).

The proposed DSC types for transportation in MP197HB are listed in Table 1-1.

Table 1-1 DSC Types and Heat Loads in MP197HB

	DSC type	DSC OD (in)	Sleeve	External Fins	Max. Heat Load for Transport (kW)
1	69BTH	69.75	No	No	26.0
2				Yes	29.2
3				Yes	32.0
4	61BTH Type 1 (1)	67.25	Yes	No	22.0
5	61BTH Type 2 (1)	67.25	Yes	No	24.0
6	61BT	67.25	Yes	No	18.3
7	37PTH	69.75	No	No	22
8	32PTH / 32PTH Type 1	69.75	No	No	26.0
9	32PTH1 Type 1	69.75	No	No	26.0
10	32PTH1 Type 2	69.75	No	No	24.0
11	32PT	67.19	Yes	No	24.0
12	24PTH Type 1 & 2 (1)	67.19	Yes	No	26.0
13	24PT4	67.19	Yes	No	24.0

Notes: (1) DSC types 61BTHF and 24PTHF have the same dimensions and use the same MP197HB features as for DSC types 61BTH and 24PTH, respectively.

Based on discussions in [10], the maximum fuel cladding and basket component temperatures for 61BTH, 61BT, 32PTH, 32PTH1, 32PT, 24PTH, and 24PT4 are bounded by the normal transfer conditions and no further analysis is required.

Four heat load zoning configurations (HLZC) are considered for the 69BTH basket, which are summarized in Table 1-2 and shown in Figure 5-1 to Figure 5-4.

Boral, metal matrix composite (MMC), or borated aluminum can be used as poison materials for HLZC # 1, # 2 and # 3 in 69BTH basket. For 69BTH basket with HLZC # 4, only borated aluminum can be used as poison material.

Only one HLZC is considered for 37PTH basket for NCT with 22 kW heat load. The HLZC for 37PTH DSC is shown in Figure 5-13. Boral plates paired with Al1100 plates or single plates of metal matrix composite (MMC) or borated aluminum can be used as poison materials in 37PTH basket with 22 kW heat load.

The considered poison materials for each HLZC are listed in Table 1-2.

Table 1-2 Heat Load Zoning Configurations for 69BTH and 37PTH DSCs in MP197HB

	DSC type	HLZC	Poison Material	Max. Heat Load (kW)
1	69BTH	1 or 2	Boral / MMC / Borated Aluminum	26.0
2	69BTH	3	Boral / MMC / Borated Aluminum	29.2
3	69BTH	4	Borated Aluminum	32.0
4	37PTH	1 (1)	Boral Paired Al Single MMC/Borated Al	22

Note: (1) The HLZC for 37PTH in the input files is assigned as HLZC # 8

Thermal performances of 69BTH and 37PTH baskets are evaluated for hot and cold NCT at 100, -20, and -40°F ambient.

Effective properties of 69BTH and 37PTH baskets are determined in Section 5.3 for the purpose of transient analysis in other calculations.

For the purpose of structural evaluation, a heat load of 23.2 kW is considered for 37PTH DSC. Since the considered heat load of 23.2 kW is higher than the design heat load of 22.0 kW, this approach is conservative for structural evaluation of 37PTH DSC. The HLZC and the maximum component temperatures for 37PTH DSC with 23.3 kW are collected in APPENDIX D. The temperatures plots for DSC shell resulted from analyses in [10] are collected in APPENDIX E.

Justification for using DSC types previously evaluated for storage conditions as the bounding results for transportation in MP197HB cask is discussed in APPENDIX F.

Justification for assumed gaps in the 69BTH DSC as limiting case is addressed in APPENDIX G.

The effect of high burnup damaged fuel assemblies under NCT is discussed in APPENDIX H.

Justification for thermal properties assumed for poison materials in Section 5.3.1 is addressed in APPENDIX I.

2.0 REFERENCES

1 Updated Final Safety Analysis Report for the Standardized NUHOMS® Horizontal Modular Storage System for Irradiated Nuclear Fuel, NUH-003, Rev. 11.

2 Updated Final Safety Analysis Report for the Standardized Advanced NUHOMS® Horizontal Modular Storage System for Irradiated Nuclear Fuel, ANUH-01.0150, Rev. 3.

3 Not used.

4 Final Safety Analysis Report for NUHOMS® HD Horizontal Modular Storage System for Irradiated Nuclear Fuel, Rev. 2.

5 Spent Fuel Project Office, Interim Staff Guidance, ISG-11, Rev 3, "Cladding Considerations for the Transportation and Storage of Spent Fuel".

6 Project MP197HB, "Design Criteria Document (DCD) for the NUHOMS® MP197HB Transport Package," Transnuclear, Inc., Specification No. MP197HB.0101, Rev. 3.

7 Oak Ridge National Laboratory, "Physical Characteristics of GE BWR Fuel Assemblies," by R. S. Moore and K. J. Notz, ORNL/TM-10902, June 1989.

8 Calculation, "NUHOMS®-61BTH DSC Thermal Evaluation for Storage and Transfer Conditions," Transnuclear, Inc., Calculation No. NUH61BTH-0403, Rev. 0.

9 Calculation, "NUHOMS® -24PTH DSC Thermal Evaluation for Storage and Transfer Conditions," Transnuclear, Inc., Calculation No. NUH24PTH-0403, Rev. 5.

10 Calculation, "Thermal Analysis of MP197HB Transport Cask for Normal Transport Conditions," Transnuclear, Inc., Calculation No. MP197HB-0401, Rev. 2.

11 Calculation, "NUH69BTH DSC Weight Properties (weight, Volume, Center of Gravity, and Momentum of Inertia) Calculation," Transnuclear, Inc., Calculation No. NUH69BTH-0200, Rev. 0.

12 Calculation, "NUH37PTH DSC Weight Properties (Weight, Volume, Center of Gravity, and Momentum of Inertia) Calculation," Transnuclear, Inc., Calculation No. NUH37PTH-0200, Rev. 0.

13 Calculation, "Minimum Effective Fuel Conductivity for NUHOMS® -32PT Design," Transnuclear, Inc., Calculation No. NUH32PT-0410, Rev. 0.

14 Calculation, "Fuel Effective Thermal Properties Calculation for the NUHOMS® -24PTH DSC Design for Helium Backfill and Vacuum Conditions," Transnuclear, Inc., Calculation No. NUH24PTH-0402 Rev. 0.

15 Calculation, "Fuel Effective Thermal Properties Calculation for the NUHOMS® -61BTH DSC Design for Helium Backfill and Vacuum Conditions," Transnuclear, Inc., Calculation No. NUH61BTH-0402, Rev. 0.

16 Calculation, "NUHOMS®-32PT DSC Thermal Evaluation for 10 CFR, Part 72 Storage Conditions," Transnuclear, Inc., Calculation No. NUH32PT-0403, Rev. 2

17 Calculation, "NUHOMS® -32PTH1 DSC Thermal evaluation for Storage and Transfer Conditions," Transnuclear, Inc., Calculation No. NUH32PTH1-0403, Rev. 1.

18 ASME Boiler and Pressure Vessel Code, Section II, Part D, "Material Properties", 2004.

19 Rohsenow, Hartnett, Cho, "Handbook of Heat Transfer", 3rd Edition, 1998.

20 AAR Brooks & Perkins, Advanced Structural Division, "Boral® The Neutron Absorber", Product Performance Report 624.

21 Pacific Northwest National Laboratory, "Evaluation of Effect of Fuel Assembly Loading Patterns on Thermal and Shielding Performance of a Spent Fuel Storage/Transportation Cask", by J.M. Cuta, U.P. Jenquin, and M.A. McKinnon, PNNL-13583, November 2001.

22 Kreith, Frank, "Principles of Heat Transfer", 3rd Edition, 1973.

23 M. M. Yovanovich, J. R. Culham, P. Teertstra, "Calculating Interface Resistance", Electronics Cooling, Vol. 3, No. 2, May 1997.

24 Amiss, J. M., et al., "Machinery's Handbook", 24th Edition, Industrial Press, 1992 - Fig. 5, pg 672.

25 Aluminum Association, Inc., "Aluminum Standards and Data", 10th Edition, 1990 - Table 2.1, pg 33.

26 ASME Boiler and Pressure Vessel Code, Section II, Part A, "Ferrous Material Specification", 1998 and 2000 addenda.

27 Gordon England Company, "Microhardness Test", http://www.gordonengland.co.uk/hardness/microhardness.htm

28 ANSYS computer code and On-Line User's Manuals, Version 8.1 and 10.0.

29 U.S Department of Energy, "Characteristics of Spent Nuclear Fuel, High-Level Waste, and Other Radioactive Wastes Which May Require Long-Term Isolation, Appendix 2A", U.S Department of Energy, Office of Civilian Radioactive Waste Management, DOE/RW-0184, Volume 3 of 6, December, 1987.

30 U.S Department of Energy, "Topical Report on Actinide-Only Burnup Credit for PWR Spent Fuel Packages", Office of Civilian Radioactive Waste Management, DOE/RW-0472, Revision 2, September 1998.

31 Perry, R. H., Chilton, C. H., “Chemical Engineers' Handbook”, 5th Edition, 1973

32 Roth, A., “Vacuum Technology,” 2nd Edition, 1982.

33 Lide, David, R., “CRC Handbook of Chemistry and Physics”, 83rd edition, 2002-2003, CRC Press.

34 Chun, Ramsey; Witte, Monika; Schwartz, Martin, “Dynamic Impact Effects on Spent Fuel Assemblies”, Lawrence Livermore National Laboratory, Report UCID-21246, October, 1987.

35 Consolidated Safety Analysis Report for IF-300 Shipping Cask, CoC 9001, Rev. 35.

36 Calculation, “TN-24P Benchmarking Analysis Using ANSYS,” Transnuclear, Inc., Calculation No. NUH32PT.0408, Revision 0.

37 Calculation, “Effective Thermal Properties of Fuel Assemblies in MP197HB Transport Cask,” Transnuclear, Inc., Calculation No. MP197HB-0400, Revision 0.

38 Calculation, “Thermal Analysis of 24PTHF and 61BTHF DSCs for Normal and Hypothetical Accident Conditions of Transport in MP197HB Transport Cask,” Transnuclear, Inc., Calculation No. MP197HB-0408, Revision 1.

39 Oak Ridge National Laboratory, “Effect of Fuel Failure on Criticality Safety and Radiation Dose for Spent Fuel Casks,” by K.R. Elam, J.C. Wagner and C.V. Parks, NUREG/CR-6835 (ORNL/TM-2002/255), September 2003.

40 Idaho National Engineering and Environmental Laboratory, “SCDAP/RELAP5/MOD 3.3 Code Manual, MATPRO – A Library of Materials Properties for Light-Water-Reactor Accident Analysis”, by L.J. Siefken, E.W. Coryell and E.A. Harvego, NUREG/CR-6150, Vol.4, Rev.2 (INEL-96/0422), January 2001.

41 Not used.

42 PRL-801, “Thermal Conductivity of Aluminum-Boron Alloy”, Taylor, R.E., et al., Properties Research Laboratory, Purdue University, May 1989.

43 Neutron Absorber Materials, Ceradyne, Inc., http://www.ceradyneboron.com/products/boron-alloy.aspx.

3.0 ASSUMPTIONS AND CONSERVATISM

Radial and axial effective conductivities for 69BTH and 37PTH basket are calculated based on slice models of the baskets described in Section 5.3. For conservatism, only 95% of the calculated values from slice models are considered as bounding values for transient runs.

3.1 Assumptions and conservatism for 69BTH DSC

The following assumptions are considered for the 69BTH basket/DSC model.

The fuel assemblies contained in 69BTH basket are intact fuel assemblies.

No convection is considered within the DSC cavity.

Only helium conduction is considered from the basket upper surface to the DSC top shield plug.

Heat transfer through the hold-down ring is conservatively modeled as conduction through helium.

No convection or radiation is considered between the aluminum dummy assemblies and the fuel compartments. The length of aluminum dummy assembly is considered equal to the active fuel length.

A uniform gap of 0.0625" is considered around the cross section of the dummy assembly within the fuel compartment for calculation of effective conductivities.

Radiation is considered only implicitly between the fuel rods and the fuel compartment walls in the calculation of effective fuel conductivity. No other radiation heat exchange is considered within the basket model.

Active fuel length for BWR fuel assemblies is 144" [7] and starts about 7.5" from the bottom of the basket [7].

The following gaps are considered in the 69BTH basket/DSC model at thermal equilibrium:

- 0.30" diametrical hot gap between the basket outer surface and the canister inner surface. This assumption is justified in APPENDIX A.
- 0.125" axial gap between the bottom of the basket and the DSC bottom inner cover plate
- 0.01" gap between any two adjacent plates or components in the cross section of the basket.
- Three 0.125" gaps in axial direction between the aluminum rail pieces.
- 0.01" gap between the sections of the paired aluminum and poison plates in axial direction.
- 0.1" gap between the two small aluminum rails at the basket corners.
- 0.1" gap between the two pieces of large aluminum rails at 0-180 and 90-270 orientations.
- 0.0625" gap between DSC shield plugs and DSC cover plates for calculation of effective conductivities in axial direction.

- 0.09" radial gap between top shield plug and DSC shell equal to nominal cold gap
- 0.25" diametrical gap between bottom shield plug and DSC shell equal to nominal cold gap

No gap is considered between the paired poison and aluminum plates. The 0.01" gaps considered on either side of the paired plates account for the thermal resistance between the multiple plates. This assumption is justified in APPENDIX B.

The gaps considered between the aluminum rail segments are larger than the nominal cold gaps and are therefore conservative. The axial gaps considered between the aluminum rail pieces in the axial direction is larger than the tolerances considered for the rail and are therefore conservative.

The benchmarking of finite element models against test data in [36] shows that the 0.01" gaps considered between adjacent plates or components in the cross section of the basket account conservatively for the tolerances and contact resistances.

The thickness of paired aluminum and poison plates within the wrapped compartment blocks of 69BTH basket is 0.25" [11]. This thickness is reduced to 0.21" to accommodate for the size of the gaps and maintain the outer basket diameter contained within the DSC inner diameter. An effective conductivity is calculated for these plates in Section 5.1.1 to maintain the conductivity of plates within the basket. All other dimensions are based on nominal dimensions for 69BTH basket model from [11].

Mesh sensitivity of 69BTH DSC model is discussed in APPENDIX C. It is demonstrated in APPENDIX C that the mesh density of 69BTH DSC model is adequate for thermal analysis.

3.2 Assumptions and conservatism for 37PTH DSC

The following assumptions are considered for the 37PTH basket/DSC model.

The fuel assemblies contained in 37PTH basket are intact fuel assemblies.

No convection is considered within the DSC cavity.

Radiation is considered only implicitly between the fuel rods and the fuel compartment walls in the calculation of effective fuel conductivity. No other radiation heat exchange is considered within the basket model.

The modeled active fuel length for PWR fuel assemblies is 144" with the length of the bottom fitting about 4" based on WE 14x14 PWR fuel assembly [29]. The total length of the basket assembly is 162" [12].

The following gaps are considered in the 37PTH basket/DSC model at thermal equilibrium:

- 0.45" diametrical hot gap between the basket outer surface and the canister inner surface. This assumption is justified in APPENDIX A.

- 0.45” diametrical hot gap between the shield plugs and the canister shell inner surface. The maximum diametrical cold gaps between the top and bottom shield plugs and the canister shell inner surface are 0.18” and 0.25”, respectively [12]. The assumed hot gap is therefore conservative.
- 0.01” gap between the basket rails and compartment plates.
- 0.0075” gap between any two adjacent plates or components within the cross section of fuel compartments.
- 0.125” gap in axial direction between the aluminum rail pieces. This gap is larger than the axial tolerances considered for rail aluminum pieces and therefore conservative.
- Two pieces of MMC plates with 0.0075” contact gap as shown in Figure 5-17 are conservatively assumed to model single MMC plate in the model.
- 0.01” gap between any two adjacent plates between shield plugs and canister cover plates.
- 0.1” axial gap between the canister inner bottom plate and bottom basket assembly.

It has been shown in [1], Appendix M, that the 0.01” and 0.0075” gaps considered in the basket cross section account adequately for tolerances and contact resistances in a similar basket design.

Fourteen single aluminum plates with 0.125” nominal thickness are considered in the fuel compartments [12]. The thickness of single aluminum plate is modeled as 0.1325”. To account for this thickness change, an effective conductivity is estimated by a conservative reduction factor of 0.926 (=0.125”/0.135”) to maintain the conductivity of aluminum plates within the basket. All other dimensions are based on nominal dimensions for 37PTH basket/DSC model from [12].

A total thickness of 0.075” is considered for Boral plates with a maximum core thickness of 0.06”. It is considered that the single MMC or borated aluminum plates have a thickness of 0.125”.

The nominal widths of fuel compartments are 9” for four corner compartments and 8.725” for all other compartments [12]. The corresponding nominal compartment opening sizes are 8.875” for fuel assemblies in the corner compartments and 8.6” for the other fuel assemblies [12]. The widths of all compartments are reduced to 8.6” in 37PTH DSC model to accommodate for the size of the gaps and maintain the outer basket diameter contained within the canister inner diameter. Due to reduced size of the compartments, the compartment opening widths are 8.46” for all the fuel assemblies in the 37PTH DSC model.

Due to the reduced compartment opening in 37PTH DSC model, the related heat generation rates are increased by 10.0% ($=8.875^2 / 8.46^2$) for corner fuel assemblies and 3.3% ($=8.6^2 / 8.46^2$) for all other fuel assemblies. The transverse effective fuel conductivity is calculated using the following equation from [15], Section 5.2.

$$k_{eff} = \frac{q''' \, a^2}{(T_c - T_o)}(0.29468)$$

With

k_{eff} = tranverse effective fuel conductivity (Btu/hr-in-°F)
q''' = volumetric heat generation rate (Btu/hr-in^3)

$$q''' = \frac{Q}{4a^2 \, L_a}$$

Q = decay heat load (Btu/hr)
a= half of the compartment width (in)
L_a = Active fuel length (in)
T_c = maximum temperature of fuel assembly (°F)
T_o = compartment wall temperature (°F)

Since the increase of the heat generation rate and the decreases of the compartment opening size cancel each other out in the above equation, the transverse effective fuel conductivity calculated for compartment openings of 8.875" and 8.6" can be used in the 37PTH DSC model with compartment openings of 8.46" without affecting the maximum fuel cladding temperature.

Except for the four corner compartments, 32PT and 37PTH baskets have similar fuel compartment material and configuration. Since the opening size of these compartments in 37PTH DSC (8.6") is smaller than the compartment opening size of 32PT DSC (8.7"), the bounding (lowest) effective properties for homogenized PWR fuel assemblies in 32PT basket taken from [13] (used in [1], Section M.4.2) can be used conservatively for 37PTH DSC model for all fuel assemblies except the ones located in the four corner compartments. The corresponding fuel assembly is WE 14x14 PWR fuel assembly.

Only 95% of the axial effective fuel conductivity calculated for 32PT DSC in [13] is considered for use in the 37PTH DSC model for conservatism. This value is utilized in 37PTH DSC model for all fuel assemblies except the ones located in the four corner compartments.

Based on [1], drawing NUH24PTH-1003 SAR, sheet 2 of 7, Rev. 1, the compartment opening size for 24PTH DSC is 8.9" and the material of the compartments for 24PTH DSC is stainless steel SA 240, type 304. Since the compartment opening size for the four corner compartments in 37PTH DSC (8.875") is smaller than the compartment opening size of 24PTH DSC (8.9") and the emissivity of anodized aluminum used in the four corner compartments of 37PTH is higher than the emissivity of stainless steel, the bounding (lowest) effective fuel properties calculated for 24PTH DSC in [14] (used in [1], Section P.4.2) can be used conservatively for the fuel assemblies located in the four corner compartments in the 37PTH DSC model. These values are not derated for application in 37PTH DSC model.

The bounding effective fuel conductivity used for the four corner fuel assemblies in the 37PTH DSC model belongs to WE 14x14 PWR fuel assembly taken from [14].

Mesh sensitivity of 37PTH DSC model is discussed in APPENDIX C. It is demonstrated in APPENDIX C that the mesh density of 37PTH DSC model is adequate and accurate for thermal analysis.

The design basis HLZCs for all DSCs in the MP197HB transport cask are symmetrical and show maximum allowable heat load per FA and per DSC, which result in bounding maximum fuel cladding and DSC component temperatures. Possible asymmetry in HLZC (within specified FA and DSC limits) means reduction of heat load in particular FA resulting in reduction of local and maximum temperatures of fuel cladding and DSC components.

4.0 DESIGN INPUT

Material properties for 69BTH and 37PTH baskets are listed in Section 4.1.

4.1 Thermal Properties of Materials

Materials used in 69BTH basket model are listed in Table 4-1.

Table 4-1 Material Numbers in ANSYS Model for 69BTH Basket

Component	Mat # in ANSYS Model	Material
Homogenized Fuel Assembly	1	Effective conductivity
Fuel Compartment	2	SA 240, type 304
Al/Poison plates (0.25"), 90-270 orientation	3	Al1100/Boral
Al/Poison plates (0.25"), 0-180 orientation	4	Al1100/Boral
Fuel compartments wrap	5	SA 240, type 304
Al/Poison plates (0.375"), 0-180 orientation	6	Al1100/Boral
Al/Poison plates (0.375"), 90-270 orientation	12	Al1100/Boral
Aluminum rails	7	Al6061
DSC cavity gas	8	Helium
DSC shell	9	SA 240, type 304
DSC inner top cover	13	SA 240, type 304 (1)
DSC inner bottom cover	9	SA 240, type 304
DSC top shield plug	10	A36
DSC bottom shield plug	11	A36 (1)
DSC outer cover plates (top & bottom)	9	SA 240, type 304
Al/Poison plates (0.25"), 90-270 orientation	23	Al1100/Borated Al
Al/Poison plates (0.25"), 0-180 orientation	24	Al1100/Borated Al
Al/Poison plates (0.375"), 0-180 orientation	26	Al1100/Borated Al
Al/Poison plates (0.375"), 90-270 orientation	32	Al1100/Borated Al
Aluminum dummy assemblies	101	Effective conductivity

Note: (1) Effective conductivities are calculated for this component, see Table 4-11

The bounding (lowest) effective properties for homogenized BWR fuel assemblies are taken from [15] (used in [1], Section T.4.2). These properties are applicable to 69BTH basket since this basket handles the same fuel assemblies as 61BTH basket and has the same compartment material and compartment opening of nominal 6" square. It has been shown in [37] that the effective fuel properties used in 61BTH basket are the bounding (lowest) values for all the fuel assemblies proposed for 69BTH DSC.

The bounding effective properties for homogenized BWR fuel assemblies used in 69BTH DSC model belongs to FANP9 9×9-2 assembly in transverse direction and QFA 9×9 in axial direction [15].

Paired aluminum and poison plates are considered as one homogenized material in the 69BTH basket model. The effective conductivities for paired aluminum poison plates are calculated in Section 5.1.1.

To reduce the complexity of the 69BTH basket model, the contact resistances between the DSC shield plugs and DSC cover plates are integrated into the bottom shield plug and top inner cover plate. Axial effective conductivities are calculated for top and bottom shield plugs of DSC in [10] and listed in Table 4-11. The conductivities of these components remain unchanged in the radial direction.

Effective conductivities for aluminum dummy assemblies used in HLZC#2, HLZC#3, and HLZC# 4 for 69BTH basket are calculated in Section 5.1.2.

Materials used in 37PTH baskets model are listed in Table 4-2.

Table 4-2 Material Numbers in ANSYS Model for 37PTH Basket

Component	Mat # in ANSYS Model	Material
Homogenized Fuel Assembly in Four Corner Compartments (1)	19	Effective conductivity
Homogenized Fuel Assembly in Other Compartments (2)	9	Effective conductivity
Fuel Compartment	4	SA 240, type 304
Aluminum plates (0.125")	10	Al1100 (3)
Aluminum plates (0.05")	6	Al1100
Boral Poison plates (0.075" with 0.06" core)	24	Boral
MMC Poison plates (0.125")	25	MMC (4)
Aluminum rails	3	Al6061
DSC cavity gas	2, 8	Helium
Contact gap (0.075") among neutron absorber plates	7	Helium
Gaps among DSC top/bottom end plates	22	Air
DSC shell and cover plates	1	SA 240, type 304
DSC top and bottom shield plugs	20	A36

Notes: (1) The opening size for corner compartments is 8.875" [12].
(2) The opening size for other compartments is 8.6" [12].
(3) Effective thermal conductivities as discussed in Section 3.2 is used for these plates.
(4) Minimum thermal conductivities is taken from [1] shown in Table 4-8. Two piece of MMC plates with 0.0075" contact gap as shown in Figure 5-17 are assumed in the model.

Thermal conductivity values used in this calculation are listed in Table 4-3 through Table 4-11. The densities and specific heats used for calculation of effective basket properties are listed in Table 4-12.

Table 4-3 Homogenized BWR Fuel Assembly in Helium ([15] and [1])

Temperature (F)	Transverse Conductivity (Btu/min-in-°F)	Transverse Conductivity (Btu/hr-in-°F)	Axial Conductivity (Btu/min-in-°F)	Axial Conductivity (Btu/hr-in-°F)
200	2.618E-04	0.0157	6.7E-4	0.0402
300	3.021E-04	0.0181		
400	3.520E-04	0.0211		
500	4.104E-04	0.0246		
600	4.756E-04	0.0285		
700	5.468E-04	0.0328		
800	6.250E-04	0.0375		

Table 4-4 Homogenized PWR Fuel Assembly in Helium

For Four Corner Fuel Assemblies from [14], used [1], Appendix P

Temperature (°F)	Transverse Conductivity (Btu/min-in-°F)	Transverse Conductivity (Btu/hr-in-°F)	Temperature (°F)	Axial Conductivity (Btu/min-in-°F)	Axial Conductivity (Btu/hr-in-°F)
178	2.798E-04	0.0168	200	7.596E-04	0.0456
267	3.257E-04	0.0195	300	8.014E-04	0.0481
357	3.828E-04	0.0230	400	8.432E-04	0.0506
448	4.547E-04	0.0273	500	8.781E-04	0.0527
541	5.389E-04	0.0323	600	9.129E-04	0.0548
635	6.326E-04	0.0380	800	9.896E-04	0.0594
730	7.398E-04	0.0444			
826	8.558E-04	0.0513			

For Other Fuel Assemblies from [13], used [1], Appendix M

Temperature (°F)	Transverse Conductivity (Btu/min-in-°F)	Transverse Conductivity (Btu/hr-in-°F)	Temperature (°F)	Axial Conductivity (Btu/min-in-°F)	Axial Conductivity (Btu/hr-in-°F) (1)
138	2.894E-04	0.0174	200	7.949E-04	0.0454
233	3.317E-04	0.0199	300	8.387E-04	0.0478
328	3.968E-04	0.0238	400	8.824E-04	0.0503
423	4.744E-04	0.0285	500	9.189E-04	0.0524
519	5.668E-04	0.0340	600	9.554E-04	0.0545
616	6.715E-04	0.0403	800	1.036E-03	0.0591
714	7.879E-04	0.0473			
812	9.208E-4	0.0552			

Note: (1) Only 95% of the axial effective conductivity calculated in [13] for 32PT DSC is considered in the 37PTH DSC model for conservatism.

Table 4-5 Stainless Steel Properties

Stainless Steel	Thermal conductivity SA 240, Type 304 ASME 2004, Group J [6], [18]	
Temperature (°F)	(Btu/hr-ft-°F)	(Btu/hr-in-°F)
70	8.6	0.717
100	8.7	0.725
200	9.3	0.775
300	9.8	0.817
400	10.4	0.867
500	10.9	0.908
600	11.3	0.942
700	11.8	0.983
800	12.3	1.025
900	12.7	1.058
1000	13.1	1.092
1100	13.6	1.133
1200	14.0	1.167
1300	14.5	1.208
1400	14.9	1.242

Table 4-6 Carbon Steel Properties

Carbon Steel	Thermal conductivity A36 ASME 2004, Group B [6], [18]	
Temperature (°F)	(Btu/hr-ft-°F)	(Btu/hr-in-°F)
70	27.3	2.275
100	27.6	2.300
200	27.8	2.317
300	27.3	2.275
400	26.5	2.208
500	25.7	2.142
600	24.9	2.075
700	24.1	2.008
800	23.2	1.933
900	22.3	1.858
1000	21.1	1.758
1100	19.8	1.650
1200	18.3	1.525
1300	16.9	1.408
1400	15.7	1.308

Table 4-7 Aluminum Alloys Properties

Aluminum	Thermal conductivity Al 1100 ASME 2004 [6], [18]		Thermal conductivity Al 6061 ASME 2004, [6], [18]	
Temperature (°F)	(Btu/hr-ft-°F)	(Btu/hr-in-°F)	(Btu/hr-ft-°F)	(Btu/hr-in-°F)
70	133.1	11.092	96.1	8.008
100	131.8	10.983 (1)	96.9	8.075
150	130.0	10.833	98.0	8.167
200	128.5	10.708	99.0	8.250
250	127.3	10.608	99.8	8.317
300	126.2	10.517	100.6	8.383
350	125.3	10.442	101.3	8.442
400	124.5	10.375	101.9	8.492

Note: (1) Thermal conductivity of 11.150 Btu/hr-in-°F (133.8 Btu/hr-ft-°F) is used in the file "Mat69BTH.inp" and "MatInp_37pth.mac" for the material properties. Since the basket temperature is over 150°F for all analyzed cases, this value does not affect the results in this calculation.

Table 4-8 Poison Material

Boral Core Matrix		
Temperature (°F)	Conductivity (W/cm-K) [20]	Conductivity (Btu/hr-in-°F)
100	0.859	4.136
500	0.768	3.698
Metal Matrix Composite (MMC)		
Temperature (°F)	Conductivity (Btu/min-in-°F),	Conductivity (Btu/hr-in-°F)
212 to 572	0.116 [8]	6.96
All temperatures	0.0964 [1] (1)	5.78
Borated Aluminum		
Temperature (°F)	Conductivity (Btu/min-in-°F) [1], [8]	Conductivity (Btu/hr-in-°F)
68	0.123	7.38
212	0.132	7.92
392	0.141	8.46
482	0.145	8.70

Note: (1) The lower conductivity is selected to calculate effective conductivity in Section 5.1.1.

Table 4-9 Helium Thermal Conductivity

Temperature (K)	Thermal conductivity (W/m-K)	Temperature (°F)	Thermal conductivity (Btu/hr-in-°F)
300	0.1499	80	0.0072
400	0.1795	260	0.0086
500	0.2115	440	0.0102
600	0.2466	620	0.0119
800	0.3073	980	0.0148
1000	0.3622	1340	0.0174
1050	0.3757	1430	0.0181

The above data are calculated base on the following polynomial function from [19]

$k = \sum C_i\, T_i$ for conductivity in(W/m-K) and T in (K)

For 300 < T < 500 K		for 500< T < 1050 K	
C0	-7.761491E-03	C0	-9.0656E-02
C1	8.66192033E-04	C1	9.37593087E-04
C2	-1.5559338E-06	C2	-9.13347535E-07
C3	1.40150565E-09	C3	5.55037072E-10
C4	0.0E+00	C4	-1.26457196E-13

Table 4-10 Air Thermal Conductivity

Temperature (K)	Thermal conductivity (W/m-K)	Temperature (°F)	Thermal conductivity (Btu/hr-in-°F)
250	0.02228	-10	0.0011
300	0.02607	80	0.0013
400	0.03304	260	0.0016
500	0.03948	440	0.0019
600	0.04557	620	0.0022
800	0.05698	980	0.0027
1000	0.06721	1340	0.0032

The above data are calculated base on the following polynomial function from [19]

$k = \sum C_i\, T_i$ for conductivity in(W/m-K) and T in (K)

For 250 < T < 1050 K	
C0	-2.2765010E-03
C1	1.2598485E-04
C2	-1.4815235E-07
C3	1.7355064E-10
C4	-1.0666570E-13
C5	2.4766304E-17

Table 4-11 Axial Effective Conductivity for Bottom Shield plug and Inner Top Cover Plate

69BTH inner top cover plate
Plate thickness = 0.75 in (1)
Gap thickness = 0.0625 in
Two axial gaps

Temp (°F)	k_SS304 (Btu/hr-in-°F) [Table 4-5]	Temp (K)	k_air (W/m-K) [Table 4-10]	k_air (Btu/hr-in-°F)	k_eff (Btu/hr-in-°F)
70	0.717	294.4	0.0257	0.0012	0.0086
100	0.725	311.1	0.0269	0.0013	0.0090
200	0.775	366.7	0.0308	0.0015	0.0103
300	0.817	422.2	0.0345	0.0017	0.0115
400	0.867	477.8	0.0381	0.0018	0.0127
500	0.908	533.3	0.0415	0.0020	0.0138
600	0.942	588.9	0.0449	0.0022	0.0149
700	0.983	644.4	0.0482	0.0023	0.0160
800	1.025	700.0	0.0514	0.0025	0.0171
900	1.058	755.6	0.0545	0.0026	0.0181
1,000	1.092	811.1	0.0576	0.0028	0.0191

69BTH bottom shield plug
Plate thickness = 3 in
Gap thickness = 0.0625 in
Two axial gaps

Temp (°F)	k_A36 (Btu/hr-in-°F) [Table 4-6]	Temp (K)	k_air (W/m-K) [Table 4-10]	k_air (Btu/hr-in-°F)	k_eff (Btu/hr-in-°F)
70	2.275	294.4	0.0257	0.0012	0.030
100	2.300	311.1	0.0269	0.0013	0.032
200	2.317	366.7	0.0308	0.0015	0.037
300	2.275	422.2	0.0345	0.0017	0.041
400	2.208	477.8	0.0381	0.0018	0.045
500	2.142	533.3	0.0415	0.0020	0.049
600	2.075	588.9	0.0449	0.0022	0.053
700	2.008	644.4	0.0482	0.0023	0.056
800	1.933	700.0	0.0514	0.0025	0.060
900	1.858	755.6	0.0545	0.0026	0.063
1,000	1.758	811.1	0.0576	0.0028	0.067

Note: (1) The smallest thickness for DSC top cover plate among all the DSC types proposed for transportation in MP197HB is 0.75". This value is considered to calculate the axial effective conductivity for conservatism.

Table 4-12 Density and Specific Heat

SA 240, Type 304 ASME 2004, Group J [18]		
Temperature (°F)	Specific Heat [6] (Btu/lbm-°F)	Density [6] (lbm/in^3)
70	0.116	0.284 (1)
100	0.117	
200	0.121	
300	0.125	
400	0.128	
500	0.131	
600	0.132	
700	0.134	
800	0.136	
900	0.137	
1000	0.138	

Aluminum 6061 or 6063 ASME 2004 [18]		
Temperature (°F)	Specific Heat [6] (Btu/lbm-°F)	Density [6] (lbm/in^3)
70	0.213	0.098
100	0.215	
200	0.221	
300	0.226	
400	0.230	

BWR Fuel Assembly		
Temperature (°F)	Specific Heat [15] (Btu/lbm-°F)	Density [15] (lbm/in^3)
---	0.0575	0.103

PWR Fuel Assembly		
Temperature (°F)	Specific Heat [14] (Btu/lbm-°F)	Density [14] (lbm/in^3)
80	0.05924	0.1114
260	0.06538	
692	0.07255	
1502	0.07779	

Note: (1) The density of SA 240, Type 304 in [6] is 0.29 lbm/in^3. Using a lower density of 0.284 is conservative to maximize the component temperatures for a transient run.

4.2 Design Criteria

To establish the integrity of the fuel cladding, a fuel cladding temperature limit of 350°C (662°F) is selected for fuel assemblies in 69BTH and 37PTH basket. This temperature limit is below the fuel cladding temperature limit of 400°C (752°F) established in [5] and [6] and therefore acceptable.

The fuel cladding temperature limit for fuel assemblies for other baskets is 400°C (752°F), which is equal to the value established in [5] and [6].

Based on ISG-11 [5], the fuel cladding temperature is limited to 400°C (752°F) for short term operation such as vacuum drying. Temperature differences greater than 65°C (117°F) are not permitted by [5] for repeated cycling of fuel cladding temperature during drying and backfilling operations

Materials of the baskets in all DSC types can be subjected to a minimum environment temperature of -40°F (-40°C) without any adverse effects.

5.0 METHODOLOGY

Thermal evaluations for 69BTH DSC and 37PTH DSC for NCT are performed based on finite element models of the DSCs using ANSYS computer code, version 8.1 [28]. These models are described in the following sections.

5.1 Model for 69BTH DSC

A half-symmetric, three-dimensional finite element model of 69BTH basket and DSC is developed using ANSYS [28], version 8.1. The model contains the DSC shell, the DSC cover plates, shield plugs, aluminum rails, basket plates, and homogenized fuel assemblies. Only SOLID70 elements are used in the 69BTH DSC/basket model.

The DSC shell temperatures for NCT at 100°F, -20°F and -40°F are retrieved from the MP197HB transfer cask model described in [10] and transferred to the basket models via runs listed in Section 8.0, Table 8-1.

Decay heat load is applied as heat generation boundary conditions over the elements representing homogenized fuel assemblies.

The base heat generation rates used in this analysis is calculated as follows.

$$\dot{q}''' = \left(\frac{q}{a^2 L_a} \times PF \right) \times CF \qquad (5.1)$$

Where,
q = Decay heat load per assembly defined for each loading zone
a = Width of the homogenized fuel assembly = 6.0”
L_a =Active fuel length = 144”
PF = Peaking Factor from Section 5.1.3
CF = correction factor = 1.00697 for 69BTH (see Section 5.1.3)

The base heat generation rates used in 69BTH basket model are listed in Table 5-1.

Table 5-1 Base Heat Generation Rates for 69BTH

Heat Load in the Model (KW)	$\dot{q}'''$ value without PF (Btu/hr-in^3)	Heat Load in the Model (KW)	$\dot{q}'''$ value without PF (Btu/hr-in^3)
0.10	0.0663	0.50	0.3314
0.25	0.1657	0.55	0.3646
0.30	0.1988	0.60	0.3977
0.40	0.2651	0.70	0.4640
0.45	0.2983		

The base heat generation rate is multiplied by peaking factors along the axial fuel length to represent the axial decay heat profile. Axial decay heat profile for BWR fuel assemblies is described in [8] and used in [1]. The peaking factors from [8] are converted to match the regions defined for the fuel assembly in the finite element model. Section 5.1.3 describes the conversion method and lists the peaking factors used in 69BTH model.

The active fuel length for fuel assembly LaCrosse is only 85" [6], which is significantly shorter than the other fuel assemblies considered for transport in 69BTH DSC. The heat load of this fuel assembly fuel should be lower than the longer fuel assemblies to maintain the same temperature distribution in 69BTH DSC.

Since conduction and effective conductivities are the only heat transfer paths considered in the 69BTH DSC, the temperatures are directly proportional to the fuel assembly heat load and reversely proportional to the active fuel length and effective fuel conductivity. Therefore, the following equations determine the reduction in heat load for fuel assembly LaCrosse to maintain the 69BTH temperatures at the same level as those determined for the bounding fuel assembly.

$$\left(\frac{q}{L_a\ k_{eff}}\right)_{LaCrosse} = \left(\frac{q}{L_a\ k_{eff}}\right)_{BoundingFA} \qquad (5.2)$$

$$q_{LaCrosse} = q_{boundingFA}\ \frac{L_{a,LaCrosse}}{L_{a,BoundingFA}} \cdot \frac{k_{eff,LaCrosse}}{k_{eff,boundingFA}}$$

With,
k_{eff} = effective fuel assembly conductivity (Btu/hr-in-°F)
q = Decay heat load per assembly defined for each loading zone (Btu/hr)
L_a =Active fuel length (in)
= 144" for bounding fuel assembly
= 85" for LaCrosse fuel assembly

Based on studies in [37], the transverse and axial effective conductivities of fuel assembly LaCrosse are at least 19.9% higher than those for the bounding fuel assembly. Substitution of these values in equation (5.2) gives the reduction of the heat load for fuel assembly LaCrosse.

$$q_{LaCrosse} = q_{boundingFA} \left(\frac{85}{144} \times 1.199\right) = 0.708\, q_{boundingFA} \qquad (5.3)$$

The heat load for LaCrosse fuel assembly should be reduced to 70% of the heat load for bounding fuel assembly to maintain the 69BTH DSC temperatures at the same level calculated for the bounding fuel assembly.

The heat generating rates for the elements representing the active fuel are calculated based on the HLZCs for each basket type. The HLZCs and their restrictions for 69BTH basket are shown in Figure 5-1 through Figure 5-4.

		Z6	Z6	Z6	Z6	Z6		
	Z6	Z5	Z5	Z4	Z5	Z5	Z6	
Z6	Z5	Z4	Z4	Z3	Z4	Z4	Z5	Z6
Z6	Z5	Z4	Z3	Z2	Z3	Z4	Z5	Z6
Z6	Z4	Z3	Z3	Z1	Z3	Z3	Z4	Z6
Z6	Z5	Z4	Z3	Z2	Z3	Z4	Z5	Z6
Z6	Z5	Z4	Z4	Z3	Z4	Z4	Z5	Z6
	Z6	Z5	Z5	Z4	Z5	Z5	Z6	
		Z6	Z6	Z6	Z6	Z6		

	Zone 1	Zone 2	Zone 3	Zone 4	Zone 5	Zone 6
Max. Decay Heat (kW/FA) (3)	0.10	0.27	0.30	0.40	0.55	0.45
No. of Fuel Assemblies (1)	1	2	10	16	16	24
Max. Decay Heat per Zone (kW) (3)	0.10	0.54	3.0	6.4	8.8	10.8
Max. Decay Heat per DSC (kW)	26.0 (2) (3)					

Notes: (1) Total number of fuel assemblies is 69 for HLZC # 1
(2) Adjust payload to maintain the total DSC heat load within the specified limit
(3) Reduce the maximum decay heat to 70% of the listed values for LaCrosse Fuel assembly. The total decay heat for LaCrosse fuel assembly is 18.2 kW per DSC for HLZC No. 1.

Figure 5-1 Heat Load Zoning Configuration No. 1 for 69BTH Basket

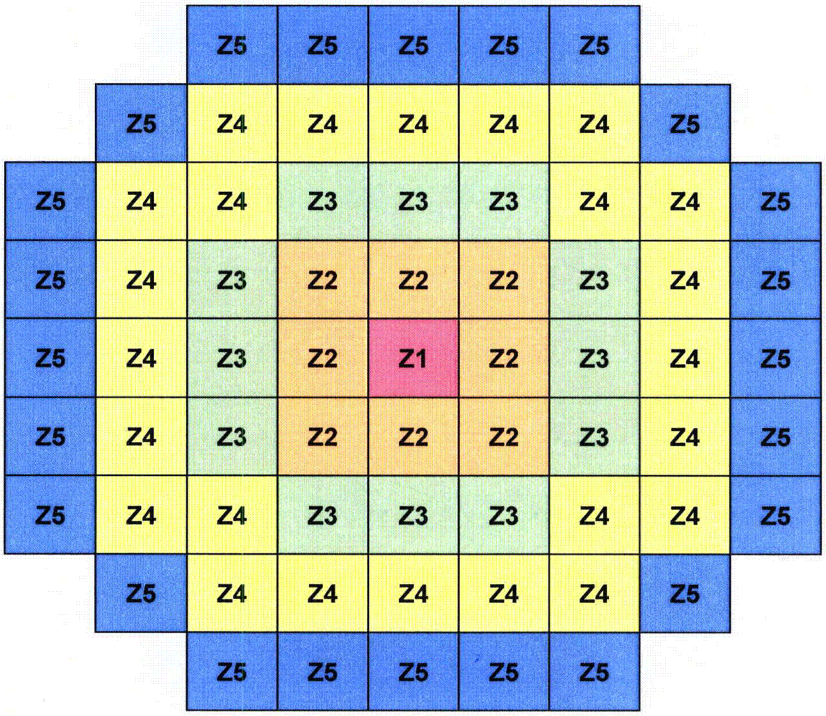

	Zone 1	Zone 2	Zone 3	Zone 4	Zone 5
Max. Decay Heat (kW/FA) (4)	0.25	0.0 (1)	0.40	0.60	0.50
No. of Fuel Assemblies (2)	1	0	12	24	24
Max. Decay Heat per Zone (kW) (4)	0.25	0	4.8	14.4	12.0
Max. Decay Heat per DSC (kW)	26.0 (3) (4)				

Notes: (1) Aluminum dummy assemblies replace the fuel assemblies in zone 2
(2) Total number of fuel assemblies is 61 for HLZC # 2
(3) Adjust payload to maintain the total DSC heat load within the specified limit
(4) Reduce the maximum decay heat to 70% of the listed values for LaCrosse Fuel assembly. The total decay heat for LaCrosse fuel assembly is 18.2 kW per DSC for HLZC No. 2.

Figure 5-2 Heat Load Zoning Configuration No. 2 for 69BTH Basket

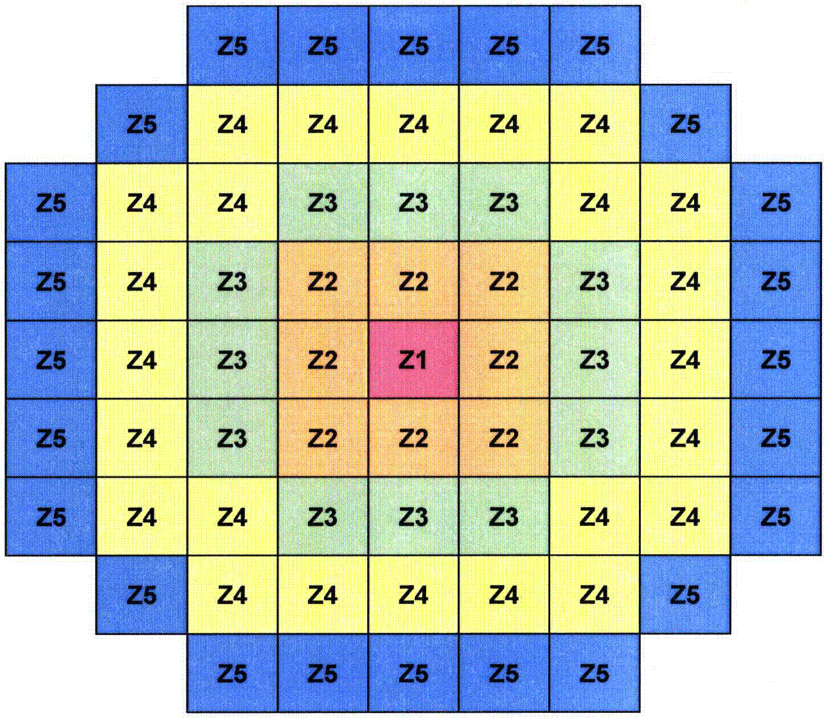

	Zone 1	Zone 2	Zone 3	Zone 4	Zone 5
Max. Decay Heat (kW/FA) (4)	0.25	0.0 (1)	0.40	0.60	0.50
No. of Fuel Assemblies (2)	1	0	12	24	24
Max. Decay Heat per Zone (kW) (4)	0.25	0	4.8	14.4	12.0
Max. Decay Heat per DSC (kW)	29.2 (3) (4)				

Notes: (1) Aluminum dummy assemblies replace the fuel assemblies in zone 2
(2) Total number of fuel assemblies is 61 for HLZC # 3
(3) Adjust payload to maintain the total DSC heat load within the specified limit
(4) Reduce the maximum decay heat to 70% of the listed values for LaCrosse Fuel assembly. The total decay heat for LaCrosse fuel assembly is 20.4 kW per DSC for HLZC No. 3.

Figure 5-3 Heat Load Zoning Configuration No. 3 for 69BTH Basket

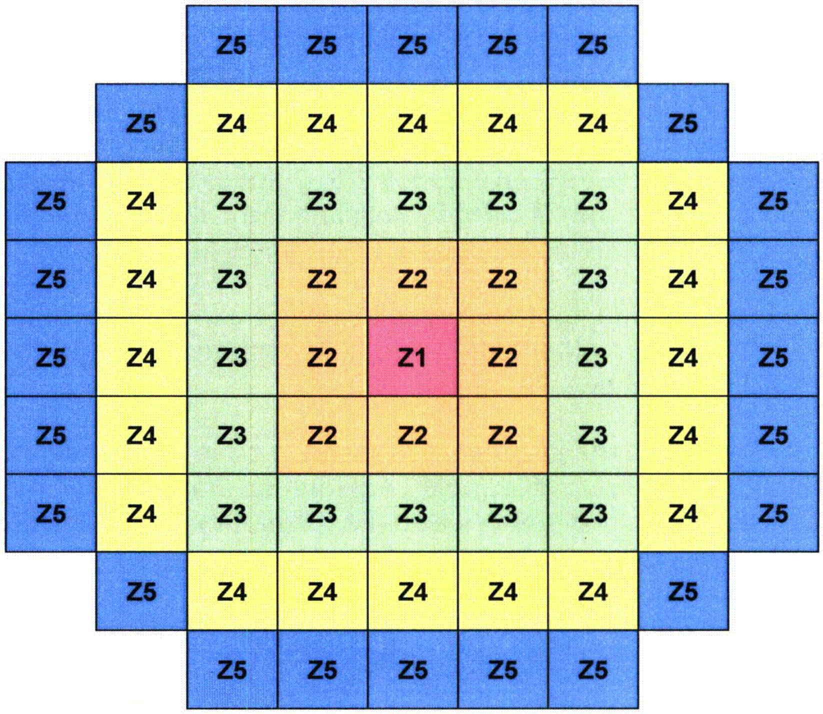

	Zone 1	Zone 2	Zone 3	Zone 4	Zone 5
Max. Decay Heat (kW/FA) (4)	0.0 (1)	0.45	0.0 (2)	0.70	0.60
No. of Fuel Assemblies (3)	0	8	0	20	24
Max. Decay Heat per Zone (kW) (4)	0	3.6	0	14.0	14.4
Max. Decay Heat per DSC (kW)	32.0 (4)				

Notes: (1) The fuel compartment in zone 1 remains empty
(2): Aluminum dummy assemblies replace the fuel assemblies in zone 3
(3): Total number of fuel assemblies is 52 for HLZC # 4
(4) Reduce the maximum decay heat to 70% of the listed values for LaCrosse Fuel assembly. The total decay heat for LaCrosse fuel assembly is 22.4 kW per DSC for HLZC No. 4.

Figure 5-4 Heat Load Zoning Configuration No. 4 for 69BTH Basket

Because of the total heat load restriction in HLZC # 1 for 69BTH basket (total heat load 26 kW), all the zones cannot be loaded with the maximum defined heat load per assembly. A study of the loading patterns in [21] concludes that for a given decay heat load in a cask, loading assemblies with higher decay heat output around the outside of the cask will result in lower peak fuel cladding temperature. Based on this study, the peak cladding temperature is maximized if the heat load is concentrated in the inner core compartments. It concludes that the fuel cladding temperature for HLZC #1 is maximized if zones 1 to 5 (inner zones) are loaded at the maximum heat load and zone 6 (outer zone) is used to maintain the total heat load at 26 kW. This bounding pattern is assigned in Table 5-2 as configuration A.

In order to assure that the configuration A results in the bounding maximum fuel cladding temperature for HLZC # 1, two other extreme loading patterns, configuration B and C, are considered for HLZC #1 as shown in Table 5-2.

In configuration B, the heat loads in zones 1 to 4 and in zone 6 are maximized. The heat load in zone 5 is lower than the maximum allowable heat load so that the total heat load is maintained at 26 kW. In this case the fuel assemblies with the maximum heat loads are located in the core compartments and in the outermost compartments.

In configuration C, the zones with the maximum heat loads are shrunken by one further zone to the center. In this configuration, heat loads in zones 1, 2, 3, 5, and 6 are maximized. The heat load in zone 4 is lower than the maximum allowable and maintains the total heat load at 26 kW.

Table 5-2 HLZC # 1A, # 1B, and # 1C for 69BTH Basket

		HLZC # 1A (1)		HLZC # 1B		HLZC # 1C	
Zone #	No. of FA	Heat load per FA (kW)	Heat load (kW)	Heat load per FA (kW)	Heat load (kW)	Heat load per FA (kW)	Heat load (kW)
Zone 1	1	0.100	0.10	0.100	0.1	0.100	0.10
Zone 2	2	0.270	0.54	0.270	0.54	0.270	0.54
Zone 3	10	0.300	3.00	0.300	3.00	0.300	3.00
Zone 4	16	0.400	6.40	0.400	6.40	0.1725	2.76
Zone 5	16	0.550	8.80	0.3225	5.16	0.550	8.80
Zone 6	24	0.2983	7.16	0.450	10.80	0.450	10.80
Total	69		26.0		26.0		26.0

Note: (1) Total number of fuel assemblies loaded in HLZC#1 is 69.

The maximum fuel cladding temperatures for HLZC # 1 discussed in Section 6.0 show that the bounding value is reached in HLZC # 1A as expected based on study in [21]. The same pattern is valid for all other configurations. Therefore, the bounding maximum fuel cladding temperature for the other HLZCs are determined based on loading patterns in which the core assemblies are loaded at the maximum allowable heat load for each zone. The maximum allowable total heat load is then maintained by loading the outermost compartments with fuel assemblies having heat loads lower than the allowable limit. The bounding heat load patterns for HLCZ # 2, # 3, and # 4 are listed in Table 5-3.

Table 5-3 Bounding Configurations for HLZC #2, # 3, and # 4

HLZC # 2 (1)			
Zone #	No. of FA	Heat load per FA (kW)	Heat load (kW)
Zone 1	1	0.250	0.25
Zone 2 (4)	8	0.000	0.00
Zone 3	12	0.400	4.80
Zone 4	24	0.600	14.40
Zone 5	24	0.2729	6.55
Total	69		26.0

HLZC # 3 (2)			
Zone #	No. of FA	Heat load per FA (kW)	Heat load (kW)
Zone 1	1	0.250	0.25
Zone 2 (4)	8	0.000	0.00
Zone 3	12	0.400	4.80
Zone 4	24	0.600	14.40
Zone 5	24	0.4063	9.75
Total	69		29.2

HLZC # 4 (3)			
Zone #	No. of FA	Heat load per FA (kW)	Heat load (kW)
Zone 1 (5)	1	0.000	0.00
Zone 2	8	0.450	3.60
Zone 3 (4)	16	0.000	0.00
Zone 4	20	0.700	14.00
Zone 5	24	0.600	14.40
Total	69		32.0

Notes: (1) Total number of fuel assemblies loaded in HLZC#2 is 61.
(2) Total number of fuel assemblies loaded in HLZC#3 is 61.
(3) Total number of fuel assemblies loaded in HLZC#4 is 52.
(4) Aluminum dummy assemblies replace fuel assemblies in this zone.
(5) The fuel compartment in this zone remains empty.

The material properties used in the 69BTH basket/DSC model are listed in Section 4.0.

The effective thermal conductivities for paired aluminum/poison plates and for dummy aluminum assemblies are calculated in Section 5.1.1 and Section 5.1.2, respectively.

The peaking factors used in the finite element model to create axial heat profile for the BWR fuel assemblies are discussed in Section 5.1.3.

The effective properties of the 69BTH basket are calculated in Section 5.3. These properties can be used in transient analysis.

The geometry of the 69BTH basket model and its mesh density are shown in Figure 5-5 through Figure 5-9.

Typical boundary conditions for 69BTH basket model are shown in Figure 5-10.

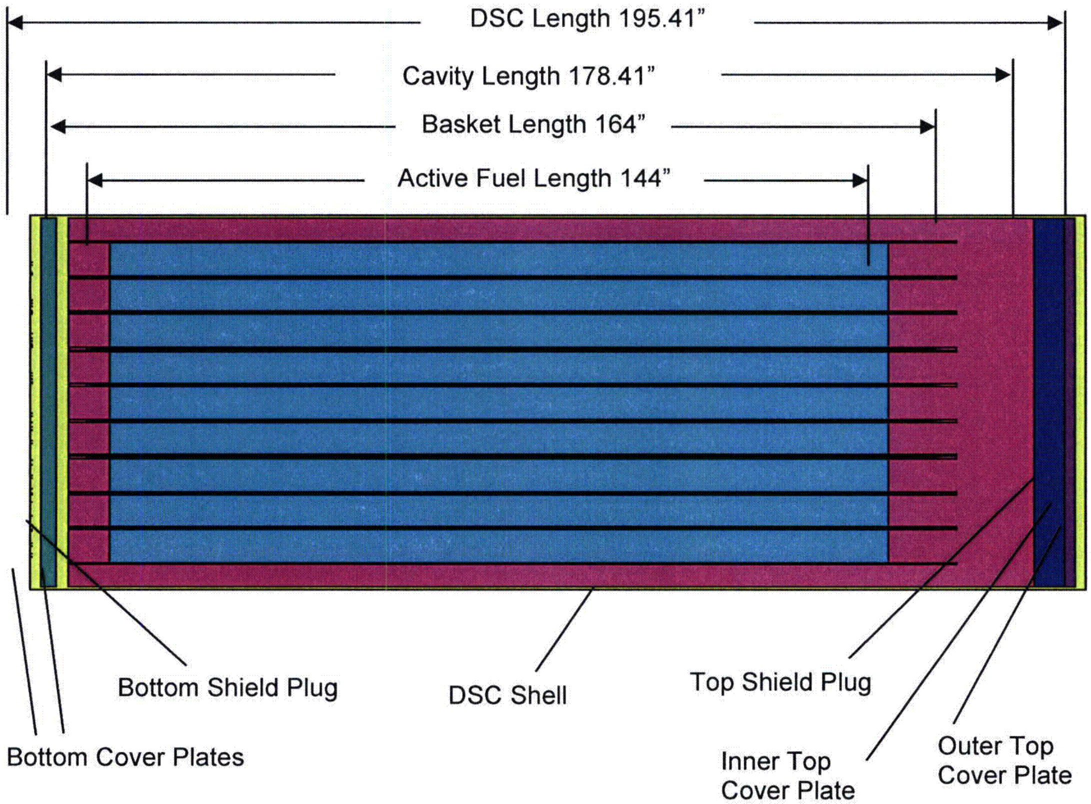

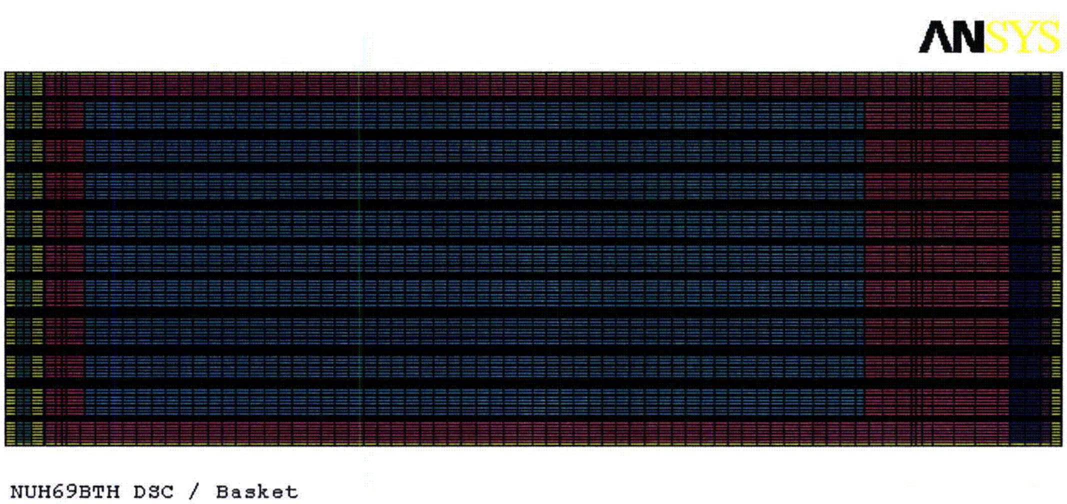

Mesh Density

Figure 5-5 Finite Element Model of 69BTH DSC/Basket

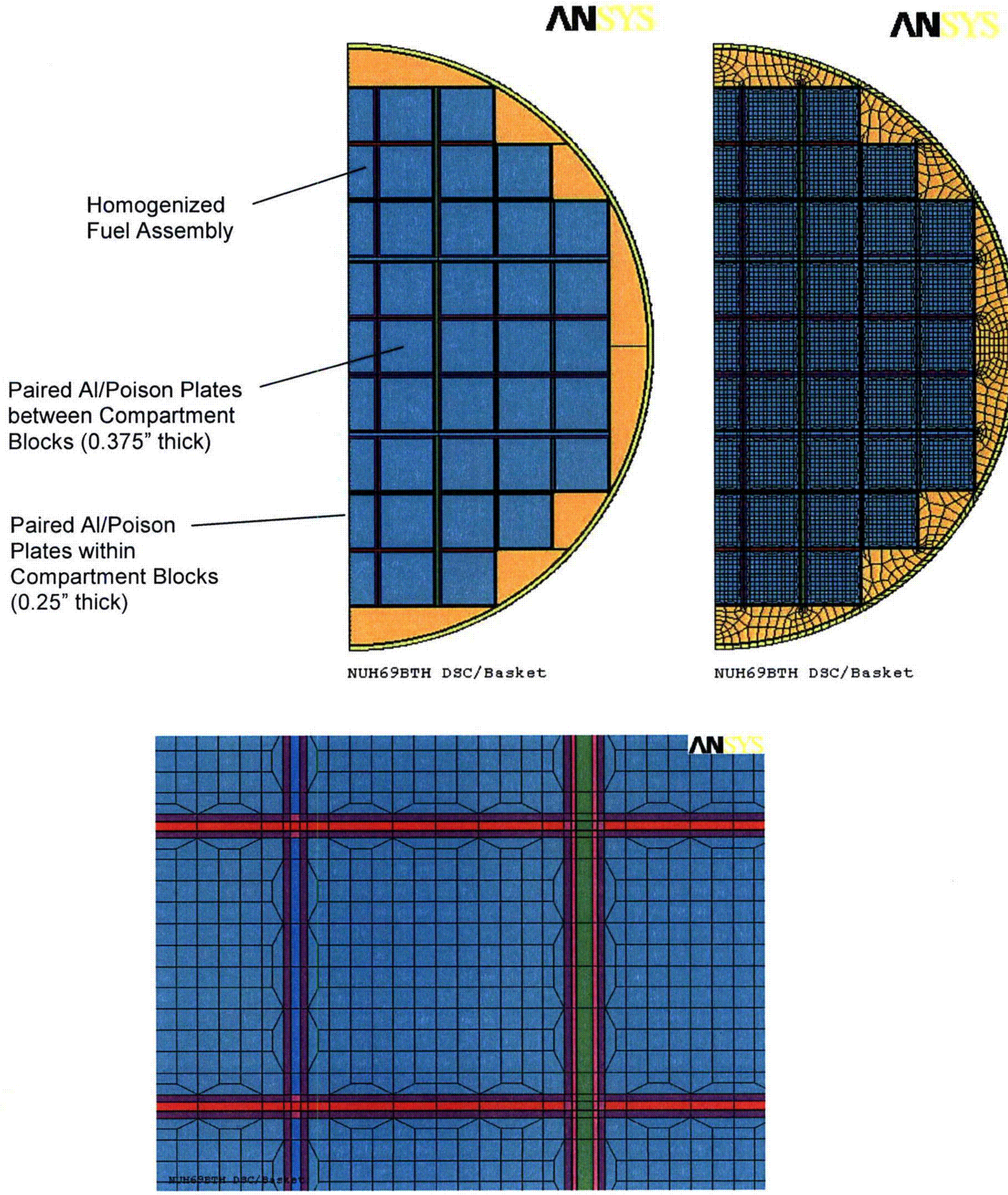

Mesh Density

Figure 5-6 69BTH DSC/Basket – Cross Section

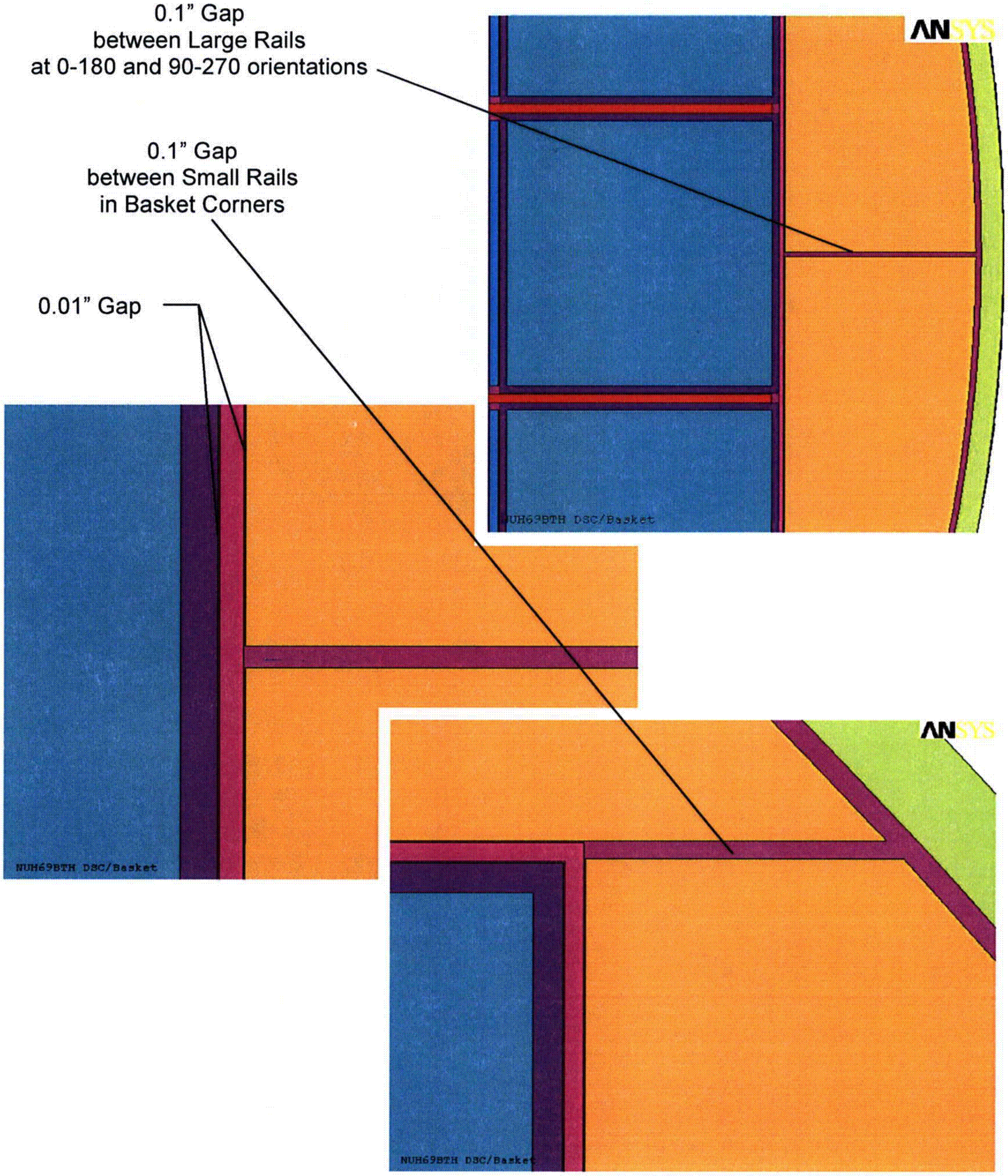

Figure 5-7 69BTH DSC/Basket – Gaps between Rail Sections at Cross Section

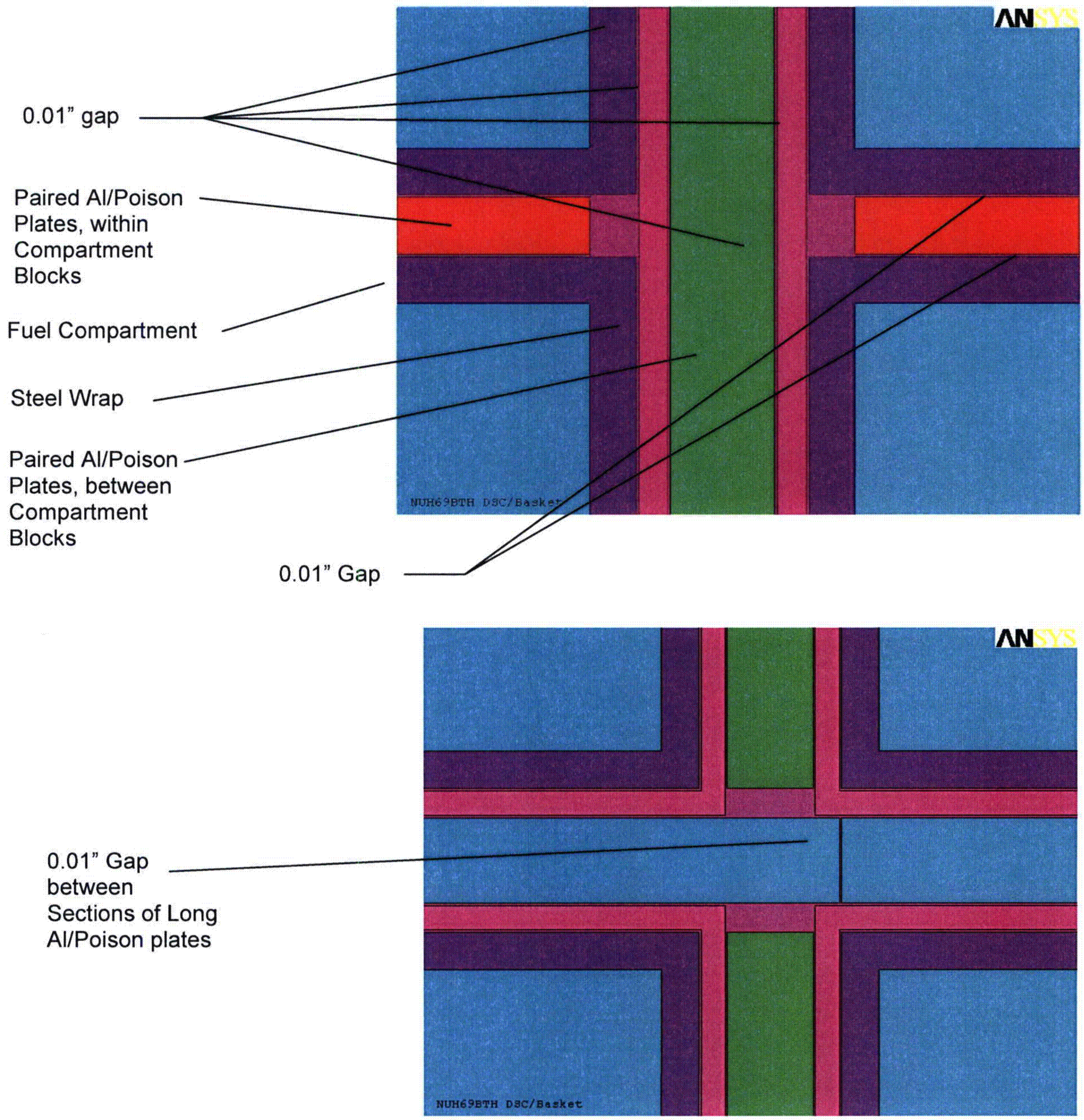

Figure 5-8 69BTH DSC/Basket – Gaps between Basket Plates at Cross Section

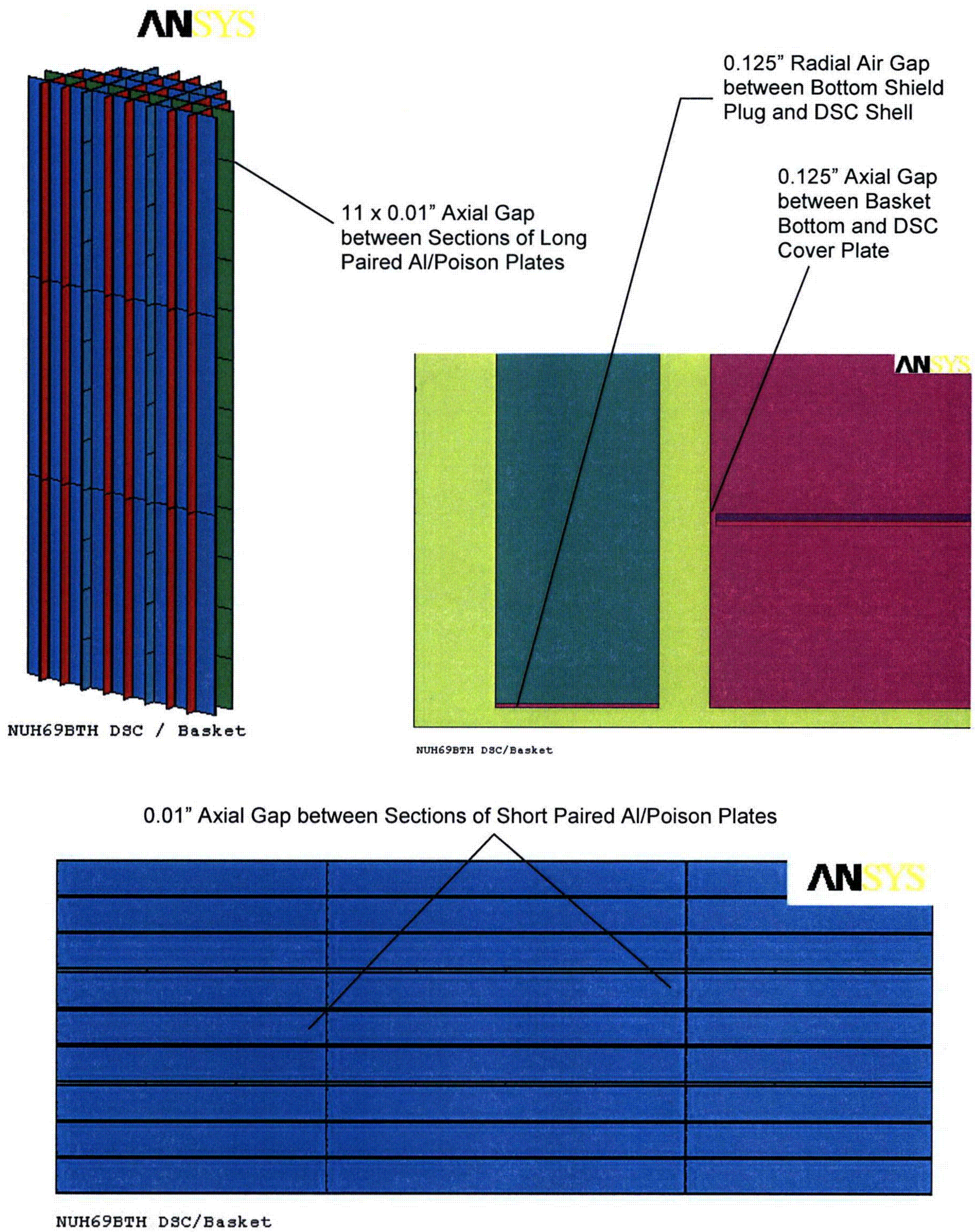

Figure 5-9 69BTH DSC/Basket – Axial Gaps

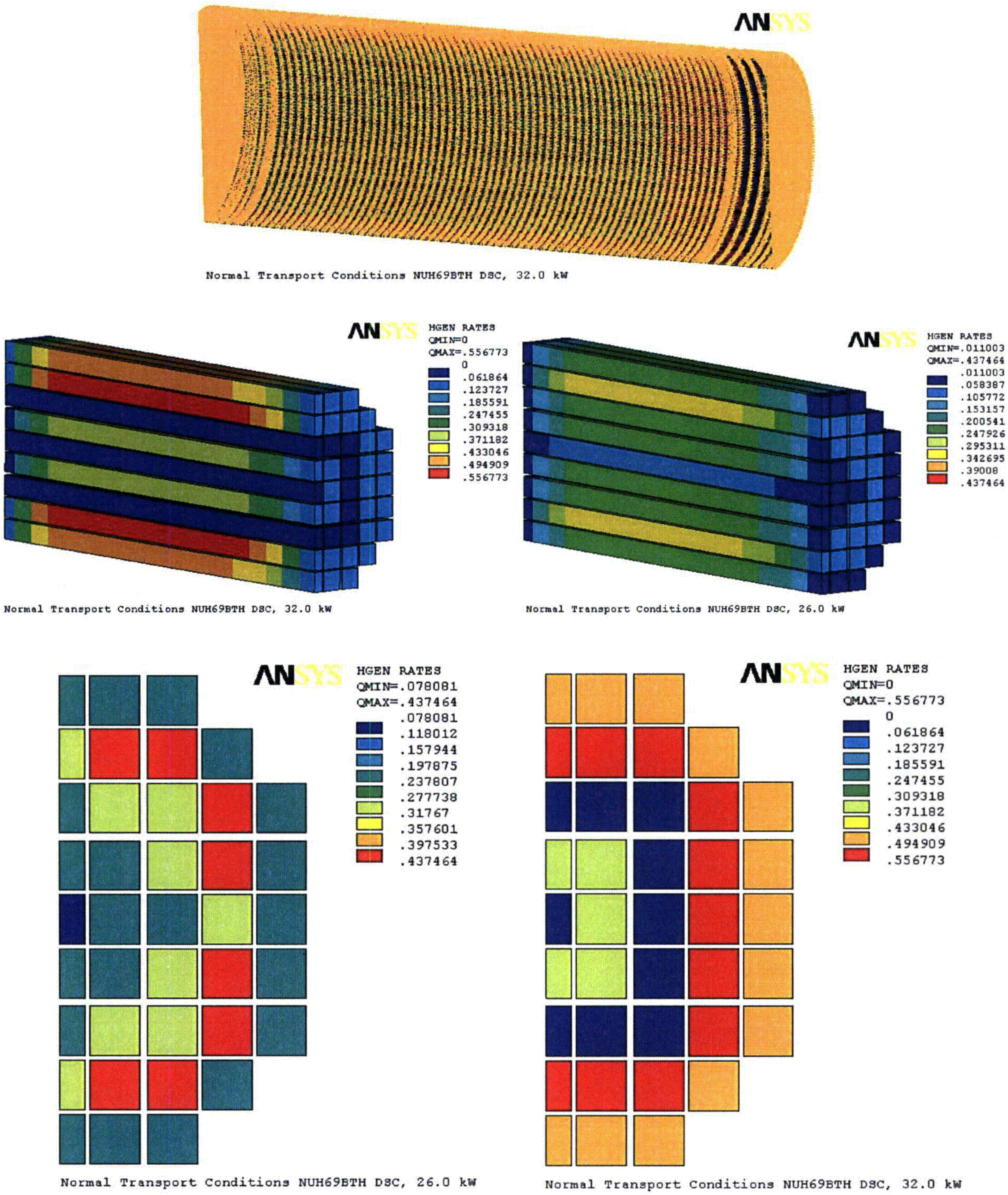

Figure 5-10 Typical Boundary Conditions for 69BTH Basket

5.1.1 Effective Conductivity for Paired Aluminum and Poison Plates in 69BTH DSC

Paired aluminum and poison plates are considered as one homogenized material in the 69BTH basket model. The possible combinations for paired aluminum and poison plates are summarized in Table 5-4.

Table 5-4 Combinations for Paired Al/Poison Plates in 69BTH Basket

		Paired Plated within Compartment Blocks	Paired Plated between Compartment Blocks
	Total Thickness	0.25"	0.375"
Al/Boral	Boral Plate Thickness	0.25"	0.25"
	Boral Core Thickness	0.16"	0.16"
	Al Plate Thickness	0	0.125"
Al/Borated Al or Al/MMC	Total Thickness	0.25"	0.375"
	Poison Plate Thickness	0.175"	0.175"
	Al Plate Thickness	0.075"	0.200"

The paired plates built up parallel thermal resistances along their length and serial thermal resistances across their thickness. The gaps considered between the paired plates and their adjacent basket plates at the cross section account for the contact resistance between the plates. The adequacy of these gaps for contact resistances is justified in APPENDIX B.

The effective conductivities of the paired plates are calculated as follows:

$$k_{eff,along} = \frac{k_{poison} \times t_{poison} + k_{Al} \times t_{Al}}{t_{model}} \quad (5.4) \text{ along the length (parallel resistances)}$$

$$k_{eff,across} = \frac{t_{model}}{\dfrac{t_{poison}}{k_{poison}} + \dfrac{t_{Al}}{k_{Al}}} \quad (5.5) \text{ across the thickness (serial resistances)}$$

Where,
k_{poison} = conductivity of poison plate or conductivity of core material for Boral (Btu/hr-in-°F)
t_{poison} = thickness of poison plate or thickness of core material for Boral (in)
k_{Al} = conductivity of Al 1100 (Btu/hr-in-°F)
t_{Al} = thickness of aluminum plate or aluminum clad for Boral (in)
t_{model} = thickness paired Al/Poison plates in the model (in)

The total thickness of paired aluminum and poison plates in 69BTH baskets are 0.25" for the plates within the compartment blocks and 0.375" for the plates between the compartment blocks. The plates within the compartment blocks are modeled with a total thickness of 0.21" to accommodate for the size of the gaps considered within the basket and maintain the outer basket diameter contained within the DSC inner diameter. The thickness of the plates between the compartment blocks is 0.375" in the model which is equal to their nominal thickness.

Borated aluminum and metal matrix composites (MMC) can be considered as isotropic materials while Boral is an orthotropic material. For the isotropic materials, the conductivity and thickness of poison plates can be used directly in the equations (5.4) and (5.5).

Since Boral cladding and the paired aluminum plates are both Al-1100, The thickness of the Boral aluminum clad and the thickness of the aluminum plate are added together and the conductivity and thickness of Boral core material is used for k_{poison} and t_{poison} in the equations (5.4) and (5.5) to calculate the effective conductivities for paired aluminum and Boral plates.

For conservatism, the conductivity of Boral core is reduced by 10% for calculation of effective conductivities.

The calculated effective conductivity values for paired aluminum and poison plates are listed in Table 5-5 through Table 5-7.

Borated aluminum plates can be used for all HLZCs in 69BTH basket. Boral or MMC plates paired with aluminum 1100 plates can be used for HLZC # 1, 2, # 3 but shall not be used for HLZC # 4 with 32 kW heat load.

A comparison between Table 5-5 and Table 5-6 shows that the effective conductivities for paired aluminum and MMC plates are higher than those for paired aluminum and Boral plates for the entire temperature range. Therefore, the effective conductivities of paired aluminum and Boral plates are considered to bound the maximum component temperatures for HLZC # 1, # 2, and # 3.

The effective conductivities for paired aluminum and borated aluminum plates are used only for HLZC # 4.

Table 5-5 Effective Conductivity for Paired Aluminum and Boral in 69BTH DSC

Conductivity of Boral Core Material		
Temp	k_c (1)	$k_{c\ 90\%}$
(°F)	(Btu/hr-in-°F)	(Btu/hr-in-°F)
100	4.136	3.723
500	3.698	3.328

t_{total} = 0.25" total thk for paired Al/Poison t_{model} = 0.21" total thk for paired Al/Poison as modeled t_{core} = 0.16" Boral core thickness t_{Al} = 0.09" Aluminum thickness				t_{total} = 0.375" total thk for paired Al/Poison t_{model} = 0.375" total thk for paired Al/Poison as modeled t_{core} = 0.16" Boral core thickness t_{Al} = 0.215" Aluminum thickness			
Temp	k_{Al} [18]	k_{core} (3)	$k_{eff,across}$	Temp	k_{Al} [18]	k_{core} (3)	$k_{eff,across}$
(°F)	(Btu/hr-in-°F)	(Btu/hr-in-°F)	(Btu/hr-in-°F)	(°F)	(Btu/hr-in-°F)	(Btu/hr-in-°F)	(Btu/hr-in-°F)
70	11.092	3.752	4.137	70	11.092	3.752	6.046
100	10.983 (4)	3.723	4.104 (4)	100	10.983 (4)	3.723	5.995 (4)
200	10.708	3.624	3.996	200	10.708	3.624	5.839
300	10.517	3.525	3.893	300	10.517	3.525	5.697
400	10.375	3.427	3.793	400	10.375	3.427	5.563
650	10.042 (2)	3.180	3.543	650	10.042 (2)	3.180	5.229
Temp	k_{Al} [18]	k_{core} (3)	$k_{eff,along}$	Temp	k_{Al} [18]	k_{core} (3)	$k_{eff,along}$
(°F)	(Btu/hr-in-°F)	(Btu/hr-in-°F)	(Btu/hr-in-°F)	(°F)	(Btu/hr-in-°F)	(Btu/hr-in-°F)	(Btu/hr-in-°F)
70	11.092	3.752	7.612	70	11.092	3.752	7.960
100	10.983 (4)	3.723	7.543 (4)	100	10.983 (4)	3.723	7.885 (4)
200	10.708	3.624	7.350	200	10.708	3.624	7.686
300	10.517	3.525	7.193	300	10.517	3.525	7.534
400	10.375	3.427	7.057	400	10.375	3.427	7.410
650	10.042 (2)	3.180	6.727	650	10.042 (2)	3.180	7.114

Notes: (1) Taken from data in [20] shown in Table 4-8
(2) Extrapolated from data in [18] shown in Table 4-7
(3) Inter- and extrapolated from data of 90% Boral core conductivity
(4) Instead of 10.983 Btu/hr-in-°F, mistakenly a conductivity of 11.150 Btu/hr-in-°F is used for k_{Al} at 100°F. This error increases the effective conductivity by approximately 1% for paired aluminum and Boral plates in the file "Mat69BTH.inp" for the material properties in the ANSYS model. Since the basket temperature is over 100°F for all analyzed cases, this error does not affect the results in this calculation.

Table 5-6 Effective Conductivity for Paired Aluminum and MMC in 69BTH DSC

t_{total} = 0.25" total thk for paired Al/Poison t_{model} = 0.21" total thk for paired Al/Poison as modeled t_{core} = 0.175" MMC thickness t_{Al} = 0.075" Aluminum thickness				t_{total} = 0.375" total thk for paired Al/Poison t_{model} = 0.375" total thk for paired Al/Poison as modeled t_{core} = 0.175" MMC thickness t_{Al} = 0.200" Aluminum thickness			
Temp	k_{Al} [18]	k_{MMC} (1)	$k_{eff,across}$	Temp	k_{Al} [18]	k_{MMC} (1)	$k_{eff,across}$
(°F)	(Btu/hr-in-°F)	(Btu/hr-in-°F)	(Btu/hr-in-°F)	(°F)	(Btu/hr-in-°F)	(Btu/hr-in-°F)	(Btu/hr-in-°F)
70	11.092	5.78	5.673	70	11.092	5.78	7.766
100	10.983	5.78	5.663	100	10.983	5.78	7.737
200	10.708	5.78	5.636	200	10.708	5.78	7.664
300	10.517	5.78	5.617	300	10.517	5.78	7.611
400	10.375	5.78	5.602	400	10.375	5.78	7.571
650	10.042 (2)	5.78	5.567	650	10.042 (2)	5.78	7.474
Temp	k_{Al} [18]	k_{MMC} (1)	$k_{eff,along}$	Temp	k_{Al} [18]	k_{MMC} (1)	$k_{eff,along}$
(°F)	(Btu/hr-in-°F)	(Btu/hr-in-°F)	(Btu/hr-in-°F)	(°F)	(Btu/hr-in-°F)	(Btu/hr-in-°F)	(Btu/hr-in-°F)
70	11.092	5.78	8.781	70	11.092	5.78	8.615
100	10.983	5.78	8.743	100	10.983	5.78	8.557
200	10.708	5.78	8.644	200	10.708	5.78	8.410
300	10.517	5.78	8.576	300	10.517	5.78	8.308
400	10.375	5.78	8.525	400	10.375	5.78	8.233
650	10.042 (2)	5.78	8.406	650	10.042 (2)	5.78	8.055

Notes: (1) The lowest conductivity is taken from data in [1] shown in Table 4-8
(2) Extrapolated from data in [18] shown in Table 4-7

Table 5-7 Effective Conductivity for Paired Aluminum and Borated Aluminum in 69BTH DSC

t_{total} = 0.25" total thk for paired Al/Poison t_{model} = 0.21" total thk for paired Al/Poison as modeled t_{core} = 0.175" Borated Aluminum thickness t_{Al} = 0.075" Aluminum thickness				t_{total} = 0.375" total thk for paired Al/Poison t_{model} = 0.375" total thk for paired Al/Poison as modeled t_{core} = 0.175" Borated Aluminum thickness t_{Al} = 0.200" Aluminum thickness			
Temp	k_{Al} [18]	k_{BAl} (1)	$k_{eff,across}$	Temp	k_{Al} [18]	k_{BAl} (1)	$k_{eff,across}$
(°F)	(Btu/hr-in-°F)	(Btu/hr-in-°F)	(Btu/hr-in-°F)	(°F)	(Btu/hr-in-°F)	(Btu/hr-in-°F)	(Btu/hr-in-°F)
70	11.092	7.39	6.896	70	11.092	7.39	8.988
100	10.983 (3)	7.50	6.962 (3)	100	10.983 (3)	7.50	9.027 (3)
200	10.708	7.88	7.185	200	10.708	7.88	9.169
300	10.517	8.18	7.365	300	10.517	8.18	9.282
400	10.375	8.48	7.537	400	10.375	8.48	9.396
650	10.042 (2)	9.15	7.895	650	10.042 (2)	9.15	9.604
Temp	k_{Al} [18]	k_{BAl} (1)	$k_{eff,along}$	Temp	k_{Al} [18]	k_{BAl} (1)	$k_{eff,along}$
(°F)	(Btu/hr-in-°F)	(Btu/hr-in-°F)	(Btu/hr-in-°F)	(°F)	(Btu/hr-in-°F)	(Btu/hr-in-°F)	(Btu/hr-in-°F)
70	11.092	7.39	10.118	70	11.092	7.39	9.363
100	10.983 (3)	7.50	10.173 (3)	100	10.983 (3)	7.50	9.358 (3)
200	10.708	7.88	10.387	200	10.708	7.88	9.386
300	10.517	8.18	10.576	300	10.517	8.18	9.428
400	10.375	8.48	10.773	400	10.375	8.48	9.491
650	10.042 (2)	9.15	11.210	650	10.042 (2)	9.15	9.625

Notes: (1) Inter- and extrapolated from data in [1] shown in Table 4-8
(2): Extrapolated from data in [18] shown in Table 4-7
(3) Instead of 10.983 Btu/hr-in-°F, mistakenly a conductivity of 11.150 Btu/hr-in-°F is used for k_{Al} at 100°F. This error increases the effective conductivity by less than 1% for paired aluminum and borated aluminum plates in the file "Mat69BTH.inp" for the material properties in the ANSYS model. Since the basket temperature is over 100°F for all analyzed cases, this error does not affect the results in this calculation.

5.1.2 Effective Conductivity for Dummy Aluminum Assemblies

Aluminum dummy assemblies replace the fuel assemblies in assigned compartments defined in Figure 5-2 through Figure 5-4 for 69BTH basket with HLZC # 2 through # 4.

The dummy assemblies are aluminum blocks with a cross section of 5.875" × 5.875" and a length equal to BWR fuel assemblies. A uniform gap of 0.0625" is considered around the cross section of the dummy assembly within the fuel compartment.

The effective conductivity in transverse direction is a combination of serial and parallel thermal resistances shown in Figure 5-11. The transverse effective conductivity for dummy assembly is calculated as follows.

$$k_{eff,tr,dummy} = \frac{1}{R_{eff,tr,dummy}} \qquad (5.6)$$

with

$$R_{eff,tr,dummy} = 2R_{th,He1} + \frac{1}{\left(\frac{2}{R_{th,He2}} + \frac{1}{R_{th,Al}}\right)}$$

Where

$$R_{th,He1} = \frac{t_{gap}}{k_{He}\ w_{comp}}; \qquad R_{th,He2} = \frac{a_{dummy}}{k_{He}\ t_{gap}}; \qquad R_{th,Al} = \frac{a_{dummy}}{k_{Al6061}\ a_{dummy}} = \frac{1}{k_{Al6061}}$$

a_{dummy} = width of dummy assembly = 5.875"
w_{comp} = inner width of fuel compartment = 6.0"
t_{gap} = thickness of gap between dummy assembly and fuel compartment =0.0625"
k_{Al6061} = conductivity of Al 6061 (Btu/hr-in-°F)
k_{He} = conductivity of Helium (Btu/hr-in-°F)

The conductivity of helium is conservatively ignored in the axial direction. The axial transverse effective conductivity for dummy assembly is calculated as follows.

$$k_{eff,ax,dummy} = \frac{a_{dummy}^2}{w_{comp}^2} k_{Al6061} \qquad (5.7)$$

The calculated effective conductivities for dummy assembly are listed in Table 5-8.

Table 5-8 Effective Conductivity for Aluminum Dummy Assembly

a_{dummy} = 5.875 in
t_{gap} = 0.0625 in
w_{comp} = 6 in

Temp	k_{Al6061} (1)
(°F)	(Btu/hr-in-°F)
70	8.008
100	8.075
200	8.250
300	8.383
400	8.492
650	8.492 (2)

Temp	k_{He} (3)	Temp	k_{He} (4)
(°F)	(Btu/hr-in-°F)	(°F)	(Btu/hr-in-°F)
-10	0.0064	70	0.0071
80	0.0072	100	0.0074
260	0.0086	200	0.0081
440	0.0102	300	0.0090
620	0.0119	400	0.0098
980	0.0148	650	0.0121
1340	0.0174		

Temp	$R_{th\ He1}$	$R_{th\ Al6061}$	$R_{th\ He2}$	$R_{th,tr,dummy}$	$k_{eff,tr,dummy}$	$k_{eff,ax,dummy}$
(°F)	(Btu/hr-in-°F)	(Btu/hr-in-°F)	(Btu/hr-in-°F)	(Btu/hr-in-°F)	(Btu/hr-in-°F)	(Btu/hr-in-°F)
70	1.4648	0.1249	13218.8	3.0546	0.327	7.678
100	1.4162	0.1238	12779.5	2.9562	0.338	7.742
200	1.2807	0.1212	11557.4	2.6827	0.373	7.910
300	1.1632	0.1193	10496.3	2.4456	0.409	8.037
400	1.0581	0.1178	9548.5	2.2340	0.448	8.142
650	0.8579	0.1178	7741.9	1.8336	0.545	8.142

Notes: (1) See Table 4-7 for aluminum conductivity
(2) Al6061 conductivity increases at higher temperatures. Increasing of the Al6061 conductivity is conservatively ignored for calculation of effective conductivity of aluminum dummy assembly.
(3) See Table 4-9 for helium conductivity
(4) Interpolated based on data in Table 4-9.

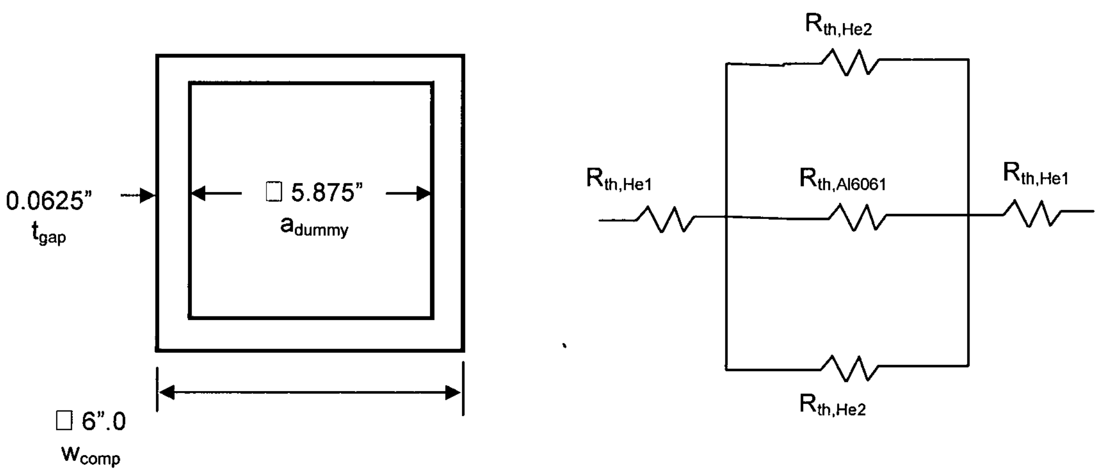

Figure 5-11 Thermal Resistances for Aluminum Dummy Assembly

5.1.3 Axial Decay Heat Profile for BWR Fuel Assemblies

The axial decay heat profile for BWR fuel assemblies considered in 69BTH basket is identical to that described in [8] and used in [1]. The peaking factors for this axial heat profile are shown in Table 5-9. The discussion in [8] shows that the selected axial decay heat profile covers conservatively the low and high burnup fuels.

The active fuel length for 69BTH basket is divided into 19 sections. The peaking factors from [8] are converted as follows to match the 19 regions defined for the active fuel length.

- An average height is calculated for each section of peaking factors defined in [8].
- An average height is calculated for each section of active fuel length defined in the finite element model (FEM) of 69BTH basket.
- The peaking factor for each section in FEM is calculated by interpolation between the peaking factors in [8] using the average heights.

The peaking factors for 69BTH basket are shown in Table 5-10 and illustrated in Figure 5-12.

As seen in Table 5-10, the normalized area under peaking factor curve is smaller than 1.0. To avoid any degradation of decay heat load, a correction factor of 1.00697 calculated as follows is used when applying the peaking factors.

$$\textit{Nomalized Area under Curve} = \frac{\text{Area under Axial Heat Profile}}{\text{Active Fuel Length}} = 0.99308$$

Active fuel length = 144"

$$\textit{Correction Factor} = \frac{1}{\textit{Normalized Area under Curve}} = 1.00697$$

Table 5-9 Peaking Factors for BWR Fuel Assemblies

Region #	Active Fuel Length (in) from	to	Average Height (in)	Peaking Factor [8]
1	0.00	2.17	1.09	0.075
2	2.17	8.20	5.19	0.405
3	8.20	11.69	9.95	0.763
4	11.69	14.37	13.03	0.897
5	14.37	20.40	17.39	1.02
6	20.40	23.89	22.15	1.101
7	23.89	26.57	25.23	1.126
8	26.57	30.84	28.71	1.152
9	30.84	36.09	33.47	1.178
10	36.09	43.03	39.56	1.188
11	43.03	60.49	51.76	1.2
12	60.49	77.44	68.97	1.2
13	77.44	81.40	79.42	1.197
14	81.40	84.89	83.15	1.19
15	84.89	87.57	86.23	1.178
16	87.57	93.60	90.59	1.164
17	93.60	97.09	95.35	1.147
18	97.09	99.77	98.43	1.136
19	99.77	105.79	102.78	1.111
20	105.79	107.61	106.70	1.084
21	107.61	111.97	109.79	1.07
22	111.97	116.24	114.11	1.044
23	116.24	119.75	118.00	0.987
24	119.75	124.02	121.89	0.918
25	124.02	133.69	128.86	0.759
26	133.69	140.64	137.17	0.441
27	140.64	144.00	142.32	0.116

Table 5-10 Peaking Factors for 69BTH Basket

Region #	Fuel Model Z-Coord (in) from	to	Average Height from Bottom (in)	Peaking Factor	Area under Curve
1	7.375	11.80	2.213	0.166	0.733
2	11.80	19.60	8.325	0.641	5.001
3	19.60	27.40	16.125	0.984	7.678
4	27.40	35.20	23.925	1.115	8.700
5	35.20	43.00	31.725	1.168	9.114
6	43.00	50.80	39.525	1.188	9.266
7	50.80	58.60	47.325	1.196	9.326
8	58.60	66.40	55.125	1.200	9.360
9	66.40	74.20	62.925	1.200	9.360
10	74.20	82.00	70.725	1.199	9.356
11	82.00	89.80	78.525	1.197	9.339
12	89.80	97.60	86.325	1.178	9.186
13	97.60	105.40	94.125	1.151	8.981
14	105.40	113.20	101.925	1.116	8.704
15	113.20	121.00	109.725	1.070	8.348
16	121.00	128.80	117.525	0.994	7.752
17	128.80	136.60	125.325	0.840	6.548
18	136.60	144.40	133.125	0.596	4.646
19	144.40	151.375	140.513	0.230	1.604
				Sum	143.003
				Normalized	0.99308
				Corr. Factor	1.00697

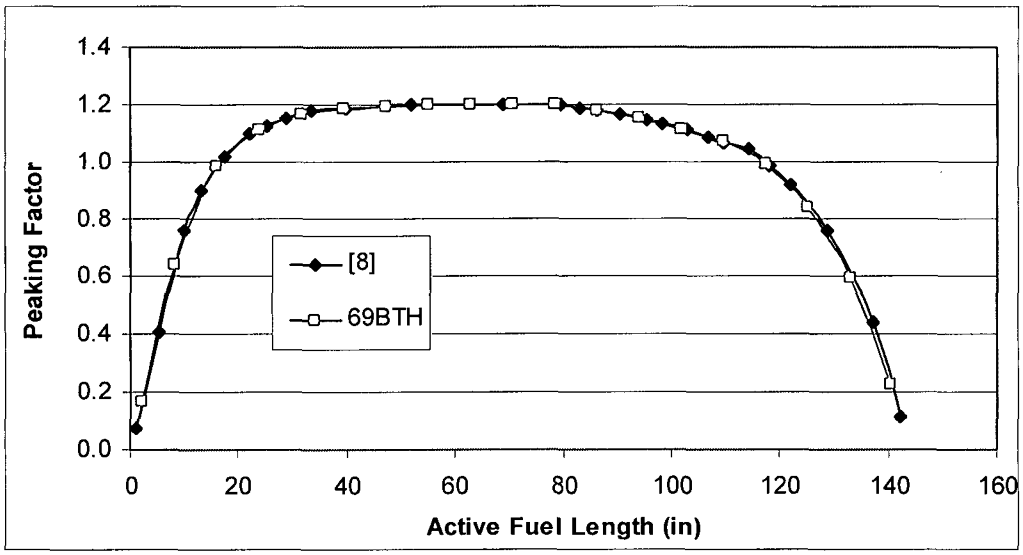

Figure 5-12 Peaking Factor Curve for BWR Fuels

5.2 Model for 37PTH DSC

The three-dimensional finite element model of 37PTH basket/DSC model is developed using ANSYS [28], version 8.1. The model contains the DSC shell, the DSC cover plates, shield plugs, aluminum rails, basket plates, and homogenized fuel assemblies. Only SOLID70 elements are used in the 37PTH DSC/basket model.

The DSC shell temperatures for NCT at 100°F, -20°F and -40°F are retrieved from the MP197HB transfer cask model described in [10] and transferred to the basket models via runs listed in Section 8.0, Table 8-1.

Decay heat load is applied as heat generation boundary conditions over the elements representing homogenized fuel assemblies.

The base heat generation rates used in this analysis is calculated as follows.

$$\dot{q}''' = \left(\frac{q}{a^2 L_a} \times PF \right) \times CF \qquad (5.8)$$

Where,

q = Decay heat load per assembly defined for each loading zone
a = Width of the homogenized fuel assembly in model = 8.46"
L_a =Active fuel length = 144"
PF = Peaking Factor from Section 5.2.1.
CF = correction factor = 1.002 for 37PTH (see Section 5.2.1)

The base heat generation rates used in 37PTH basket model are listed in Table 5-11.

Table 5-11 Base Heat Generation Rates for 37PTH

Heat Load in the Model (KW)	$\dot{q}'''$ value without PF (Btu/hr-in^3)
0.40	0.1327
0.60	0.1991
0.70	0.2322

The base heat generation rate is multiplied by peaking factors along the axial fuel length to represent the axial decay heat profile. Axial decay heat profile for PWR fuel assemblies is described in DOE/RW-0472 [30]. The peaking factors from [30] are converted to match the regions defined for the fuel assembly in the finite element model. Section 5.2.1 describes the conversion method and lists the peaking factors used in 37PTH model.

The heat generating rates for the elements representing the active fuel are calculated based on the HLZC for 37PTH DSC. The HLZC and its restrictions for 37PTH basket are shown in Figure 5-13.

The material properties used in the 37PTH basket/DSC model are listed in Section 4.0.

Table 4-8 shows that the conductivity of MMC plate is lower than those for borated aluminum plate. Therefore, the conductivity of MMC plate is considered for single poison plates in the 37PTH basket model to bound the maximum component temperatures.

The effective thermal conductivities for Boral plates are calculated in Section 5.2.1.

The peaking factors used in the finite element model to create axial heat profile for the PWR fuel assemblies are discussed in Section 5.2.2.

The effective properties of the 37PTH basket are calculated in Section 5.3. These properties can be used in transient analysis.

The geometry of the 37PTH basket model and its mesh density are shown in Figure 5-14 through Figure 5-18.

Typical boundary conditions for 37PTH basket model are shown in Figure 5-19.

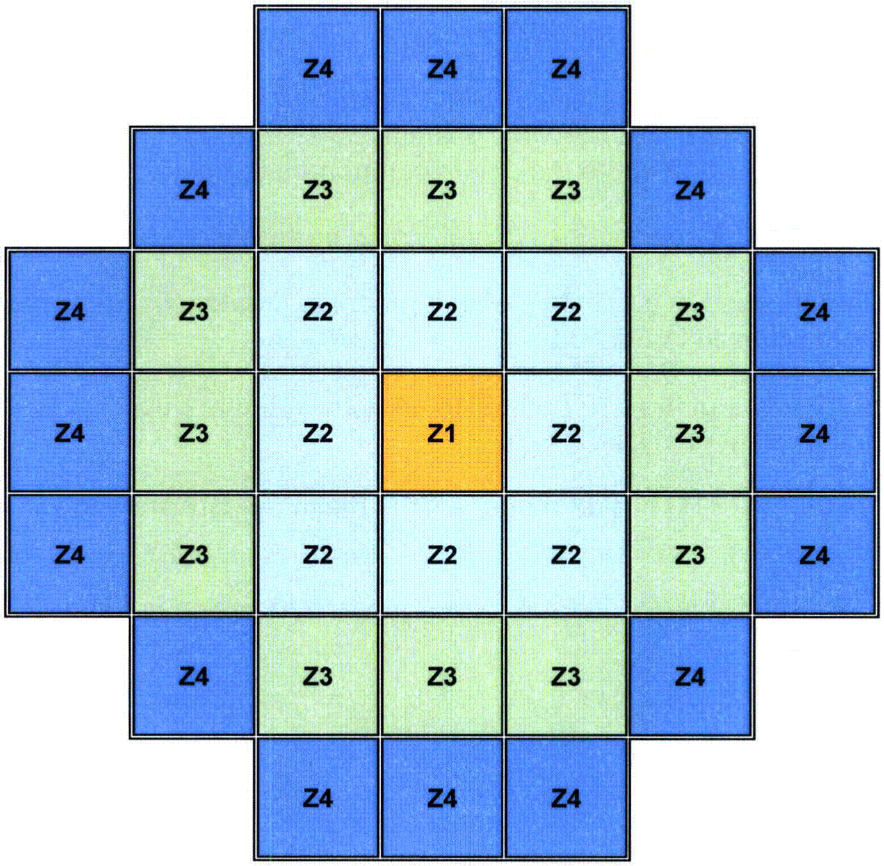

	Zone 1	Zone 2	Zone 3	Zone 4
Max. Decay Heat (kW/FA)	0.40	0.40	0.60	0.70
No. of Fuel Assemblies (1)	1	8	12	16
Max. Decay Heat per Zone (kW)	0.4	3.2	7.2	11.2
Max. Decay Heat per DSC (kW)	22.0			

Note: (1) Total number of fuel assemblies is 37 for this HLZC

Figure 5-13 Heat Load Zoning Configuration for 37PTH Basket

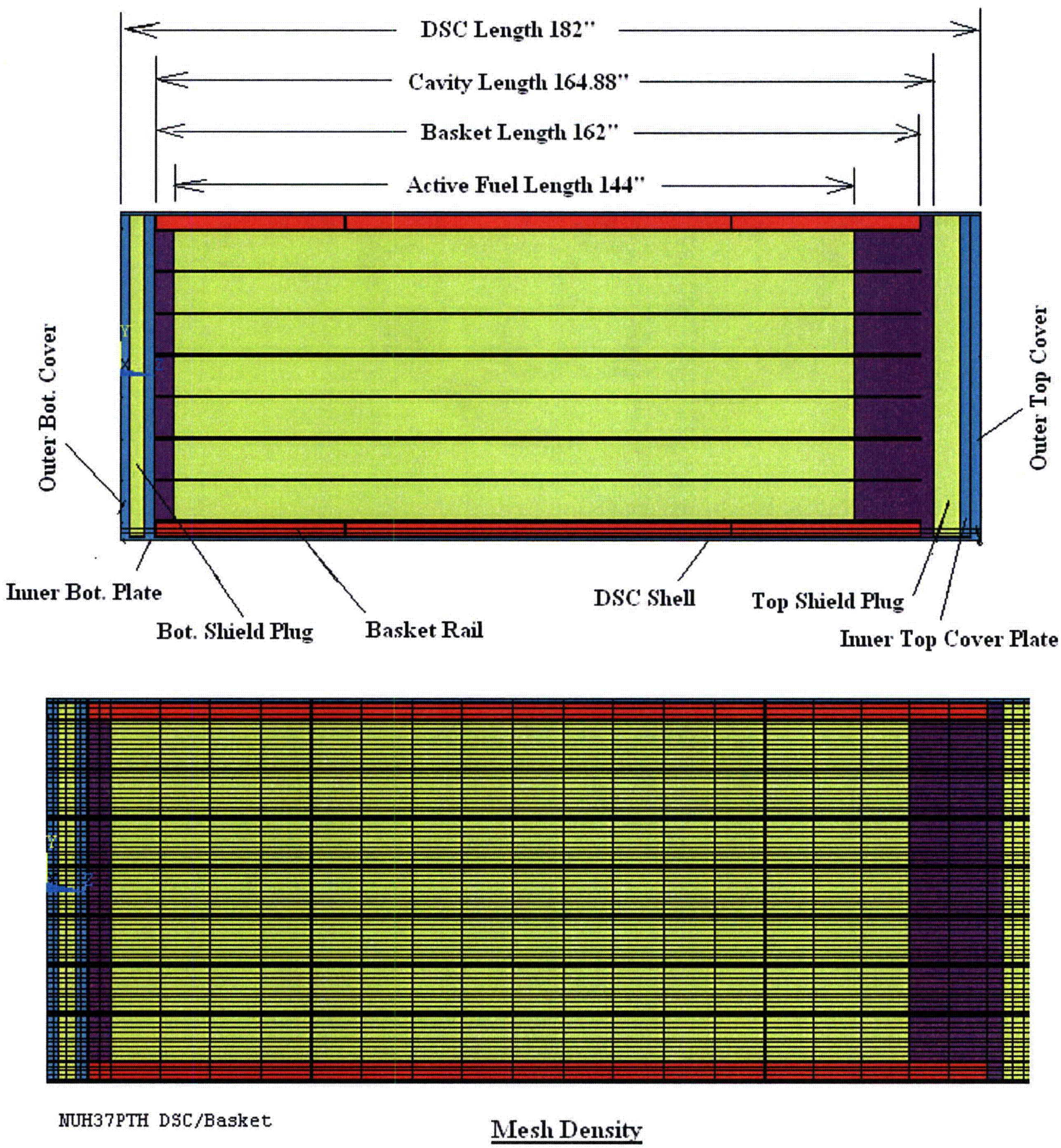

Figure 5-14 Finite Element Model of 37PTH DSC/Basket

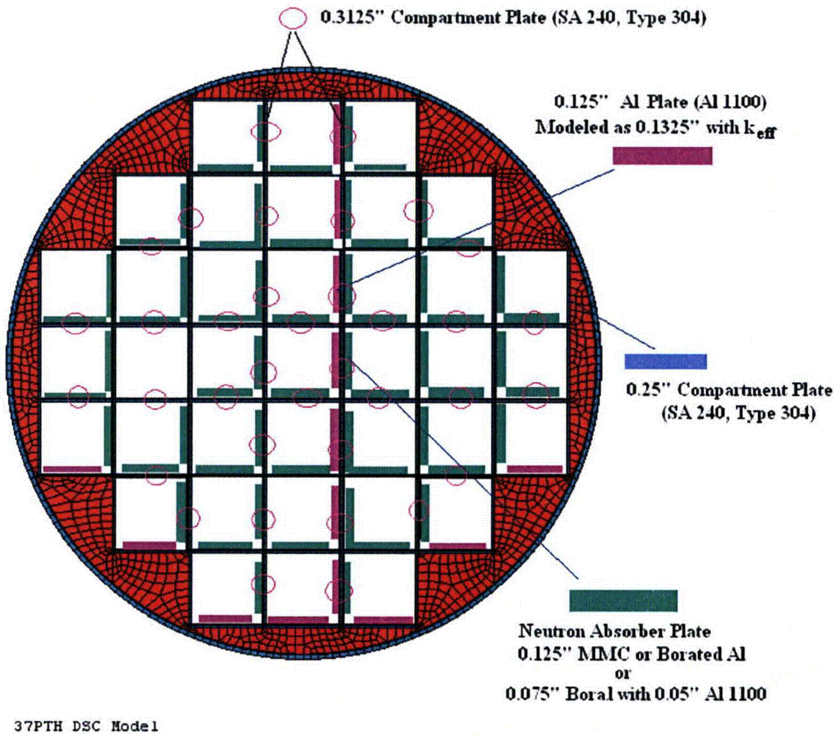

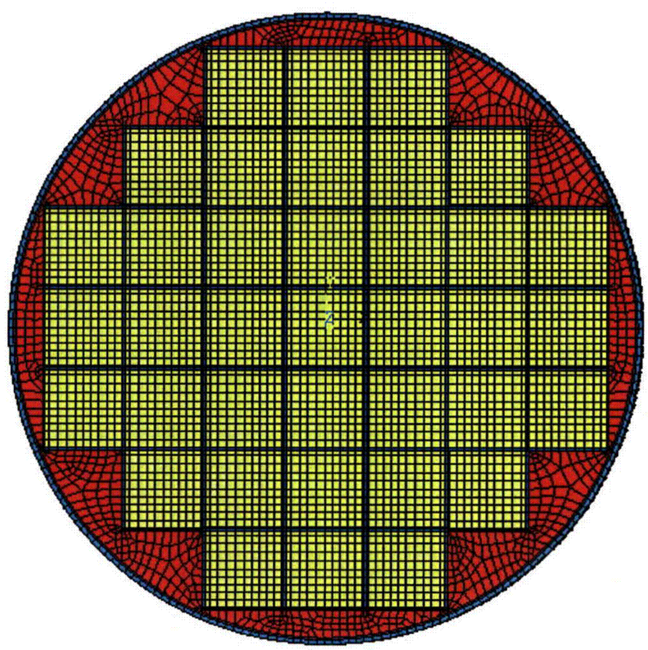

Mesh Density

Figure 5-15 37PTH DSC/Basket – Cross Section and Details

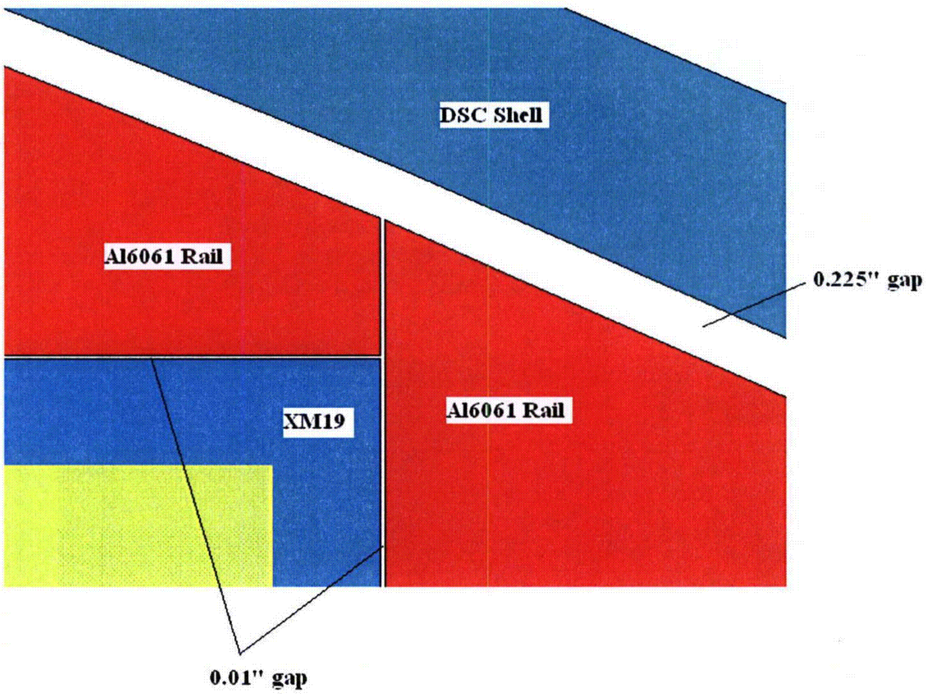

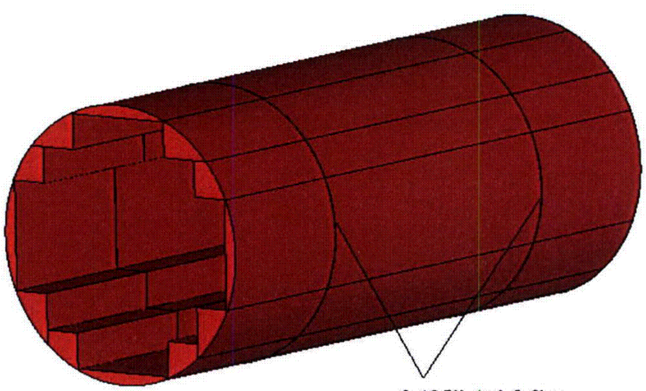

Figure 5-16 37PTH DSC/Basket – Gaps between Rail Sections

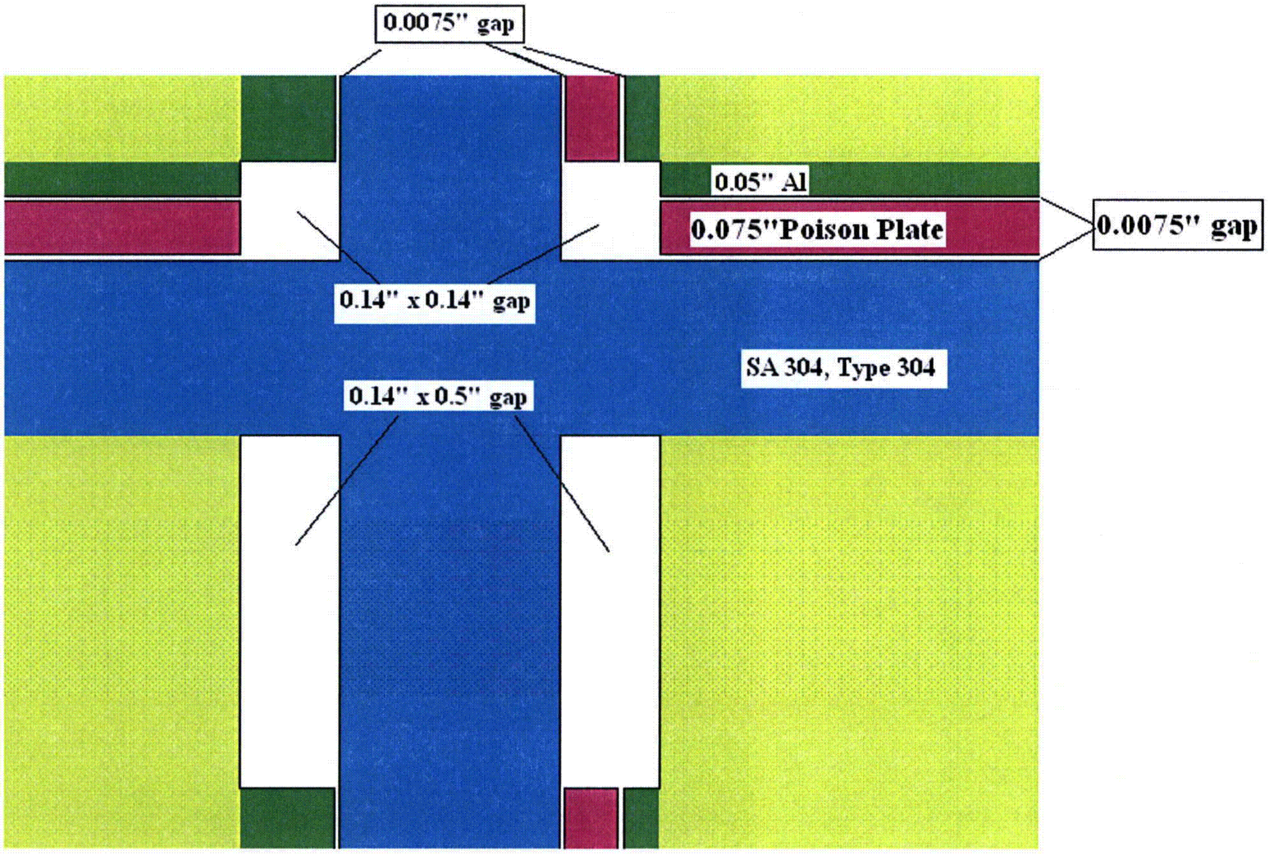

Figure 5-17 37PTH DSC/Basket – Gaps between Basket Plates at Cross Section

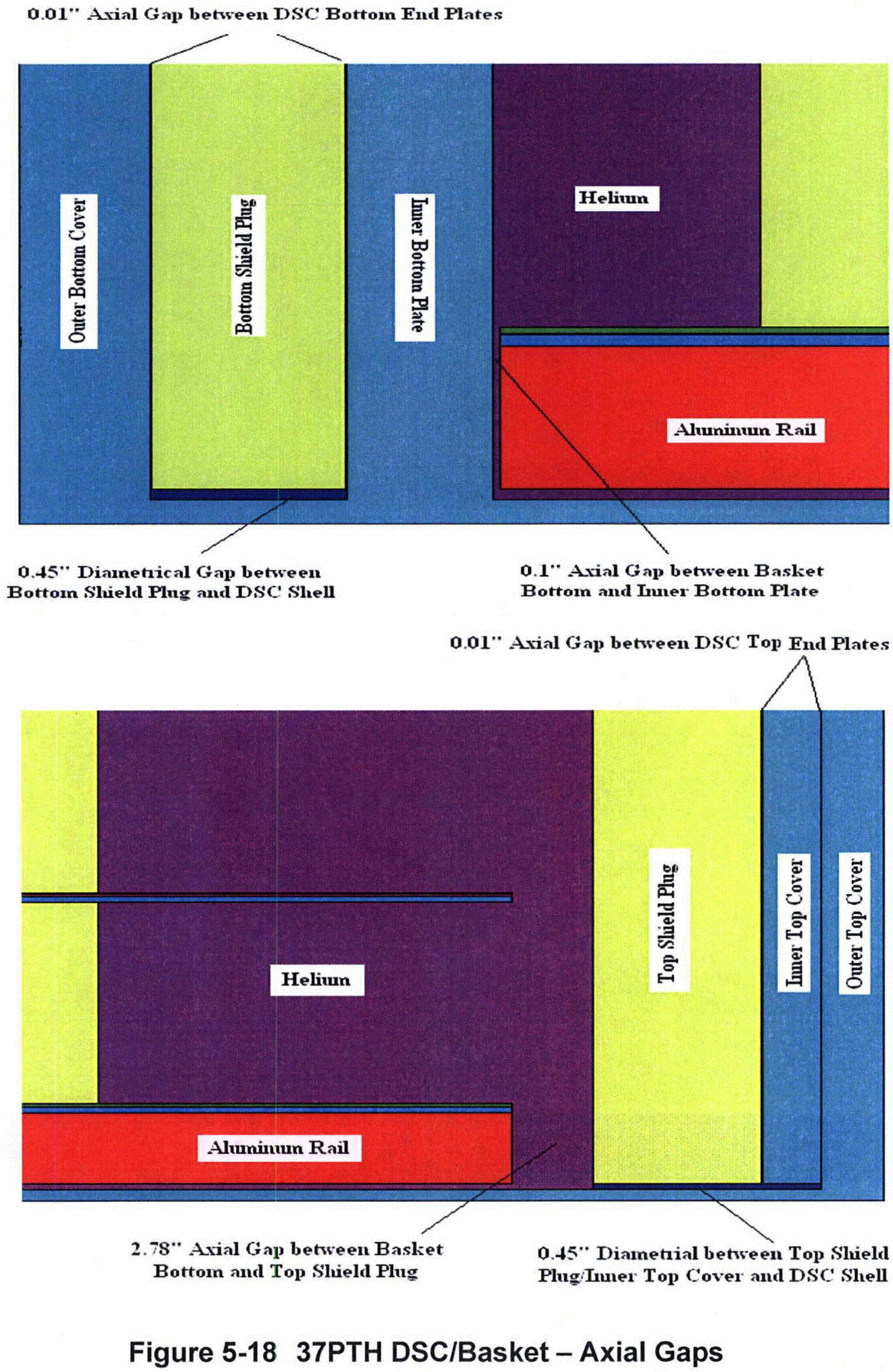

Figure 5-18 37PTH DSC/Basket – Axial Gaps

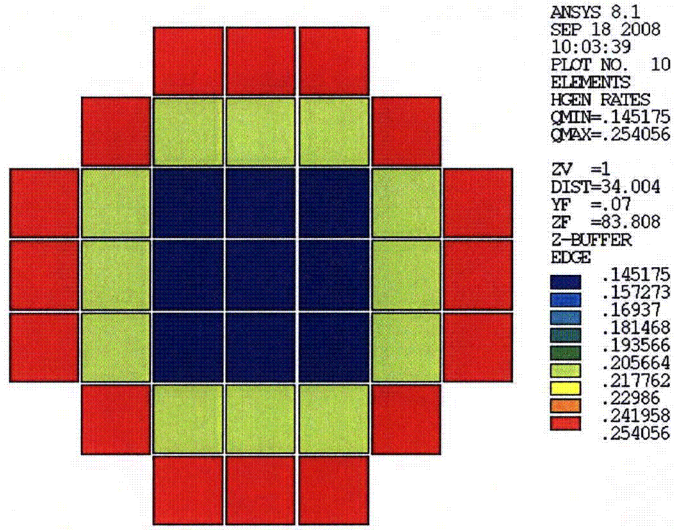

Heat Load Zone Configuration (HLZC#8 / 22.0 kW)

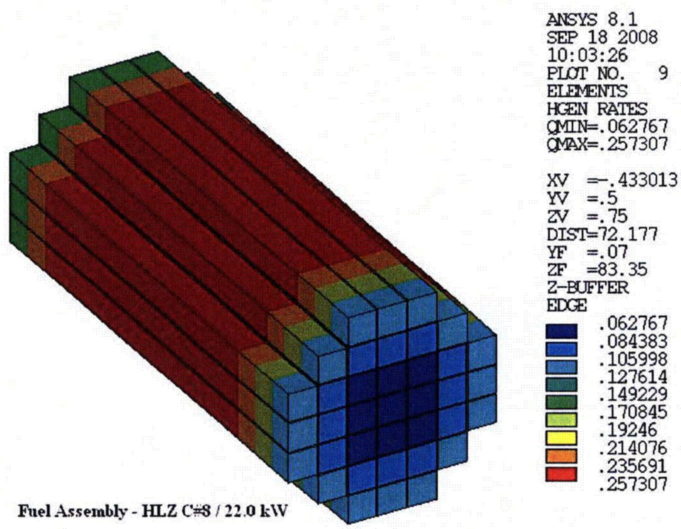

Fuel Assembly - HLZ C#8 / 22.0 kW

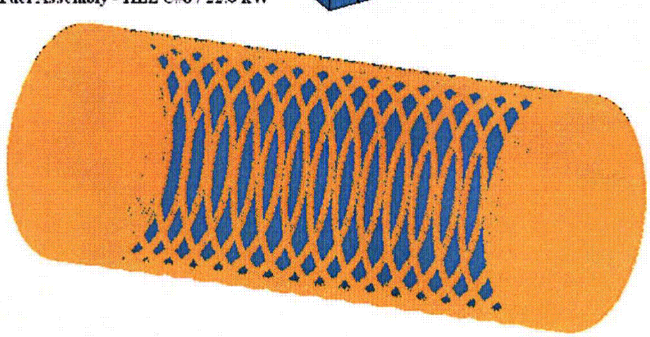

Normal Transport Condition - 37PTH DSC, 22.0 kW (HLZC#8)

Figure 5-19 Typical Boundary Conditions for 37PTH Basket

5.2.1 Effective Conductivity for Boral Plates in 37PTH DSC

Boral plates are considered as one homogenized material in the 37PTH basket model. The total thickness of the Boral plate is 0.075" with a core thickness of 0.06" in the 37PTH basket.

The Boral core and its aluminum claddings built up parallel thermal resistances along their length and serial thermal resistances across their thickness. The effective conductivities of the Boral plate are calculated using equations (5.4) and (5.5) with the following parameters.

k_{poison} = conductivity of core material for Boral (Btu/hr-in-°F)
t_{poison} = thickness of core material for Boral = 0.06 in
k_{Al} = conductivity of Al 1100 (Btu/hr-in-°F)
t_{Al} = thickness of aluminum clad for Boral = 0.015 in
t_{model} = thickness of Boral plates in the model =0.075 in

For conservatism, the conductivity of Boral core is reduced by 10% for calculation of effective conductivities.

The calculated effective conductivity values for Boral plates in 37PTH basket model are listed in Table 5-12.

Table 5-12 Effective Conductivity for Boral in 37PTH DSC

Conductivity of Boral Core Material		
Temp	k_c (1)	$k_{c\ 90\%}$
(°F)	(Btu/hr-in-°F)	(Btu/hr-in-°F)
100	4.136	3.723
500	3.698	3.328

t_{total} = 0.075" total thk for Boral plate
t_{model} = 0.075" total thk for Boral plate as modeled
t_{core} = 0.06" Boral core thickness
t_{Al} = 0.015" Aluminum clad thickness

Temp	k_{Al} [18]	k_{core}	$k_{eff,across}$
(°F)	(Btu/hr-in-°F)	(Btu/hr-in-°F)	(Btu/hr-in-°F)
100	10.983	3.723	4.290
500	10.242 (2)	3.328	3.848
Temp	k_{Al} [18]	k_{core}	$k_{eff,along}$
(°F)	(Btu/hr-in-°F)	(Btu/hr-in-°F)	(Btu/hr-in-°F)
100	10.983	3.723	5.175
500	10.242 (2)	3.328	4.711

Notes: (1) Taken from data in [20] shown in Table 4-8
(2) Extrapolated from data in [18] shown in Table 4-7

5.2.2 Axial Decay Heat Profile for PWR Fuel Assemblies

The axial decay heat profile for PWR fuel assemblies considered in 37PTH basket is identical to that described in DOE/RW-0472 [30]. The peaking factors for this axial heat profile are shown in Table 5-13. The discussions in [17], Section 7.3 and [1], Section U.4.6.3 show that the selected axial decay heat profile covers conservatively the low and high burnup fuels.

The active fuel length for 37PTH basket is divided into 18 sections. The peaking factors from [30] are converted as follows to match the 18 regions defined for the active fuel length.

- An average height is calculated for each section of peaking factors defined in [4] Section 4.7.
- An average height is calculated for each section of active fuel length defined in the finite element model (FEM) of 37PTH basket.
- The peaking factor for each section in FEM is calculated by interpolation between the peaking factors in [30] using the average heights.

The peaking factors for 37PTH basket are shown in Table 5-14 and illustrated in Figure 5-20.

As seen in Table 5-14, the normalized area under peaking factor curve is smaller than 1.0. To avoid any degradation of decay heat load, a correction factor of 1.002 calculated as follows is used when applying the peaking factors.

$$Nomalized\ Area\ under\ Curve = \frac{\text{Area under Axial Heat Profile}}{\text{Active Fuel Length}} = 0.998$$

Active fuel length = 144"

$$Correction\ Factor = \frac{1}{Normalized\ Area\ under\ Curve} = 1.002$$

Table 5-13 Peaking Factors for PWR Fuel Assemblies

% of Core Height	Length (in)	Peaking Factor [30]
0.00	0.00	0
2.78	4.00	0.652
8.33	12.00	0.967
13.89	20.00	1.074
19.44	27.99	1.103
25.00	36.00	1.108
30.56	44.01	1.106
36.11	52.00	1.102
41.67	60.00	1.097
47.22	68.00	1.094
52.78	76.00	1.094
58.33	84.00	1.095
63.89	92.00	1.096
69.44	99.99	1.095
75.00	108.00	1.086
80.56	116.01	1.059
86.11	124.00	0.971
91.67	132.00	0.738
97.22	140.00	0.462
100.00	144.00	0

Table 5-14 Peaking Factors for 37PTH Basket Model

Region #	Fuel Model Z-Coord (in) from	to	Average Height from Bottom (in)	Peaking Factor	Area under Curve
1	11.350	20.350	4.500	0.672	6.044
2	20.350	29.350	13.500	0.987	8.884
3	29.350	38.350	22.500	1.083	9.748
4	38.350	47.350	31.500	1.105	9.947
5	47.350	47.475	36.063	1.108	0.138
6	47.475	56.558	40.667	1.108	10.061
7	56.558	65.642	49.750	1.103	10.021
8	65.642	74.725	58.834	1.098	9.971
9	74.725	83.808	67.917	1.094	9.937
10	83.808	92.892	77.000	1.094	9.939
11	92.892	101.970	86.081	1.095	9.943
12	101.970	111.060	95.165	1.096	9.959
13	111.060	120.140	104.250	1.090	9.899
14	120.140	129.220	113.330	1.068	9.698
15	129.220	129.350	117.935	1.038	0.135
16	129.350	138.020	122.335	0.989	8.577
17	138.020	146.680	131.000	0.767	6.644
18	146.680	155.350	139.665	0.473	4.105
				Sum	143.650
				Normalized	0.998
				Corr. Factor	1.002

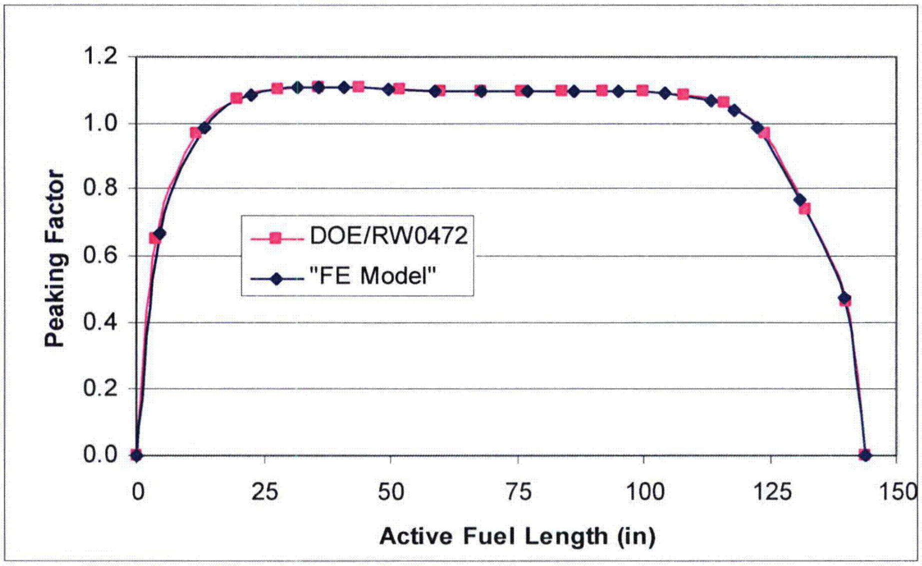

Figure 5-20 Peaking Factor Curve for PWR Fuels

5.3 Effective Thermal Properties of 69BTH and 37PTH Baskets

The 69BTH and 37PTH basket effective density, thermal conductivity and specific heat are calculated for use in the transient analyses of the 69BTH and 37PTH DSCs. The calculation of these thermal effective properties is based on the DSC components' weight data provided in [11] and [12].

The effective properties are valid only when the homogenized basket and top grid assembly are modeled with the dimensions listed in Table 5-15 :

Table 5-15 Dimensions of Homogenized Baskets

DSC Type	69BTH	37PTH
Basket OD (in)	68.75	68.75
Basket length (in)	164	162
Top grid assembly OD (in)	68.75	N/A
Top grid assembly length (in)	14.4	N/A

5.3.1 Effective Density and Specific Heat

The basket effective density $\rho_{eff\ basket}$, and specific heat $c_{p\ eff\ basket}$ are calculated as volumetric and weight average, respectively using equations (5.9), (5.10) below.

$$\rho_{eff\ basket} = \frac{\sum W_i}{V_{basket}} = \frac{W_{steel} + W_{Al} + W_{poison} + W_{fuel}}{L_{basket} \cdot \pi \cdot D_{basket}^{\ 2} / 4} \qquad (5.9)$$

$$c_{p\ eff\ basket} = \frac{\sum W_i \cdot c_{pi}}{\sum W_i} = \frac{W_{steel} \cdot c_{p\ steel} + W_{Al} \cdot c_{p\ Al} + W_{poison} \cdot c_{p\ poison} + W_{fuel} \cdot c_{p fuel}}{W_{steel} + W_{Al} + W_{poison} + W_{fuel}} \qquad (5.10)$$

Where: W_i = weight of basket components
V_{model} = total volume of basket in FE model
L_{basket} = basket length (see Table 5-15)
D_{basket} = basket OD (see Table 5-15)
$c_{p\ i}$ = specific heat of basket materials.

The following assumptions are used in the calculation of the basket effective density and specific heat calculation:

- These specific heat and density values are listed in Table 4-12.
- Specific heat of SA 240, type 304 and Al 6061 are considered for stainless steel and aluminum components, respectively.

- For poison material c_p values are conservatively assumed equal to those for 6061 aluminum.
- For aluminum at T > 400°F c_p value is conservatively assumed equal to value at 400°F.
- Conservatively, Helium is not included in density and specific heat calculation.

The same approach as described above for the basket is used to calculate the effective density $\rho_{eff\ top\ grid}$, for top grid assembly (hold-down ring) of 69BTH DSC.

$$\rho_{eff\ topgrid} = \frac{\sum W_i}{V_{topgrid}} = \frac{W_{steel}}{L_{topgrid} \cdot \pi \cdot D_{topgrid}^{\ 2} / 4} \qquad (5.11)$$

Where: W_{steel} = weight of steel in top grid assembly
$V_{topgrid}$ = total volume of top grid assembly in FE model
$L_{topgrid}$ = top grid assembly length in FE model = 14.4"
$D_{topgrid}$ = top grid assembly OD in FE model = 68.75"

Since no density and specific heat are considered for the helium, the specific heat of top grid assembly is equal to specific heat of steel.

The effective densities for 69BTH and 37PTH baskets are summarized in Table 5-16 and Table 5-17, respectively. The bounding value for the effective density of 37PTH baskets is 0.133 lbm/in^3 based on 37PTH-M basket with medium length.

The effective specific heats for 69BTH and 37PTH baskets are summarized in Table 5-18, and Table 5-19.

Table 5-16 Effective Density for 69BTH Basket

Basket		
Components	Material	Total Weight [11] (lbm)
Fuel Assembly		48,645
Fuel Compartment	SS304	13,174
Poison Plate + Alum	Aluminum	2,169
Sub-Assy Wrap	SS304	3,484
Aluminum Plates	Aluminum	1,434
Rail 90	Aluminum	6,204
Rail 45	Aluminum	3,508
Total		78,618
D_{basket}	68.75	in
L_{basket}	164.0	in
V_{basket}	608,806	in^3
$\rho_{eff\ basket}$	0.129	lbm/in^3

Top Grid Assembly		
Components	Material	Total Weight [11] (lbm)
Plates	SA182	2,123
$D_{topgrid}$	68.75	in
$L_{topgrid}$	14.4	in
$V_{topgrid}$	53,493	in^3
$\rho_{eff\ topgrid}$	0.040	lbm/in^3

Table 5-17 Effective Density for 37PTH Basket

Basket		Total Weight [12] (lbm)	
Components	Material	37PTH-S	37PTH-M
Fuel Assembly	-	61,605	60,125
Fuel Compartment	SS304	10,127	10,564
Poison Plate + Alum	Aluminum	1,263	1,318
Rail 90	Aluminum	3,172	3,309
Rail 45	Aluminum	7,762	8,098
Total		83,929	83,413
D_{basket} (in)		68.75	68.75
L_{basket} (in)		162.0	169.0
V_{basket} (in^3)		601,382	627,367
$\rho_{eff\ basket}$ (lbm/in^3)		0.140	0.133 (Bounding)

Table 5-18 Effective Specific Heat for 69BTH Basket

69BTH Basket									
Components	Fuel Assembly	Fuel compartments	Poison Plates	Sub-Assy Wrap	Aluminum Plates	Rail 90	Rail 45	Total	
Material (1)	---	Stainless Steel	Al	St. Steel	Al	Al	Al	---	
Weight (lbm) [11]	48,645	13,174	2,169	3,484	1,434	6,204	3,508	78,618	
Temperature	m.Cp	m.Cp	m.Cp	m.Cp	m.Cp	m.Cp	m.Cp	Σ m.Cp	Cp_{eff}
(°F)	(Btu/°F)	(Btu/°F)	(Btu/°F)	(Btu/°F)	(Btu/°F)	(Btu/°F)	(Btu/°F)	(Btu/°F)	(Btu/lbm-°F)
70	2,797	1,529	462	404	305	1,322	747	7,566	0.096
100	2,797	1,536	466	406	308	1,334	754	7,603	0.097
200	2,797	1,600	479	423	317	1,371	775	7,763	0.099
300	2,797	1,644	490	435	324	1,402	793	7,885	0.100
400	2,797	1,692	499	447	330	1,427	807	7,999	0.102
500	2,797	1,731	499	458	330	1,427	807	8,049	0.102
600	2,797	1,743	499	461	330	1,427	807	8,064	0.103
700	2,797	1,770	499	468	330	1,427	807	8,097	0.103
800	2,797	1,794	499	475	330	1,427	807	8,129	0.103
900	2,797	1,804	499	477	330	1,427	807	8,140	0.104
1000	2,797	1,813	499	479	330	1,427	807	8,152	0.104
1100	2,797	1,844	499	488	330	1,427	807	8,192	0.104

Top Grid Assembly (SA 240, type 304)			
Temp	Cp_{eff}	Temp	Cp_{eff}
(°F)	(Btu/lbm-°F)	(°F)	(Btu/lbm-°F)
70	0.116	600	0.132
100	0.117	700	0.134
200	0.121	800	0.136
300	0.125	900	0.137
400	0.128	1000	0.138
500	0.131	1100	0.140

Note: (1) Specific heat values are listed in Table 4-12.

Table 5-19 Effective Specific Heat for 37PTH Basket

37PTH Short Basket [1]							
Components	Fuel Assembly	Fuel compartments	Poison + Aluminum Plates	Rail 90	Rail 45	Total	
Material [2]	---	Stainless Steel	Al	Al	Al	---	
Weight (lbm) [12]	61,605	10,127	1,263	3,172	7,762	8,3929	
Temperature	m.Cp	m.Cp	m.Cp	m.Cp	m.Cp	Σ m.Cp	Cp_{eff}
(°F)	(Btu/°F)	(Btu/°F)	(Btu/°F)	(Btu/°F)	(Btu/°F)	(Btu/°F)	(Btu/lbm-°F)
70	3,628	1,175	269	676	1,653	7,402	0.088
100	3,692	1,181	272	682	1,669	7,495	0.089
200	3,902	1,230	279	701	1,716	7,827	0.093
300	4,069	1,264	285	717	1,754	8,089	0.096
400	4,171	1,301	290	730	1,785	8,277	0.099
500	4,273	1,331	290	730	1,785	8,409	0.100
600	4,375	1,340	290	730	1,785	8,521	0.102
700	4,473	1,360	290	730	1,785	8,638	0.103
800	4,512	1,379	290	730	1,785	8,697	0.104
900	4,552	1,387	290	730	1,785	8,744	0.104
1000	4,592	1,393	290	730	1,785	8,791	0.105
1100	4,632	1,418	290	730	1,785	8,855	0.106

Notes: (1) Lower weights are used conservatively, which are based on 37PTH-S basket with short basket length.
(2) Specific heat values (c_p) for materials are listed in Table 4-12.

5.3.2 Effective Thermal Conductivity

69BTH basket with Boral poison plates is chosen to calculate the effective conductivities. A 26" long slice of 69BTH basket is created by selecting the nodes and elements of the basket from the finite element model described in Section 5.1. The length of the slice model is twice the length of the aluminum plates and the axial gaps between them. The slice model is shown in Figure 5-21.

A 26.1" long slice of 37PTH basket is created by selecting the nodes and elements of the basket from the finite element model described in Section 5.2. The slice model is shown in Figure 5-21.

5.3.2.1 Axial Effective Thermal Conductivity

To calculate the axial effective conductivity of the baskets, constant temperature boundary conditions are applied at the top and bottom of the slice models. No heat generation is considered for the fuel elements in these cases. The axial effective conductivity is calculated using equation (5.12) below.

$$k_{basket,axl} = \frac{Q_{axl} \times L}{A_{slice} \times \Delta T} \times 0.95 \qquad (5.12)$$

Where: Q_{axl} = Amount of heat leaving the upper face of the slice model – reaction solution of the uppermost nodes (Btu/hr)
L = Length of the model = 26" for 69BTH
= 26.1" for 37PTH
A_{slice} = Surface area of the upper (or bottom) face of the basket slice model
= 1856 in^2 for 69BTH ($=\pi/8 \times D_{basket}^2$)
= 3712 in^2 for 37PTH ($\pi/4 \times D_{basket}^2$)
$\Delta T = (T_2 - T_1)$ =Temperature difference between upper and lower faces of the model (°F)
T_2 = Constant temperature applied on the upper face of the model (°F)
T_1 = Constant temperature applied on the lower face of the model (°F)

Only 95% of the estimated axial effective conductivity is considered for conservatism.

Typical applied boundary conditions are shown in Figure 5-22.

In determining the temperature dependent axial effective conductivities an average temperature, equal to $(T_1 + T_2)/2$, is used for the basket temperature. The axial effective conductivities for 69BTH and 37PTH baskets are listed in Table 5-20 and Table 5-19, respectively.

The axial effective conductivity for the top grid assembly of 69BTH basket is calculated considering only the 14.4" high plates. The effects of the extension, base plate, and short plates are conservatively ignored. The assumed geometry of the top grid assembly is shown in Figure

5-23. The following equation is used to calculate the axial effective conductivity for the top grid assembly.

$$k_{topgrid,axl} = k_{SS304} \frac{A_{plates}}{A_{model}} \qquad (5.13)$$

Where: k_{SS304} = conductivity of stainless steel, see Table 4-5 (Btu/hr-in-°F)
A_{plates} = Surface area of the 14.4" high plates, see Table 5-20 (in^2)
A_{model} = Surface area of the homogenized top grid assembly model
= $\pi/4 \times D_{basket}{}^2 = 3712\ in^2$

The axial effective conductivities for the top grid assembly are listed in Table 5-20.

Table 5-20 Effective Axial Conductivity for 69BTH Basket

Basket				
T_2 (T_{top})	T_1 (T_{bottom})	Q_{axl}	T_{avg}	$k_{basket, axl}$
(°F)	(°F)	(Btu/hr)	(°F)	(Btu/hr-in-°F)
50	0	6319.4	25	1.682
150	100	6389.7	125	1.701
250	200	6479.2	225	1.724
350	300	6559.4	325	1.746
450	400	6613.1	425	1.760
550	500	6615.9	525	1.761
650	600	6615.7	625	1.761
750	700	6630.8	725	1.765
850	800	6649.5	825	1.770
950	900	6665.5	925	1.774
1050	1000	6681.8	1025	1.778
1150	1100	6698.7	1125	1.783

Top Grid Assembly			
D_topgrid	68.5	in	
L_topgrid	14.4	in	
Plate Thickness	0.25	in	
	Length (in)	No. of Plates	Area (in^2)
L1	44.17	16	176.7
L2	18.71	4	18.7
L3	6.25	16	25.0
Total			220.4
A_model	3712	in^2	
A_plates	220.4	in^2	

Temp	k_{SS304} [Table 4-5]	$k_{topgrid, axl}$
(°F)	(Btu/hr-in-°F)	(Btu/hr-in-°F)
70	0.717	0.043
100	0.725	0.043
200	0.775	0.046
300	0.817	0.048
400	0.867	0.051
500	0.908	0.054
600	0.942	0.056
700	0.983	0.058
800	1.025	0.061
900	1.058	0.063
1000	1.092	0.065
1100	1.133	0.067

Table 5-21 Effective Axial Conductivity for 37PTH Basket

Basket				
T_2 (T_{top})	T_1 (T_{bottom})	Q_{axl}	T_{avg}	$k_{basket, axl}$
(°F)	(°F)	(Btu/hr)	(°F)	(Btu/hr-in-°F)
50	0	7684.6	25	1.028
150	100	7816.8	125	1.045
250	200	8078.8	225	1.080
350	300	8345.1	325	1.116
450	400	8591.5	425	1.149
550	500	8790.1	525	1.176
650	600	8974.2	625	1.200
750	700	9141.4	725	1.223
850	800	9295	825	1.243
950	900	9411.7	925	1.259
1050	1000	9521.7	1025	1.273
1150	1100	9628.2	1125	1.288

5.3.2.2 Radial Effective Thermal Conductivity

The basket slice models are also used to calculate the transverse effective conductivity of the basket. For this purpose, constant temperature boundary conditions are applied on the outermost nodes of the slice model and heat generating conditions are applied over the fuel elements.

The heat generation rates for the slice model of 69BTH basket are calculated based on the HLZC # 1A shown in Figure 5-1 and Table 5-2 with a total heat load of 26 kW and a peaking factor of 1.2 for BWR assemblies.

The heat generation rates for the slice model of 37PTH basket is based on HLZC shown in Figure 5-13 with a total heat load of 22 kW and a peaking factor of 1.11 for PWR assemblies.

The following equation is given in [22] for long solid cylinders with uniformly distributed heat sources.

$$T = T_o + \frac{\dot{q}\, r_o^{\,2}}{4k}\left[1 - \left(\frac{r}{r_o}\right)^2\right] \qquad (5.14)$$

With T_o = Temperature at the outer surface of the cylinder (°F)
T = Maximum temperature of cylinder (°F)
$\dot{q}$ = Heat generation rate (Btu/hr-in^3)
r_o = Outer radius = D_{basket} /2 = 34.375” for 69BTH basket
= 34.375” for 37PTH basket

r = Inner radius = 0 for slice model
k = Conductivity (Btu/hr-in-°F)

Equation (5.14) is rearranged to calculate the transverse effective conductivity of the basket as follows. Only 95% of the estimated radial effective conductivity is considered for conservatism.

$$\dot{q} = \frac{Q_{rad}}{V} \qquad (5.15)$$

$$k_{basket,rad} = \frac{Q_{rad} \cdot r_0^2}{4 \cdot V \cdot \Delta T} \times 0.95 = \frac{0.95\, Q_{rad}}{2\pi \cdot L \cdot \Delta T} \text{ for 69BTH}$$

$$= \frac{0.95\, Q_{rad}}{4\pi \cdot L \cdot \Delta T} \text{ for 37PTH} \qquad (5.16)$$

With Q_{rad} = Amount of heat leaving the periphery of the slice model – reaction solution of the outermost nodes (Btu/hr)
L = Length of the slice model = 26" for 69BTH
= 26.1" for 37PTH
V = Volume of the slice model = $(\pi r_0^2 L)/2$ for 69BTH
= $\pi r_0^2 L$ for 37PTH
$\Delta T = (T_{max} - T_o)$ = Difference between maximum and the outer surface temperatures in (°F)

Since the surface area of the fuel assemblies at the basket cross section is much larger than the other components, assuming a uniform heat generation is a reasonable approximation to calculate the radial effective conductivity.

Typical applied boundary conditions are shown in Figure 5-22.

In determining the temperature dependent transverse effective conductivities an average temperature, equal to $(T_{max} + T_o)/2$, is used for the basket temperature.

The transverse effective conductivities of 69BTH and 37PTH basket are listed in Table 5-22 and Table 5-23, respectively.

The effect of stainless steel in top grid assembly is ignored conservatively in the radial direction. The effective conductivity of top grid assembly is set equal to helium conductivity in the radial direction.

Table 5-22 Effective Radial Conductivity for 69BTH Basket

69BTH Basket				
T_{max} (°F)	T_o (°F)	Q_{rad} (Btu/hr)	T_{avg} (°F)	k_{basket_rad} (Btu/hr-in-°F)
336	0	9678	168	0.167
429	100	9678	264	0.171
519	200	9678	360	0.176
603	300	9678	451	0.186
688	400	9678	544	0.195
776	500	9678	638	0.204
866	600	9678	733	0.211
959	700	9678	830	0.217
1054	800	9678	927	0.222
1148	900	9678	1024	0.227
1243	1000	9678	1122	0.231
1339	1100	9678	1219	0.236

Table 5-23 Effective Radial Conductivity for 37PTH Basket

37PTH Basket				
T_{max} (°F)	T_o (°F)	Q_{rad} (Btu/hr)	T_{avg} (°F)	k_{basket_rad} (Btu/hr-in-°F)
416	0	15148	208	0.105
492	100	15148	296	0.112
566	200	15148	383	0.120
642	300	15148	471	0.128
720	400	15148	560	0.137
799	500	15148	649	0.147
882	600	15148	741	0.156
971	700	15148	835	0.162
1064	800	15148	932	0.166
1159	900	15148	1030	0.169
1255	1000	15148	1127	0.172
1351	1100	15148	1225	0.175

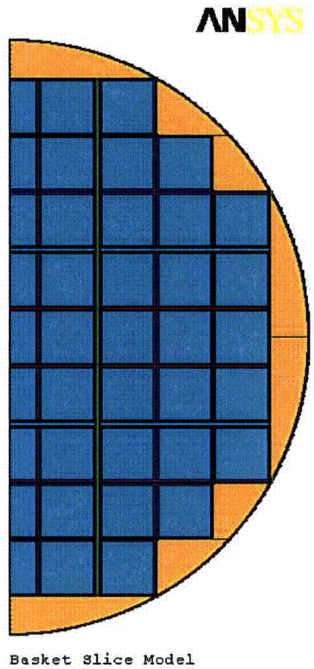

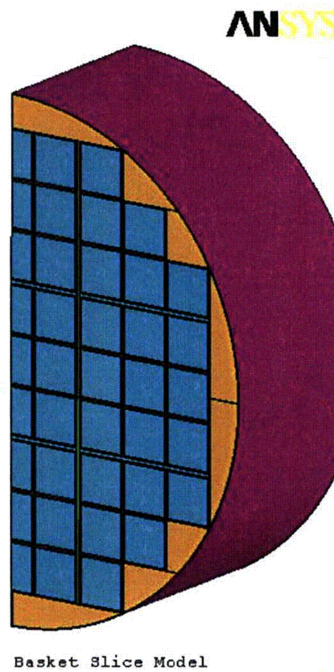

For 69BTH DSC

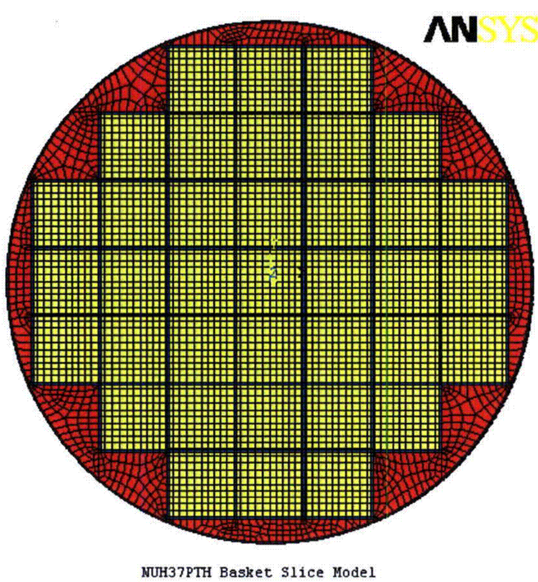

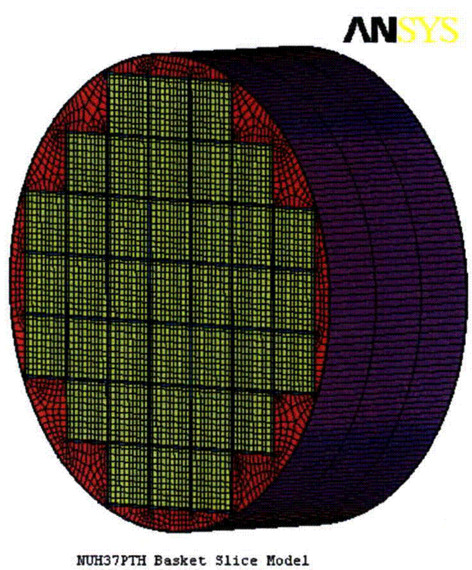

For 37PTH DSC

Figure 5-21 Basket Slice Models

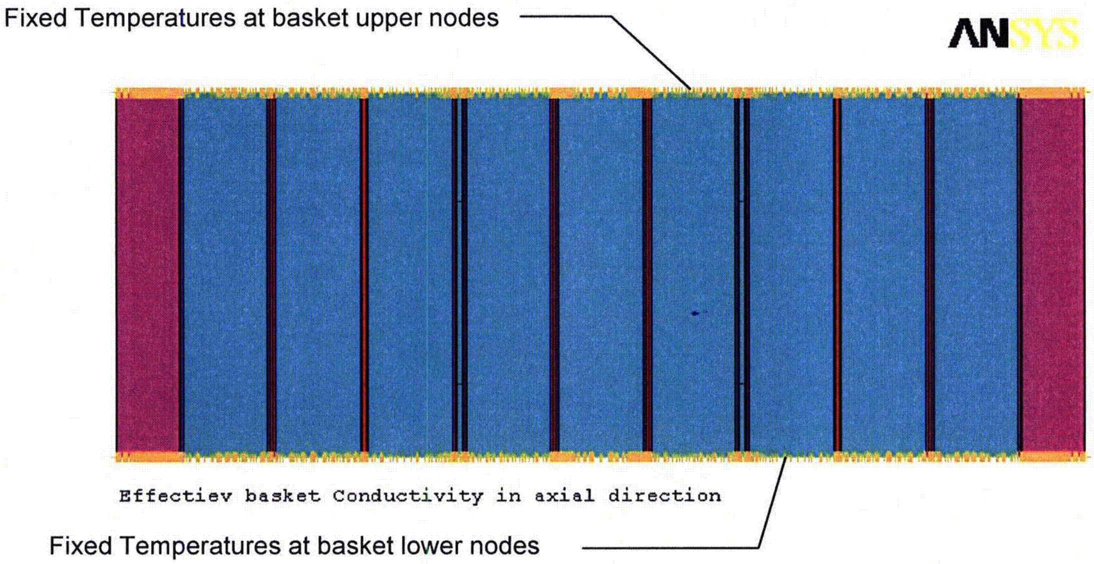

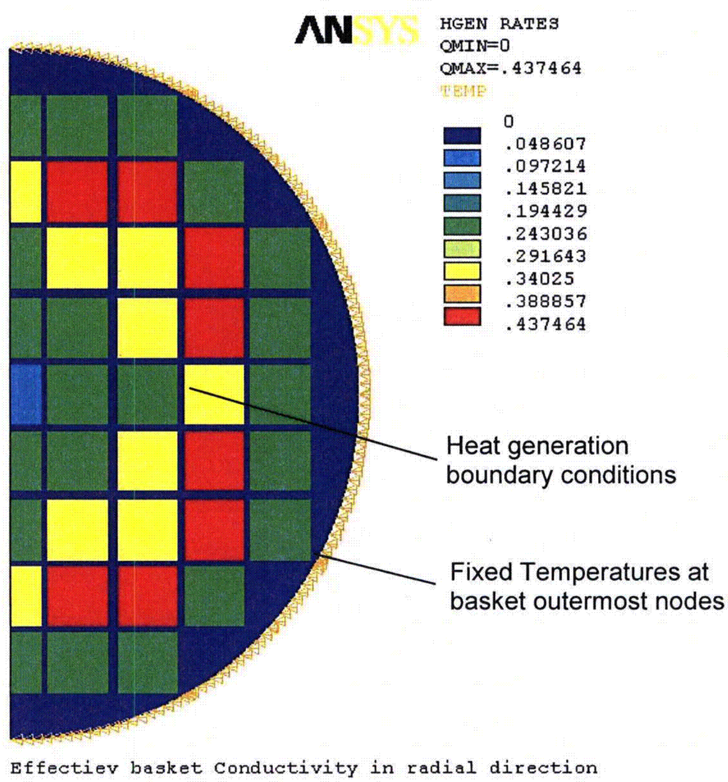

Figure 5-22 Typical Boundary Conditions for Basket Slice Model

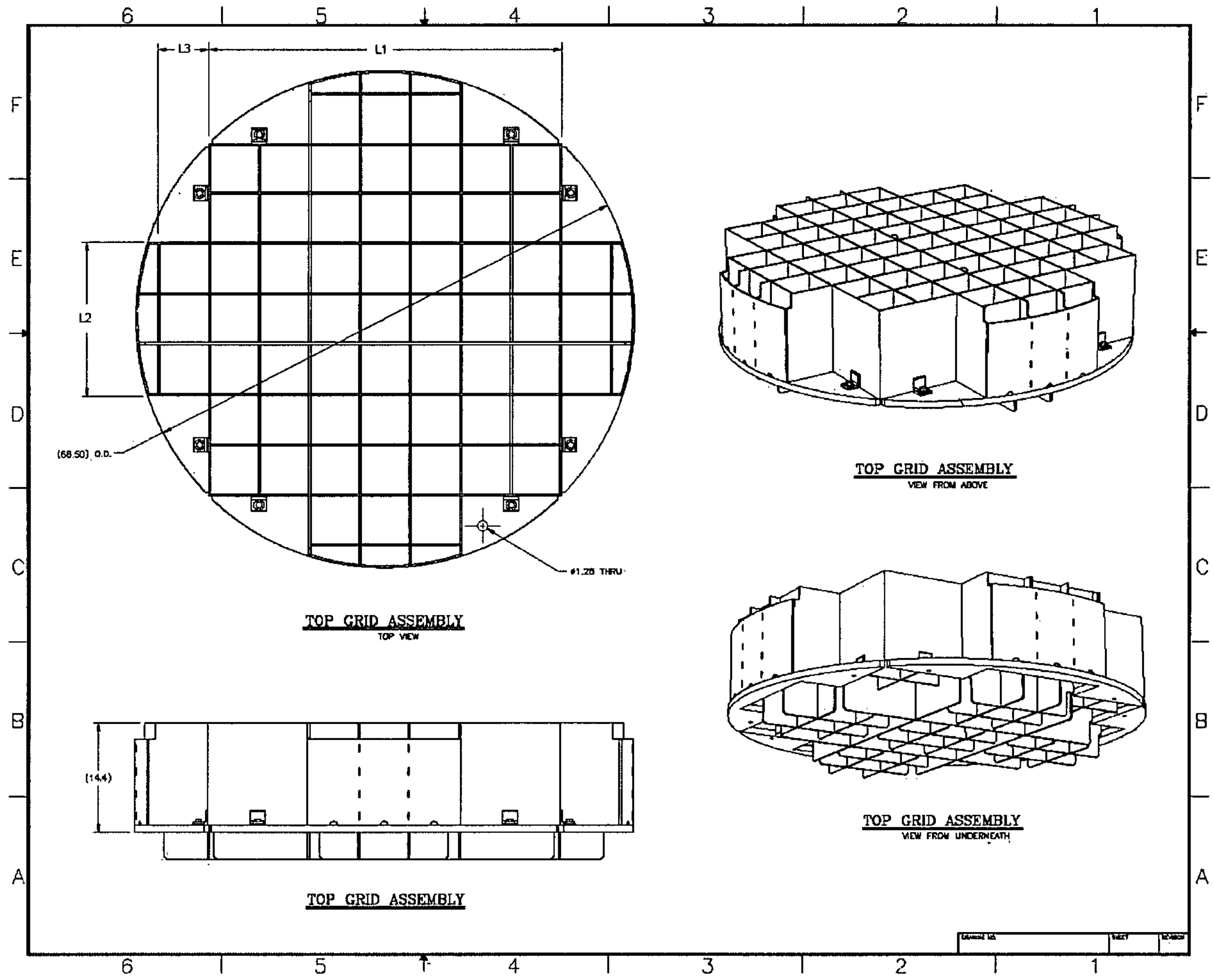

Figure 5-23 Schematic View of Top Grid Assembly (Hold-Down Ring)

5.4 Loading/Unloading Operations

Vacuum drying is considered as normal conditions for wet loading operations. The fuel transfer operations for wet loading occur when the MP197HB and the loaded DSC are in the spent fuel pool. The fuel is always submerged in free-flowing pool water permitting heat dissipation. After completion of fuel loading, the TC and DSC are removed from the pool and the DSC is drained, dried, sealed and backfilled with helium. These operations occur when the annulus between the TC and DSC remains filled with water.

The water in the annulus is replenished with fresh water to prevent boiling and maintain the water level if excessive evaporation occurs. Presence of water within the annulus maintains the maximum DSC shell temperature below the boiling temperature of water in open atmosphere (212°F).

Water in the DSC cavity is forced out of the cavity (blowdown operation) before the start of vacuum drying. Helium is used as the medium to remove water and subsequent vacuum drying occurs with a helium environment in the DSC cavity. The vacuum drying operation does not reduce the pressure sufficiently to reduce the thermal conductivity of the helium in the canister cavity [31], [32], and [33].

With helium being present during vacuum drying operations, the maximum temperatures including the maximum fuel cladding temperature are bounded by those calculated for transport operation if the DSC shell temperature under NCT is higher than the DSC shell temperature of 212°F maintained during vacuum drying.

Presence of helium during blowdown and vacuum drying operations eliminates the thermal cycling of fuel cladding during helium backfilling of the DSCs subsequent to vacuum drying. Therefore, the thermal cycling limit of 65°C (117°F) for short term operations set by [5] is irrelevant for vacuum drying operation in MP197HB.

The bounding unloading operation considered is the reflood of the DSCs with water. For unloading operations, the DSC is filled with the spent fuel pool water through its siphon port. During this filling operation, the DSC vent port is maintained open with effluents routed to the plant's off-gas monitoring system.

The maximum fuel cladding temperature during reflooding event is significantly less than the vacuum drying condition owing to the presence of water/steam in the canister cavity. Based on the above rational, the maximum cladding temperature during unloading operation is bounded by the maximum fuel cladding for vacuum drying operation.

Initially, the pool water is added to the canister cavity containing hot fuel and basket components, some of the water will flash to steam causing internal cavity pressure to rise. This steam pressure is released through the vent port. The procedures specify that the flow rate of the reflood water be controlled such that the internal pressure in the canister cavity does not exceed 20 psig ([1], [2], and [4]). This is assured by monitoring the maximum internal pressure in the canister cavity during the reflood event. The reflood for the DSC is considered as a

Service Level D event and the design pressures of the DSCs are well above 20 psig ([1], [2], and [4]). Therefore, there is sufficient margin in the DSC internal pressure during the reflooding event to assure that the canister will not be over pressurized.

The effects of the thermal loads on the fuel cladding during reflooding operations are evaluated in [1], Section T.4.7.3 and Section U.4.7.3 for BWR and PWR fuel assemblies respectively. Since the same fuel assemblies are handled in the DSCs contained in MP197HB, these evaluations remain valid for this calculation.

6.0 RESULTS

The maximum component temperatures for HLZC # 1 in 69BTH basket/DSC are listed in Table 6-1 for NCT. As seen, the maximum fuel cladding temperature is bounded by the HLZC # 1A and is 658°F. This confirms the discussion in Section 5.1 that the peak cladding temperature is maximized if the heat load is concentrated in the inner core compartments.

Table 6-1 Maximum Component Temperatures for HLZC #1 in 69BTH Basket for Hot NCT

	Heat Load 26 kW			
	HLZC # 1A	HLZC # 1B	HLZC # 1C	
Component	T_{max} (°F)	T_{max} (°F)	T_{max} (°F)	Limit (°F)
Fuel Cladding	658	646	632	662 (1)
Basket (compartment)	643	631	616	---
Al / Poison Plate	643	630	616	---
Basket Rails	475	475	475	---
Top Shield Plug	271	271	271	---
Bottom Shield Plug	414	411	410	---

Note: (1) A fuel cladding temperature limit of 350°C (662°F) is selected for BWR assemblies in 69BTH basket. This limit is lower than the fuel cladding temperature limit of 400°C (752°F) established in [5] and [6].

The maximum component temperatures for other HLZCs in 69BTH DSC and for 37PTH DSC are listed in Table 6-2.

Table 6-2 Maximum Component Temperatures for 69BTH and 37PTH DSCs for Hot NCT

	69BTH DSC				37PTH DSC		
Heat Load	26 kW	26 kW	29.2 kW	32 kW	22 kW		
Configuration	HLZC # 1	HLZC # 2	HLZC # 3	HLZC # 4	HLZC # 1 (2)		
Component	T_{max} (°F)	T_{max} (°F)	T_{max} (°F)	T_{max} (°F)	T_{max} (°F) (3)	T_{max} (°F) (4)	Limit (°F)
Fuel Cladding	658	639	651	650	660	655	662 (1)
Basket (compartment)	643	611	622	612	649	645	---
Al / Poison Plate	643	610	621	612	648	645	---
Basket Rails	475	473	481	507	443	443	---
Top Shield Plug	271	271	260	273	309	309	---
Bottom Shield Plug	414	420	421	442	295	295	---

Note: (1) A fuel cladding temperature limit of 350°C (662°F) is selected for BWR and PWR assemblies in 69BTH and 37PTH baskets. This limit is lower than the fuel cladding temperature limit of 400°C (752°F) established in [5] and [6].
(2) The HLZC # 1 for 37PTH is assigned as # 8 in input files.
(3) Based on 0.075" Boral plate paired with 0.05" Al1100 plate
(4) Based on single, 0.125" thick poison plate.

The maximum and minimum shell temperatures for DSCs are listed in Table 6-3. As Table 6-3 shows, the DSC shell temperatures for all DSC types are higher than 212°F. Based on discussion in Section 5.4, the maximum fuel cladding temperatures for vacuum drying conditions are bounded by those calculated for NCT for all DSC types in MP197HB.

Table 6-3 Maximum and Minimum DSC Shell Temperatures for Hot NCT

DSC Type	69BTH DSC			61BTH/ 61BTHF Type 1	61BTH/ 61BTHF Type 2	61BT
Heat Load	26 kW	29.2 kW	32 kW	22 kW	24 kW	18.3 kW
$T_{max, DSC\ shell}$ (°F) [(1)]	451	458	484	414	435	372
$T_{min, DSC\ shell}$ (°F) [(2)]	266	255	266	250	260	229

DSC Type	37PTH	32PTH / 32PTH Type1 / 32PTH1 Type 1	32PTH1 Type 2	32PT	24PTH / 24PTHF Type 1 & 2	24PT4
Heat Load	22 kW	26 kW	24 kW	24 kW	26 kW	24 kW
$T_{max, DSC\ shell}$ (°F) [(1)]	408	444	423	443	464	428
$T_{min, DSC\ shell}$ (°F) [(2)]	261	289	278	283	299	313

Note: (1) The maximum DSC shell temperatures are taken from [10], Table 6-1 and Table 6-2.

(2) The minimum DSC shell temperatures are taken from temperature plots saved with ANSYS files for each corresponding DSC. These plots are collected in APPENDIX E.

Based on evaluations in [1], Section T.4.7.3 and Section U.4.7.3, the maximum fuel cladding stresses are bounded by 22,515 psi for outer surface and 24,464 psi for inner surface of BWR and PWR fuel assemblies during reflooding operation. Since the calculation of these stresses is independent of the DSC type, they are valid in this calculation. The calculated fuel cladding stresses for reflooding conditions are much less than the yield stress of 50,500 psi [34]. Therefore, no cladding damage is expected due to the reflood event.

This is also substantiated by the operating experience gained with the loading and unloading of transportation packages like IF-300 [35] which show that fuel cladding integrity is maintained during these operations and fuel handling and retrieval is not impacted.

The highest heat load is 32 kW for 69BTH DSC. This case with the highest heat load is selected to determine the maximum temperature gradients through the 69BTH basket. The maximum component temperatures for cold NCT at -20°F and -40°F without insolance are listed in Table 6-4 for 69BTH and 37PTH DSCs.

Table 6-4 Maximum Fuel Cladding and Basket Component Temperatures for Cold NCT

DSC type	69BTH, 32 kW		37PTH, 22 kW (1)		37PTH, 22 kW (2)	
Ambient Temperature	-20°F	-40°F	-20°F	-40°F	-20°F	-40°F
Component	T_{max} (°F)	T_{max} (°F)	T_{max} (°F)	T_{max} (°F)	T_{max} (°F)	T_{max} (°F)
Fuel Cladding	582	570	593	582	589	578
Basket (compartment)	537	524	580	569	576	565
Al / Poison Plate	536	524	580	569	576	565
Basket Rails	431	419	365	353	365	353
Top Shield Plug	170	152	213	198	213	198
Bottom Shield Plug	352	337	203	187	202	187

Note: (1) Based on 0.075" Boral plate paired with 0.05" Al1100 plate
(2) Based on single, 0.125" thick poison plate.

The average temperatures of fuel assemblies, dummy assemblies, and helium within DSC cavities are listed in Table 6-5.

Table 6-5 Average Component Temperatures for Hot NCT

Basket Type	69BTH	69BTH	69BTH	69BTH	37PTH	
Heat Load	26 KW	26 kW	29.2 kW	32 kW	22 kW	
Configuration	HLZC # 1	HLZC # 2	HLZC # 3	HLZC # 4	HLZC # 1 (2)	
Component	T_{avg} (°F)	T_{avg} (°F)	T_{avg} (°F)	T_{avg} (°F)	T_{avg} (°F) (3)	T_{avg} (°F) (4)
Fuel Assemblies	534	525	535	547	517	515
Dummy Assemblies	N/A	559	568	558	N/A	N/A
Helium Elements (5)	398	404	404	432	406	405
Aluminum Rail (1)	457	457	464	490	436	436

Note: (1) The average rail temperature in the above table is the highest average temperature among aluminum rails at various locations in the basket, see Table 6-6.
(2) The HLZC # 1 for 37PTH is assigned as # 8 in input files.
(3) Based on 0.075" Boral plate paired with 0.05" Al1100 plate
(4) Based on single, 0.125" thick poison plate.
(5) This value is the volumetric, average temperature of the elements with helium properties in the model. In addition to the gaps, helium properties are considered for the elements within the fuel compartments located beyond the active fuel length for the compartments containing fuel or dummy assemblies. Helium properties are also considered for the empty compartment in 69BTH with HLZC # 4.

Table 6-6 shows the average temperatures for the aluminum rails in 69BTH and 37PTH baskets for hot NCT.

Table 6-6 Average Aluminum Rail Temperatures for Hot NCT

Basket Type	69BTH	69BTH	69BTH	69BTH	37PTH	
Heat Load	26 KW	26 kW	29.2 kW	32 kW	22 kW	
Configuration	HLZC # 1	HLZC # 2	HLZC # 3	HLZC # 4	HLZC # 1 (4)	
Component (1)	T_{avg} (°F)	T_{avg} (°F)	T_{avg} (°F)	T_{avg} (°F)	T_{avg} (°F) (2)	T_{avg} (°F) (3)
Large Rail @ 0°	457	457	464	490	436	436
Small Rail @ 45°, Upper One	451	451	457	483	434	434
Small Rail @ 45°, Lower One	448	448	454	480		
Large Rail @ 90°, Upper One	433	432	437	462	404	404
Large Rail @ 90°, Lower One	420	420	423	448		
Small Rail @ 135°, Upper One	404	404	406	430	393	393
Small Rail @ 135°, Lower One	393	393	394	418		
Large Rail @ 180°	385	386	385	409	375	375
Highest Average Temperature	457	457	464	490	436	436

Note: (1) The locations of the rails are shown below.
(2) Based on 0.075" Boral paired 0.05" Al1100 poison plate
(3) Based on single, 0.125" thick poison plate.
(4) The HLZC # 1 for 37PTH is assigned as # 8 in input files.

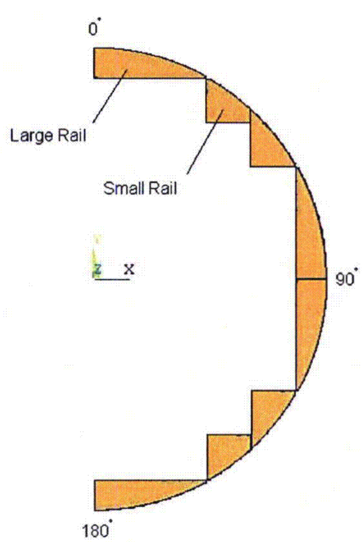

69BTH DSC Rails

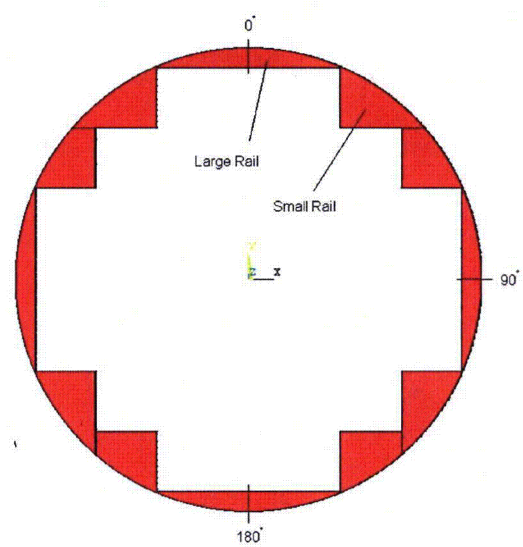

37PTH DSC Rails

Typical temperature distributions for 69BTH basket/DSC model with 26 kW and 32 kW heat loads are shown in Figure 6-1 and Figure 6-2, respectively. Temperature distributions for fuel assemblies in 69BTH basket are shown in Figure 6-3.

Typical temperature distributions for 37PTH basket/DSC model with 22 kW heat load for hot NCT are shown in Figure 6-4.

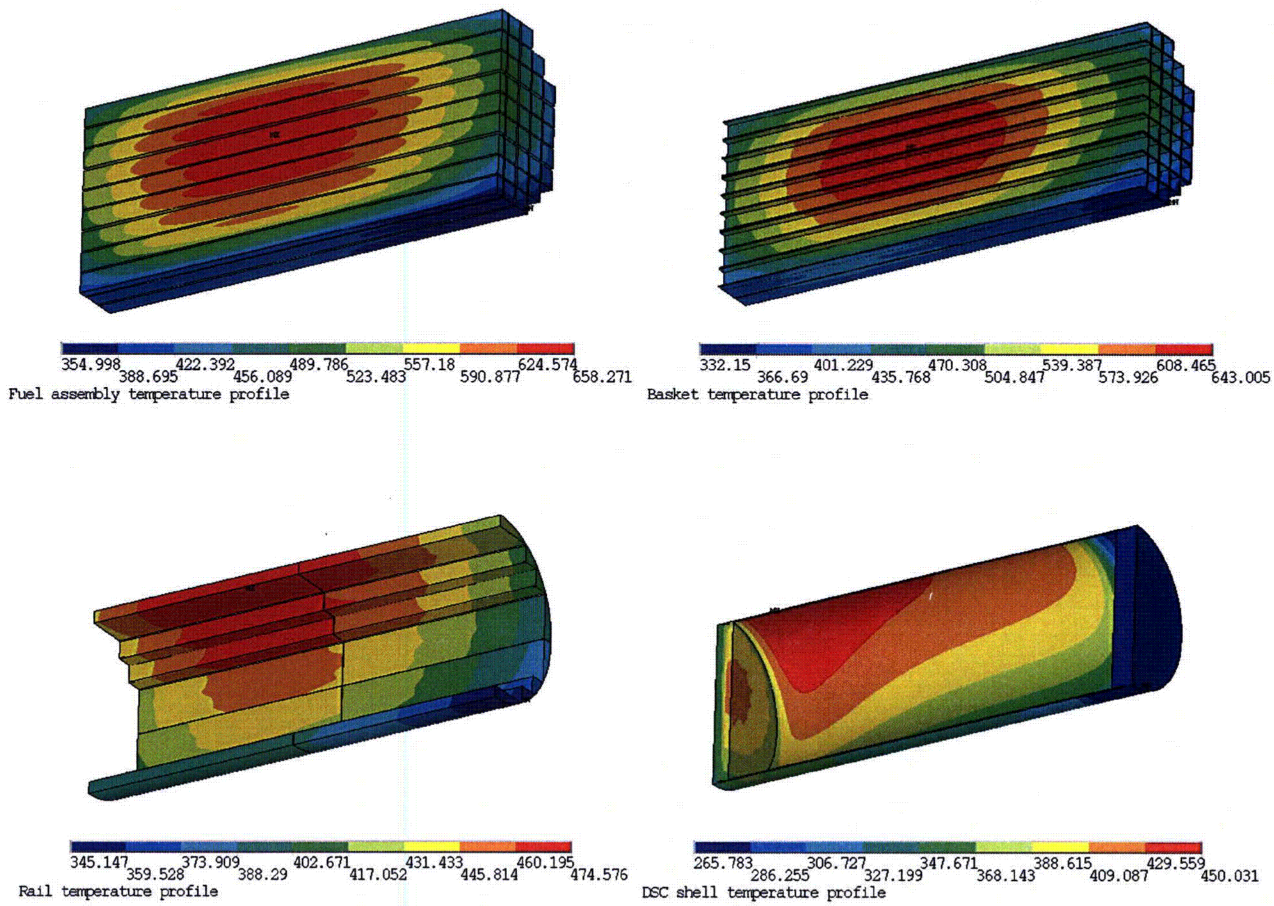

Figure 6-1 Typical Temperature Distributions for 69BTH Basket (NCT @ 100°F, HLZC#1A, 26kW)

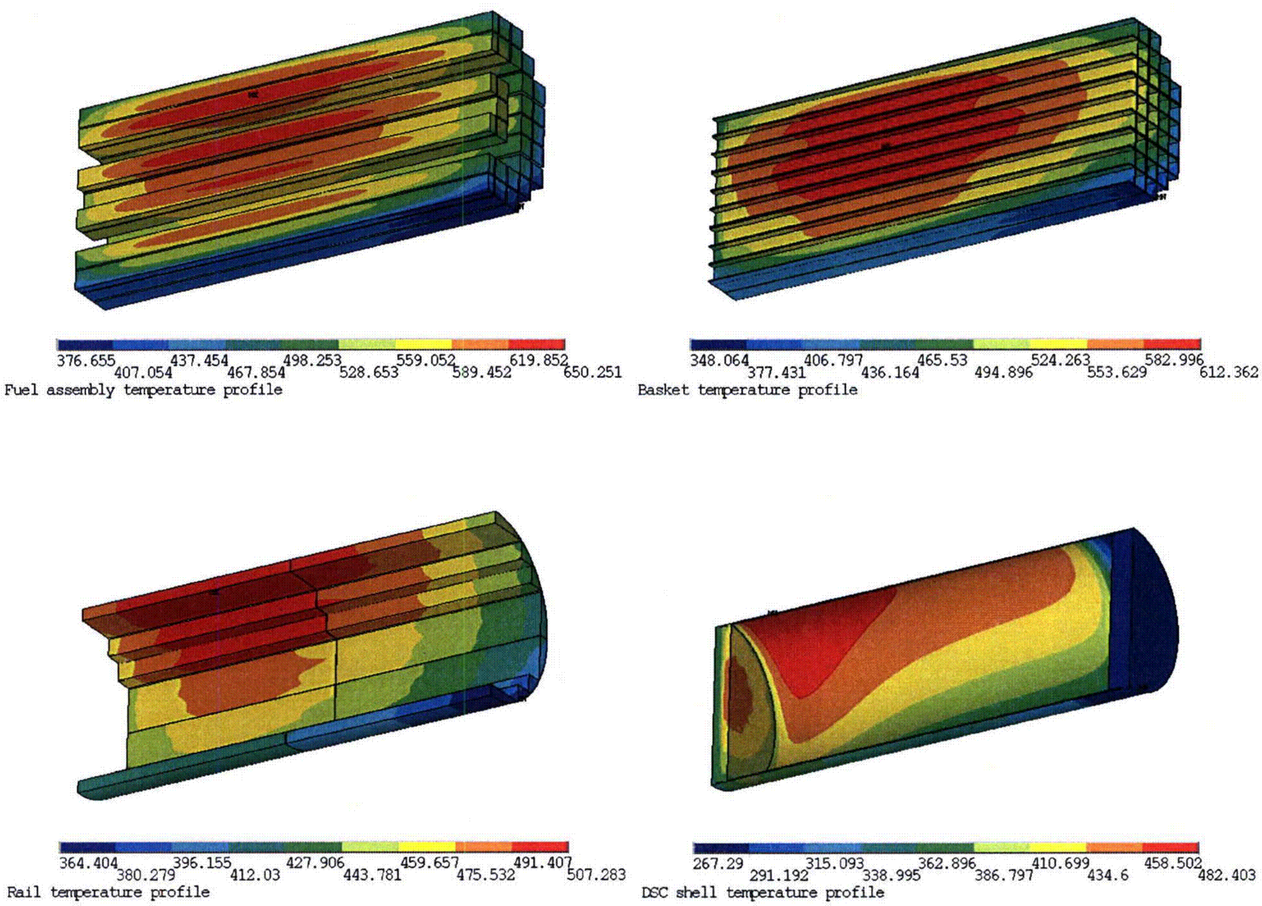

Figure 6-2 Typical Temperature Distributions for 69BTH Basket (NCT @ 100°F, HLZC#4, 32kW)

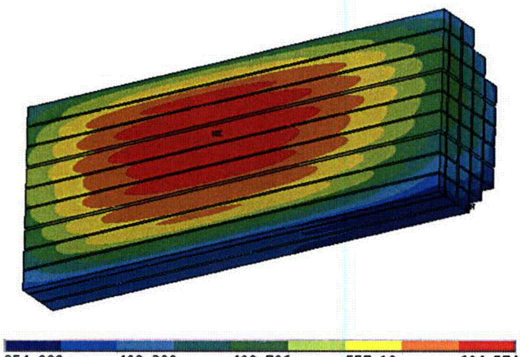

69BTH, HLZC#1A, 26kW

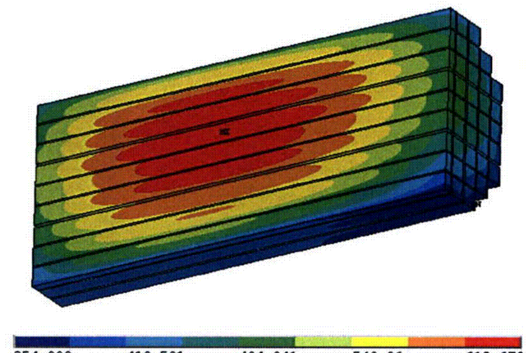

69BTH, HLZC#1B, 26kW

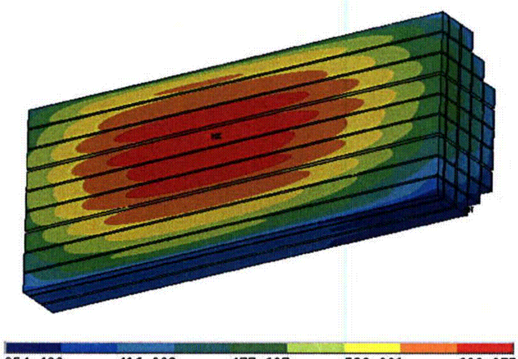

69BTH, HLZC#1C, 26kW

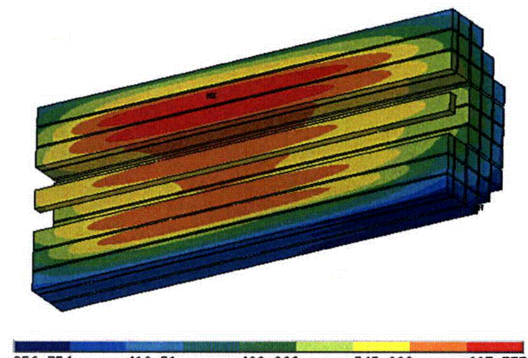

69BTH, HLZC#2, 26kW

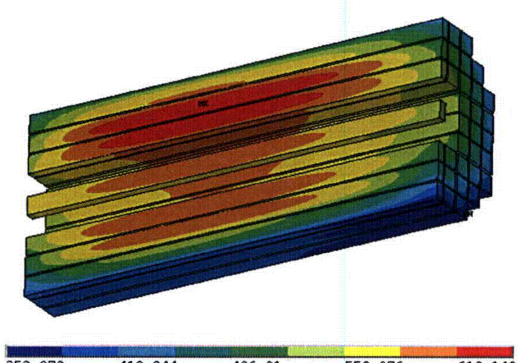

69BTH, HLZC#3, 29.2kW

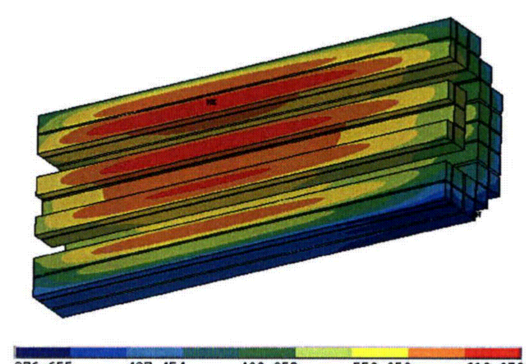

69BTH, HLZC#4, 32kW

Figure 6-3 Temperature Distributions for Fuel Assemblies in 69BTH Basket (NCT @ 100°F)

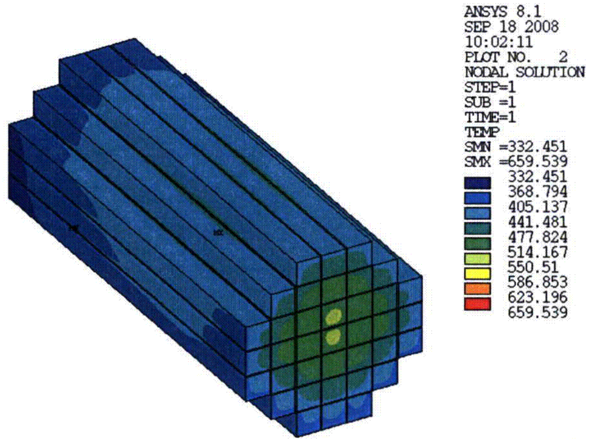

Fuel Cladding - Heat Zone Conf#8 (37PTH_22_100CS Load No. 1)

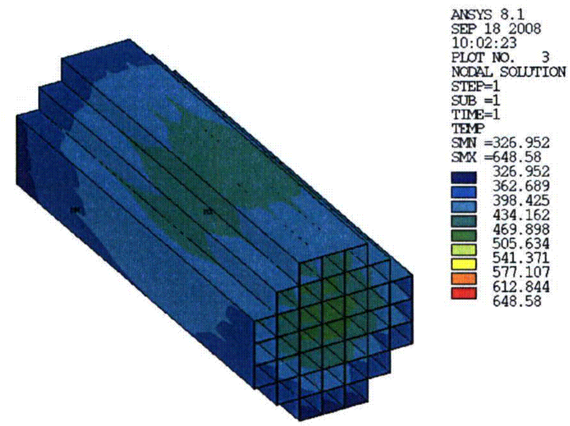

Fuel Comp - Heat Zone Conf#8 (37PTH_22_100CS Load No. 1)

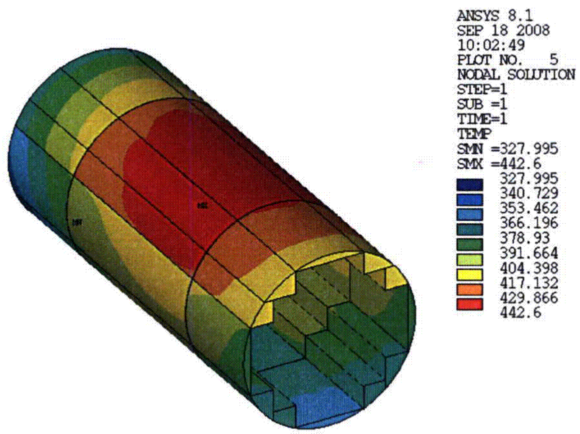

Rails - Heat Zone Conf#8 (37PTH_22_100CS Load No. 1)

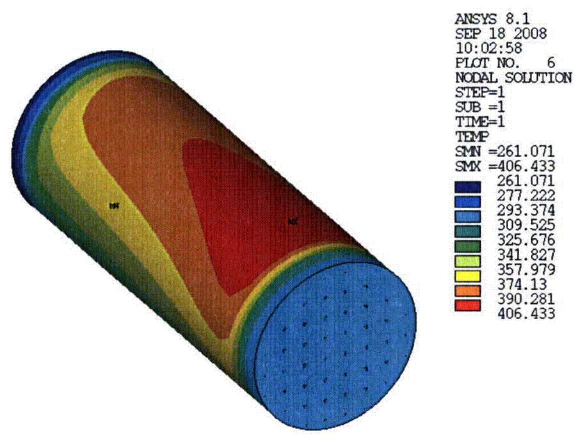

DSC Shell - Heat Zone Conf#8 (37PTH_22_100CS Load No. 1)

Figure 6-4 Typical Temperature Distributions for 37PTH Basket (NCT @ 100°F, 22 kW)

7.0 CONCLUSION

As seen in Table 6-2, the maximum fuel cladding temperatures calculated for NCT conditions are lower than the allowable limits.

The maximum fuel cladding temperature is between 650°F and 658°F for 69BTH DSC with 26 kW to 32 kW heat loads. For 37PTH DSC, the bounding maximum fuel cladding temperature is 660°F with 22 kW heat load for the basket in which 0.075" thick Boral plates are paired with 0.05" thick aluminum plates. These temperatures are below the selected limit of 662°F (350°C). The maximum fuel cladding temperature in 69BTH DSC and 37PTH DSC are well below the allowable fuel cladding temperature limit of 752°F (400°C) established in [5] and [6] and therefore acceptable.

As discussed in [10], the maximum fuel cladding and basket temperatures for all other DSC types in MP197HB cask are bounded by the values for normal transfer conditions. These values are collected in Table 7-1 and Table 7-2 for reference.

As seen in Table 7-1, the maximum fuel cladding temperatures for all DSC types are below the allowable limit of 752°F (400°C) specified in [5] and [6].

Based on discussion in Section 5.4 and the DSC shell temperatures shown in Table 6-3, the maximum fuel cladding temperatures for loading and unloading conditions are bounded by the values calculated for NCT, which are presented in Table 7-1. These values are well below the allowable fuel cladding temperature limit of 752°F (400°C) for short term operations established in [5]. Since the NCT is a steady state condition, the need for a time limit on the vacuum drying operations is eliminated.

The discussion in Section 5.4 also shows that thermal cycling limit of 117°F (65°C) is irrelevant for vacuum drying operations in MP197HB TC.

All materials can be subjected to a minimum environment temperature of -40°F (-40°C) without any adverse effects. The maximum component temperatures of 69BTH DSC and 37PTH DSC for cold conditions are summarized in Table 7-3.

All design criteria specified in Section 4.2 are herein satisfied.

The effective properties for 69BTH basket, 69BTH top grid assembly (hold-down ring), and 37PTH basket are summarized in Table 7-4 and Table 7-5 to use in transient analysis.

Table 7-1 Maximum Fuel Cladding Temperatures for NCT Conditions

DSC Type	$T_{max, Fuel}$ (°F)	Reference	Limit (°F)
69BTH, 32 kW (w/o external fins)	674	[10], Table H-1	752 [5]
69BTH, 32 kW (with external fins)	650	---	
69BTH, 29.2 kW	651	---	
69BTH, 26 kW	658	---	
61BTH Type 1	< 706	[1], Table T.4-12	
61BTH Type 2	< 715	[1], Table T.4-12	
61BT	< 638	[1], Table K.4-2	
37PTH	660	---	
32PTH, 32PTH Type 1	< 723	[4], Table 4-1	
32PTH1 Type 1	< 713	[1], Table U.4-15	
32PTH1 Type 2	< 728	[1], Table U.4-15	
32PT	< 720	[1], Table M.4-2	
24PTH Type 1 (24PTH-S or –L w/ Al inserts)	< 733	[1], Table P.4-14	
24PTH Type 2 (24PTH-S or –L w/o Al inserts)	< 733	[1], Table P.4-14	
24PTH Type 2 (24PTH-S-LC)	< 714	[1], Table P.4-14	
24PT4	< 707	[2], Table A4.4-7	

Table 7-2 Maximum Basket Component Temperatures for NCT

DSC Type	$T_{max, Comp}$ (°F)	$T_{max, Al/Posion}$ (°F)	$T_{max, Rail}$ (°F)	Reference
69BTH, 32 kW (w/o external fins)	638	622	534	[10], Table H-1
69BTH, 32 kW (with external fins)	612	612	507	---
69BTH, 29.2 kW	622	621	481	---
69BTH, 26 kW	643	643	475	---
61BTH Type 1	< 683	< 682	< 565	[1], Table T.4-13
61BTH Type 2	< 686	< 686	< 539	[1], Table T.4-14
61BT	< 615	< 615	< 493	[1], Table K.4-2
37PTH	649	648	443	---
32PTH, 32PTH Type 1	< 697	< 696	< 561	[4], Table 4-1
32PTH1 Type 1	< 677	< 676	< 520	[1], Table U.4-16
32PTH1 Type 2	< 648	< 648	< 529	[1], Table U.4-17
32PT	< 705	< 705	< 471	[1], Table M.4-3
24PTH Type 1 (24PTH-S or –L w/ Al inserts)	< 680	< 679	< 576 (1)	[1], Table P.4-16
24PTH Type 2 (24PTH-S or –L w/o Al inserts)	< 682	< 681	< 576 (1)	[1], Table P.4-16
24PTH Type 2 (24PTH-S-LC)	< 674	< 673	< 500 (1)	[1], Table P.4-17
24PT4	< 670	< 670	(2)	[2], Table A4.4-6

Notes: (1) This value is the maximum rail, R90, temperature from [9], Table B-1.

(2) Based on [2], Table A.4.4-6, the maximum spacer disc and support rod temperatures for 24PT4 DSC under normal transfer conditions are 663°F and 574°F. These temperatures are the bounding values for NCT.

Table 7-3 Maximum Component Temperatures for Cold NCT

DSC type	69BTH, 32 kW		37PTH, 22 kW	
Ambient Temperature	-20°F	-40°F	-20°F	-40°F
Component	T_{max} (°F)	T_{max} (°F)	T_{max} (°F)	T_{max} (°F)
Fuel Cladding	582	570	593	582
Basket (compartment)	537	524	580	569
Al / Poison Plate	536	524	580	569
Basket Rails	431	419	365	353
Top Shield Plug	170	152	213	198
Bottom Shield Plug	352	337	203	187

Table 7-4 Effective Thermal Properties for 69BTH Basket

Basket OD = 68.75"
Basket length = 164"

Temperature (°F)	k_{basket_rad} (Btu/hr-in-°F)	Temperature (°F)	$k_{basket,\ axl}$ (Btu/hr-in-°F)	Temperature (°F)	Cp_{eff} (Btu/lbm-°F)
168	0.167	25	1.682	70	0.096
264	0.171	125	1.701	100	0.097
360	0.176	225	1.724	200	0.099
451	0.186	325	1.746	300	0.100
544	0.195	425	1.760	400	0.102
638	0.204	525	1.761	500	0.102
733	0.211	625	1.761	600	0.103
830	0.217	725	1.765	700	0.103
927	0.222	825	1.770	800	0.103
1024	0.227	925	1.774	900	0.104
1122	0.231	1025	1.778	1000	0.104
1219	0.236	1125	1.783	1100	0.104
$\rho_{eff\ basket}$ =	0.129	lbm/in^3			

Table 7-5 Effective Thermal Properties for 69BTH Top Grid Assembly

Basket OD = 68.75"
Grid length = 14.4"

Temperature (°F)	$k_{basket\ rad}$ (Btu/hr-in-°F)	Temperature (°F)	$k_{basket,\ axl}$ (Btu/hr-in-°F)	Temperature (°F)	Cp_{eff} (Btu/lbm-°F)
80	0.0072	70	0.043	70	0.116
260	0.0086	100	0.043	100	0.117
440	0.0102	200	0.046	200	0.121
620	0.0119	300	0.048	300	0.125
980	0.0148	400	0.051	400	0.128
1340	0.0174	500	0.054	500	0.131
1430	0.0181	600	0.056	600	0.132
		700	0.058	700	0.134
		800	0.061	800	0.136
		900	0.063	900	0.137
		1000	0.065	1000	0.138
		1100	0.067	1100	0.140
$\rho_{eff\ basket}$ =	0.04	lbm/in^3			

Table 7-6 Effective Thermal Properties for 37PTH Basket

Basket OD = 68.75"
Basket length = 162"

Temperature (°F)	$k_{basket\ rad}$ (Btu/hr-in-°F)	Temperature (°F)	$k_{basket,\ axl}$ (Btu/hr-in-°F)	Temperature (°F)	Cp_{eff} (Btu/lbm-°F)
208	0.105	25	1.028	70	0.088
296	0.112	125	1.045	100	0.089
383	0.120	225	1.080	200	0.093
471	0.128	325	1.116	300	0.096
560	0.137	425	1.149	400	0.099
649	0.147	525	1.176	500	0.100
741	0.156	625	1.200	600	0.102
835	0.162	725	1.223	700	0.103
932	0.166	825	1.243	800	0.104
1030	0.169	925	1.259	900	0.104
1127	0.172	1025	1.273	1000	0.105
1225	0.175	1125	1.288	1100	0.106
$\rho_{eff\ basket}$ =	0.133	lbm/in^3			

8.0 LISTING OF COMPUTER FILES

A list of the files to retrieve the DSC shell temperature from TC models is shown in Table 8-1.

A list of the files to create geometries for 69BTH DSC and 37PTH DSC is shown in Table 8-2.

A summary of ANSYS runs is listed in Table 8-3. All the runs are performed using ANSYS version 8.1 [28] with operating system "Windows XP PRO-SP1", and CPU "Xeon 3.20 GHz".

ANSYS macros, and associated files used in this calculation are shown in Table 8-4.

The spreadsheets for this calculation are listed in Table 8-5.

Table 8-1 List of Files to Retrieve DSC Shell Temperatures

File Name (Input and Output)	Description	Required Files from [10]	Date / Time for Output File
TempMap_26CS	Transfer temp from TC to DSC/Basket model for 69BTH, 26 kW @ 100°F	TC_69BTH_26CS.db TC_69BTH_26CS.rth	08/29/08 02:38 PM
TempMap_29CS	Transfer temp from TC to DSC/Basket model for 69BTH, 29.2 kW @ 100°F	TC_69BTH_29CS.db TC_69BTH_29CS.rth	08/29/08 02:40 PM
TempMap_32CS	Transfer temp from TC to DSC/Basket model for 69BTH, 32.0 kW @ 100°F	TC_69BTH_32CS.db TC_69BTH_32CS.rth	08/29/08 02:42 PM
TempMap_20FCS	Transfer temp from TC to DSC/Basket model for 69BTH, 32.0 kW @ -20°F	TC_32kW_20FCS.db TC_32kW_20FCS.rth	08/29/08 02:44 PM
TempMap_40FCS	Transfer temp from TC to DSC/Basket model for 69BTH, 32.0 kW @ -40°F	TC_32kW_40FCS.db TC_32kW_40FCS.rth	08/29/08 02:46 PM
TempMap_22CS	Transfer temp from TC to DSC/Basket model for 37PTH, 22 kW @ 100°F	TC_22kW_23CS.db TC_22kW_23CS.rth	09/19/08 10:13 AM
	Transfer temp from TC to DSC/Basket model for 37PTH, 22 kW @ -20°F	TC_22kW_20CS.db TC_22kW_20CS.rth	
	Transfer temp from TC to DSC/Basket model for 37PTH, 22 kW @ -40°F	TC_22kW_40CS.db TC_22kW_40CS.rth	
TempMap_22CS3	Transfer temp from TC to DSC/Basket model for 37PTH, 22 kW @ 100°F (sensitivity Analysis)	TC_37PTH_22CS.db TC_37PTH_22CS.rth	09/18/08 06:34 PM

Table 8-2 List of Geometry Files

File Name (Input and Output)	Description	Date / Time for Output File
NUH69BTH	Creates geometry for 69BTH DSC	02/21/08 10:10 AM
37PTH_Model2	Creates geometry for 37PTH DSC (10×10 for FA mesh)	04/30/08 12:42 PM
37PTH_Model3	Creates geometry for 37PTH DSC (12×12 for FA mesh)	05/02/08 03:15 PM

Table 8-3 Summary of ANSYS Runs

Run Name	Description	Date / Time
69BTH_26CS_1A	69BTH basket with HLZC#1A (26kW), 100°F ambient	08/29/08 04:16 PM
69BTH_26CS_1B	69BTH basket with HLZC#1B (26kW), 100°F ambient	08/29/08 05:47 PM
69BTH_26CS_1C	69BTH basket with HLZC#1C (26kW), 100°F ambient	08/29/08 07:18 PM
69BTH_26CS_2A	69BTH basket with HLZC#2 (26kW), 100°F ambient	08/29/08 08:46 PM
69BTH_29CS_3A	69BTH basket with HLZC#3 (29.2kW), 100°F ambient	08/29/08 10:14 PM
69BTH_32CS_4	69BTH basket with HLZC#4 (32kW), 100°F ambient	08/29/08 11:42 PM
69BTH_32CS_20F	69BTH basket, 32kW, -20°F ambient	08/30/08 01:10 AM
69BTH_32CS_40F	69BTH basket, 32kW, -40°F ambient	08/30/08 02:38 AM
GAP_26CS_1A	Average component temperatures for DSC/Basket gap in 69BTH basket, HLZC#1, 26 kW	08/30/08 02:42 AM
GAP_32CS_4	Average component temperatures for DSC/Basket gap in 69BTH basket, HLZC#4, 32 kW	08/30/08 02:46 AM
bskt_eff_r	Effective conductivity for 69BTH basket in radial direction	05/12/08 09:51 PM
bskt_eff_a	Effective conductivity for 69BTH basket in axial direction	04/18/08 02:50 PM
NUH69BTH_C	69BTH basket, coarse mesh for mesh sensitivity analysis	05/12/08 10:00 PM
NUH69BTH_F	69BTH basket, fine mesh for mesh sensitivity analysis	05/12/08 10:36 PM
37PTH_22_100CS	37PTH basket, 22 kW, 100°F ambient (0.075" Boral plate)	10/06/08 05:00 PM
37PTH_22_20CS	37PTH basket, 22 kW, -20°F ambient (0.075" Boral plate)	10/06/08 05:36 PM
37PTH_22_40CS	37PTH basket, 22 kW, -40°F ambient (0.075" Boral plate)	09/19/08 02:53 PM
37PTH_22_100CS2	37PTH basket, 22 kW, 100°F ambient (0.125" MMC plate)	09/18/08 10:39 AM
37PTH_22_20CS2	37PTH basket, 22 kW, -20°F ambient (0.125" MMC plate)	09/19/08 03:58 PM
37PTH_22_40CS2	37PTH basket, 22 kW, -40°F ambient (0.125" MMC plate)	09/19/08 02:36 PM
37PTH_22_100CS3	37PTH basket for mesh sensitivity analysis	09/18/08 08:07 PM
bskt_eff_r37pth	Effective conductivity for 37PTH basket in radial direction	09/19/08 08:03 PM
bskt_eff_a37pth	Effective conductivity for 37PTH basket in axial direction	09/19/08 07:52 PM

Table 8-4 Associated Files and Macros

File Name	Description	Date / Time
Mat69BTH.inp	Material properties for 69BTH DSC	03/12/08 08:18 AM
MatInp_37pth.mac	Material properties for 37PTH DSC	09/17/08 05:29 PM
Heatgen_5Zf.inp	Heat generation for 69BTH, HLZC#1	05/05/08 01:36 PM
Heatgen_5Za.inp	Heat generation for 69BTH, HLZC#2 and HLZC#3	03/12/08 04:26 PM
Heatgen_5Zb.inp	Heat generation for 69BTH, HLZC#4	03/12/08 04:27 PM
37pthc8_22.hg	Heat generation for 37PTH	09/17/08 07:48 PM
RailAvgN.txt	Average rail temperatures	11/26/07 06:10 PM
Results.mac	Maximum and average 37PTH basket/DSC component temperatures	04/29/08 07:54 AM

Table 8-5 List of Spreadsheets

File Name	Description	Date / Time
69BTH_HLZC.xls	HLZCs for 69BTH DSC	05/05/08 05:41 PM
MatProp.xls	Material Properties for 69BTH DSC	03/14/08 02:01 PM
MatProp_Boral.xls	Effective conductivity for Boral in 37PTH	09/25/08 11:28 AM
keff_dummy.xls	Effective conductivity for Dummy Assembly	12/26/07 04:36 PM
peaking factors.xls	BWR axial heat profile	04/18/08 10:41 AM
Contact resistance.xls	Contact resistance between Al/Poison plates	04/18/08 11:46 AM
hotgap_69BTH.xls	Hot gap between 69BTH Basket/DSC shell	09/02/08 10:49 AM
Eff_Bskt_69BTH.xls	69BTH basket effective properties	05/29/08 09:08 PM
Eff_Bask_37pth.xls	37PTH basket effective properties	09/29/08 06:42 AM
PF_nuh37pth.xls	Peaking factors for PWR fuel assemblies	05/05/08 11:39 AM
TR_hot_gap_37pth.xls	Hot gap between 37PTH Basket/DSC shell	09/19/08 04:12 PM

APPENDIX A JUSTIFICATION OF HOT GAP BETWEEN BASKET AND DSC

A.1 Hot Gap for 69BTH DSC

A nominal diametrical cold gap of 0.40" is considered between the basket and the canister shell for 69BTH DSC [11]. The nominal canister inner diameter (ID) of 69BTH DSC is 68.75". The nominal basket outer diameter (OD) is then 68.35".

To calculate the minimum gap, the average temperatures for the basket, aluminum rails, and DSC shell at the hottest cross section for NCT at 100°F ambient are required to calculate the thermal expansion at thermal equilibrium. These temperatures are retrieved from 69BTH basket model via runs GAP_26_1A and GAP_32_4 listed in Section 8.0. The average temperatures are listed in Table A–1.

Table A–1 Average Temperatures at Hottest Cross Section for 69BTH Basket

Component	HLZC#1, 26kW NCT @ 100°F T_{avg} (°F)	HLZC#4, 32kW NCT @ 100°F T_{avg} (°F)
Basket (compartments & wrap plates only)	547	547
Al Rail @ 0 degree	472	504
Al Rail @ 180 degree	398	421
DSC Shell	388	408

The hot dimensions of the basket OD and DSC ID are calculated as follows.

The outer diameter of the hot basket is:

$$OD_{B,hot} = OD_B + [L_{SS,B} \times \alpha_{SS,B} (T_{avg,B} - T_{ref})] + L_{Rail} \times [\alpha_{Al,0} (T_{avg,R0} - T_{ref}) + \alpha_{Al,180} (T_{avg,R180} - T_{ref})]$$

Where:

$OD_{B,hot}$ = hot OD of the basket
OD_B = nominal cold OD of the basket
= 68.75" – 0.40" = 68.35"
$L_{SS,B}$ = width of basket at 0-180 direction
= 9 × compartment width +
9 × 2 × compartment plate +
6 × Al/Poison within nine-compartment blocks +
2 × Al/Poison between nine-compartment blocks +
6 × wrap plate
= 9 × 6 + 9 × 2 × 0.165 + 6 × 0.25 + 2 × 0.375 + 6 × 0.105 = 59.85"
L_{Al} = width of aluminum rail = $(OD_B - L_{SS,B})/2$ = 4.25"

$\alpha_{SS,B}$ = Average stainless steel axial coefficient of thermal expansion (interpolated using data in [6], Table 6-1 – in/in-°F)
α_{Al} = Average aluminum coefficient of thermal expansion (interpolated using data in [6], Table 6-3 – in/in-°F)
$T_{avg,B}$ = Average basket temperature at the hottest cross section, see Table A–1 (°F)
$T_{avg,R0}$ = Average Al rail temperature at the hottest cross section at 0 degree orientation, see Table A–1, (°F)
$T_{avg,R180}$ = Average Al rail temperature at the hottest cross section at 180 degree orientation, see Table A–1 (°F)
T_{ref} = reference temperature for stainless steel and aluminum alloys = 70°F [18]

The inner diameter of the hot DSC shell is:

$$ID_{DSC,hot} = ID_{DSC}\,[1 + \alpha_{SS,DSC}\,(T_{avg,DSC} - T_{ref})]$$

Where:
$ID_{DSC,hot}$ = Hot ID of DSC shell
ID_{DSC} = Cold ID of DSC shell = 68.75"
$\alpha_{SS,DSC}$ = Average stainless steel axial coefficient of thermal expansion (interpolated using data in [6], Table 6-1 – in/in-°F)
$T_{avg,DSC}$ = Average DSC shell temperature at hottest cross section, see Table A–1 (°F)
T_{ref} = Reference temperature for low alloy steel = 70°F [18]

The diametrical hot gap between the basket and cask inner shell is:

$$G_{hot} = ID_{DSC,hot} - OD_{B,hot}$$

The diametrical hot gap at the hottest cross section is calculated for 26kW (HLZC#1) and 32 kW ((HLZC#4) heat loads in 69BTH basket to bound the problem. The calculated hot gaps are listed in Table A–2.

A uniform diametrical hot gap of 0.30" is considered in the model between the basket and the DSC shell for 69BTH DSC. This assumption is conservative since the hot gaps calculated in Table A–2 are smaller than the assumed gap of 0.3".

Table A–2 Diametrical Hot Gaps for 69BTH Basket

26kW, HLZC # 1A					
	Cold dimension	Temp	αx10^{-6} (1)	ΔL	Hot dimension
	(in)	(°F)	(in/in/°F)	(in)	(in)
Basket width	59.85	547	9.747	0.278	60.128
Large rail @ 0°	4.25	472	13.844	0.024	4.274
Large rail @ 180°	4.25	398	13.592	0.019	4.269
Basket OD	68.35				68.671
DSC ID	68.75	388	9.464	0.207	68.957
Gap	0.4				**0.286**

32kW, HLZC # 4					
	Cold dimension	Temp	αx10^{-6} (1)	ΔL	Hot dimension
	(in)	(°F)	(in/in/°F)	(in)	(in)
Basket width	59.85	547	9.747	0.278	60.128
Large rail @ 0°	4.25	504	13.916	0.026	4.276
Large rail @ 180°	4.25	421	13.684	0.020	4.270
Basket OD	68.35				68.674
DSC ID	68.75	408	9.516	0.221	68.971
Gap	0.4				**0.297**

Note: (1) The average thermal expansion coefficient is calculated by interpolation using data in [6], Table 6-1 for stainless steel and Table 6-3 for aluminum.

A.2 Hot Gap for 37PTH DSC

A nominal diametrical cold gap of 0.4" is considered between the basket and the canister shell for 37PTH DSC. The nominal canister inner diameter (ID) of 37PTH DSC is 68.75". The nominal basket outer diameter (OD) is then 68.35".

To calculate the minimum gap, the average temperatures for the basket, aluminum rails, and DSC shell at the hottest cross section for NCT at 100°F ambient are required to calculate the thermal expansion at thermal equilibrium. These temperatures are retrieved from 37PTH basket model via macros listed in Section 8.0. The average temperatures are listed in Table A–3.

Table A–3 Average Temperatures at Hottest Cross Section for 37PTH Basket

Component	**22 kW, NCT @ 100°F T_{avg} (°F)**
Basket (compartments plates)	516
Al Rail @ 0 degree	436
Al Rail @ 180 degree	375
DSC Shell	351

The hot dimensions of the basket OD and DSC ID are calculated as follows.

The outer diameter of the hot basket is:

$$OD_{B,hot} = OD_B + [L_{SS,B} \times \alpha_{SS,B} (T_{avg,B} - T_{ref})] + L_{Rail} \times [\alpha_{Al,0} (T_{avg,R0} - T_{ref}) + \alpha_{Al,180} (T_{avg,R180} - T_{ref})]$$

Where:

$OD_{B,hot}$ = hot OD of the basket

OD_B = nominal cold OD of the basket = 68.75" – 0.4" = 68.35"

$L_{SS,B}$ = width of basket at 0-180 direction
= 7 × compartment width +
6 × thin compartment plate +
2 × thick compartment plate +
= 7 × 8.725 + 6 × 0.25 + 2 × 0.3125 = 63.20"

L_{Al} = width of aluminum rail = $(OD_B - L_{SS,B})/2$ = 2.575"

$\alpha_{SS,B}$ = Average stainless steel axial coefficient of thermal expansion (interpolated using data in [6], Table 6-1 – in/in-°F)

α_{Al} = Average aluminum coefficient of thermal expansion (interpolated using data in [6], Table 6-3 – in/in-°F)

$T_{avg,B}$ = Average basket temperature at the hottest cross section, see Table A–3 (°F)

$T_{avg,R0}$ = Average Al rail temperature at the hottest cross section at 0 degree orientation, see Table A–3 (°F)

$T_{avg,R180}$ = Average Al rail temperature at the hottest cross section at 180 degree orientation, see Table A–3 (°F)

T_{ref} = reference temperature for stainless steel and aluminum alloys = 70°F [18]

The inner diameter of the hot DSC shell is:

$$ID_{DSC,hot} = ID_{DSC} [1 + \alpha_{SS,DSC} (T_{avg,DSC} - T_{ref})]$$

Where:

$ID_{DSC,hot}$ = Hot ID of DSC shell

ID_{DSC} = Cold ID of DSC shell = 68.75"

$\alpha_{SS,DSC}$ = Average stainless steel axial coefficient of thermal expansion (interpolated using data in [6], Table 6-1 – in/in-°F)

$T_{avg,DSC}$ = Average DSC shell temperature at hottest cross section, see Table A–3 (°F)

T_{ref} = Reference temperature for low alloy steel = 70°F [18]

The diametrical hot gap between the basket and cask inner shell is:

$G_{hot} = ID_{DSC,hot} - OD_{B,hot}$

The diametrical hot gap at the hottest cross section is calculated for 22 kW heat loads in 37PTH basket. The calculated hot gaps are listed in Table A–4.

A uniform diametrical hot gap of 0.45” is considered in the model between the basket and the DSC shell for 37PTH DSC. This assumption is conservative since the hot gap calculated in Table A–4 is smaller than the assumed gap of 0.45”.

Table A–4 Diametrical Hot Gaps for 37PTH Basket

	Cold dimension	Temp	$\alpha x10^{-6}$ (1)	ΔL	Hot dimension
	(in)	(°F)	(in/in/°F)	(in)	(in)
Basket width	63.20	516	9.716	0.2740	63.474
Large rail @ 0°	2.575	436	13.746	0.0130	2.588
Large rail @ 180°	2.575	375	13.501	0.0106	2.586
Basket OD	68.35				68.648
DSC ID	68.75	351	9.353	0.181	68.931
Gap	0.4				**0.283**

Note: (1) The average thermal expansion coefficient is calculated by interpolation using data in [6], Table 6-1 for stainless steel and Table 6-3 for aluminum.

APPENDIX B CONTACT RESISTANCE ACROSS PAIRED ALUMINUM AND POISON PLATES IN 69BTH BASKET

The thermal gaps considered on both sides of the paired aluminum and poison plates account for all the thermal resistance across the paired plates. Dividing the thermal resistance into three separate resistances would only change the temperature distribution between the two paired plates without changing the overall thermal resistance. The temperature distribution among the paired aluminum and poison plates are of no particular significance.

The following calculation shows that the modeled gaps (0.01") on both sides of the paired aluminum and poison plates are adequate to bound the existing contact resistances.

According to the basket configuration, three contact resistances are recognizable for the paired aluminum / poison plates sandwiched between the fuel compartments or wrap plates:

- contact resistance between the aluminum plate and the stainless steel fuel compartment or wrap plates
- contact resistance between the aluminum plate and the poison plate
- contact resistance between the poison plate and the stainless steel fuel compartment or wrap plate

These contact resistances are shown schematically in Figure B–1.

Yovanovich suggests in [23] the following approach to calculate the thermal contact conductance.

$$h_j = h_c + h_g \qquad \text{(B.1)}$$

h_j = total thermal contact conductance (m^2-K/W)
h_c = contact conductance (m^2-K/W)
h_g = gap conductance (m^2-K/W)

The contact conductance, h_c, is given in [23] by:

$$h_c = 1.25\, k_s \,\frac{m}{\sigma}\left(\frac{P}{H_c}\right)^{0.95} \qquad \text{(B.2)}$$

Where

$k_s = 2k_1\, k_2 /(k_1 + k_2)$	Harmonic mean thermal conductivity of interface (W/m-K)
$m = \sqrt{m_1^2 + m_2^2}$	Effective mean absolute asperity slope of interface
$\sigma = \sqrt{\sigma_1^2 + \sigma_2^2}$	Effective RMS surface roughness of contacting asperities (m)

P = Contact pressure (MPa)
H_c = Microhardness of the softer of the two contacting solids (MPa)

The mean absolute asperity slope for each plate can be approximated by the following correlation from [23]:

$$m_i = 0.125\left(\sigma_i \times 10^{-6}\right)^{0.402} \text{ for } 0.216\,\mu m \le \sigma \le 9.6\,\mu m$$

As seen in equation (B.2), the contact conductance, h_c, depends heavily on contact pressure, P. Assuming a very small contact pressure of 10^{-6} psi results in a negligible contact conductance, h_c and eliminates this term in calculation of the total thermal contact conductance in equation (B.1).

Due to elimination of h_c in equation (B.1), the conductivities of the contacting plates are not required for this calculation.

The gap conductance, h_g, is given in [23] by:

$$h_g = k_g / (Y + M) \qquad \text{(B.3)}$$

Where
k_g = thermal conductivity of the gap substance (W/m-K)
Y = effective gap thickness (m)
M = gas parameter (m)

Based on [23], the effective gap thickness, Y, shown in Figure B–2, can be calculated as follows:

$$Y = 1.53\,\sigma\left(P / H_c\right)^{-0.097} \qquad \text{for } 10^{-5} < P/H_c < 2\text{x}10^{-2}$$

The gas parameter M accounts for the rarefaction effects at high temperatures and low gas pressure. This gas-surface parameter depends on the thermal accommodation coefficients, the ratio of specific heats, the Prandtl number, and the molecular mean free-path of the gas. This complex gas-surface parameter depends on gas pressure and temperature according to the following relationship:

$$M = M_0 \frac{T}{T_0} \frac{P_{g,0}}{P_g}$$

Where M_0 denotes the gas parameter value at the reference values of gas temperature and pressure, T_0 and $P_{g,0}$, respectively. The gas parameter for helium is $2.05\text{x}10^{-6}$ m at 50°C and 1 atm, as reported in reference [23].

The thermal contact resistance is:

$R_j = 1/h_j$ (B.4)

Based on Figure B–1, the total thermal contact resistance for the paired plates is:

$$R_{j,plates} = R_{j,SS-Al} + R_{j,Al-Poison} + R_{j,poison-SS} \qquad (B.5)$$

$R_{j,ss\text{-}Al}$ = contact resistance between stainless steel and aluminum plates
$R_{j,Al\text{-}Poison}$ = contact resistance between aluminum and poison plates
$R_{j,Poison\text{-}SSl}$ = contact resistance between poison and stainless steel plates

An operating temperature of 400°F (204°C) is considered for conductivity of helium. The assumed operating temperature is well below the average basket temperature in Table A–1 and is therefore conservative.

A moderate gas pressure (Pg) of 5 psig (1.34 abs atm), lower than the normal operating pressure of the 61BTH DSC ([1], Table T.4-16), is considered to evaluate the contact resistances.

Based on Table 4-9, the helium conductivity is 9.84E-3 Btu/hr-in-°F or 0.204 W/m-K at 400°F. The following data in Table B–1 are considered for roughness and hardness of the plates.

Table B–1 Surface Properties for Aluminum and Stainless Steel Plates

Material	Roughness (μm)	Hardness	Microhardness [1] (MPa)
Aluminum 1100 / Poison Plate	0.2 to 6.3 [24]	25 to 95 Brinell 500kg [25]	440 to 1079
SA 240, type 304	0.2 to 6.3 [24]	92 Rockwell B [26], Table 2	1960 to 2000

Note: (1) For conversion of roughness units see reference [27]

Surface roughness is mainly determined by the production method. The roughness values in Table B–1 correspond to average values for cold rolling / drawing process. The hardness values are collected for aluminum alloys 6063 and 6061, which are the closest to aluminum alloy 1100.

The contact resistances are calculated based on the average roughness and hardness from Table B–1.

σ_{Al} = 3.25 μm, $H_{c,Al}$ = 760 MPa
σ_{poison} = 3.25 μm, $H_{c,poison}$ = 760 MPa
σ_{SS} = 3.25 μm, $H_{c,SS}$ = 1980 MPa

The calculated contact resistances are listed in Table B–2.

Table B–2 Contact Resistances between Plates in 69BTH Basket

Contact Type	Al / Poison	SS / Al or SS/ Poison
σ (m)	4.60E-06	4.60E-06
P (MPa)	6.891E-09	6.891E-09
H_c (MPa)	760	760
P_g (atm)	1.34	1.34
T (K)	478	478
k_g (W/m-K)	0.204	0.204
P/H_c	9.073E-12	9.073E-12
Y (m)	8.283E-05	8.283E-05
M (m)	2.262E-06	2.262E-06
h_c (W/m^2-K)	0.00	0.00
h_g (W/m^2-K)	2402	2402
h_j (W/m^2-K)	2402	2402
R_j (m^2-K/W)	4.164E-04	4.164E-04

The total thermal contact resistance across the plates using equation (B.5) is:

$$R_{j,total} = 3 \times 4.164E-4 = 1.249E-3 \text{ m}^2\text{-K/W}$$

The equivalent thermal resistance for the helium gaps across the plates considered in the 69BTH basket model is:

Δx_{He} = 2 × 0.01" = 0.02" = 5.08E-4 m (total gap thickness across plates, see Figure 5-8)

$$R_{j,\text{model}} = \frac{\Delta x_{He}}{k_g} \qquad \text{(B.6)}$$

$$R_{j,\text{model}} = \frac{5.08E-4}{0.204} = 2.486E-3 \text{ m}^2\text{-K/W}$$

The total thermal resistance considered in the model ($R_{j,\text{model}}$) is about two times larger than the calculated contact resistances for the paired plates ($R_{j,\text{total}}$). This shows that the gaps considered in the model are more than adequate to bound the contact resistances and the other uncertainties, such as thickness tolerances, surface finishing, etc., involved in fabrication of the basket.

If the poison plate is paired with multiple aluminum plates, the total thermal contact resistance across the plates depends on the number of aluminum plates as follows.

$$R_{j,multiple} = R_{j,SS-Al} + (m-1)R_{j,Al-Al} + R_{j,Al-Poison} + R_{j,poison-SS} \qquad \text{(B.7)}$$

m = number of aluminum plates used to pair with poison plate

According to Table B–2, the contact resistances between Al/SS, Al/Al, and Al/poison plates are equal if the contact pressure nears zero. The total thermal resistance for multiple aluminum plates is therefore:

$$R_{j,multiple} = (n+1)R_{j,Al-Al} \qquad \text{(B.8)}$$

n = number of multiple aluminum plates including poison plate

The maximum number of multiple aluminum plates that can be used in 69BTH basket can be calculated by setting $R_{j,multiple}$ in equation (B.8) equal to the total thermal resistance considered in the model, $R_{j,model}$ in equation (B.6).

$$n_{max} = \frac{R_{j,model}}{R_{j,Al-Al}} - 1 \qquad \text{(B.9)}$$

$$n_{max} = \frac{2.486E-3}{4.164E-4} - 1 = 4.97$$

This shows that at least four plates, three aluminum plates and one poison plate can be paired together in 69BTH basket without affecting the thermal performance evaluated in this calculation.

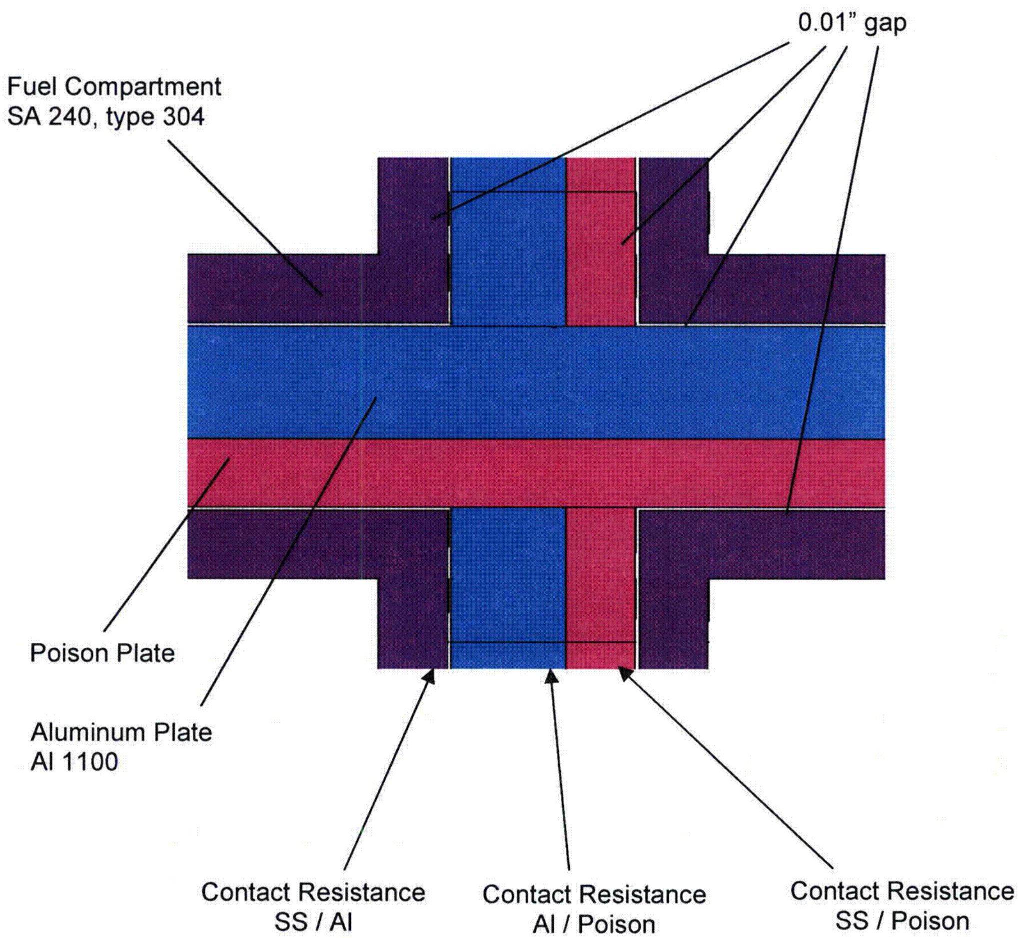

Figure B–1 Location of Contact Resistances

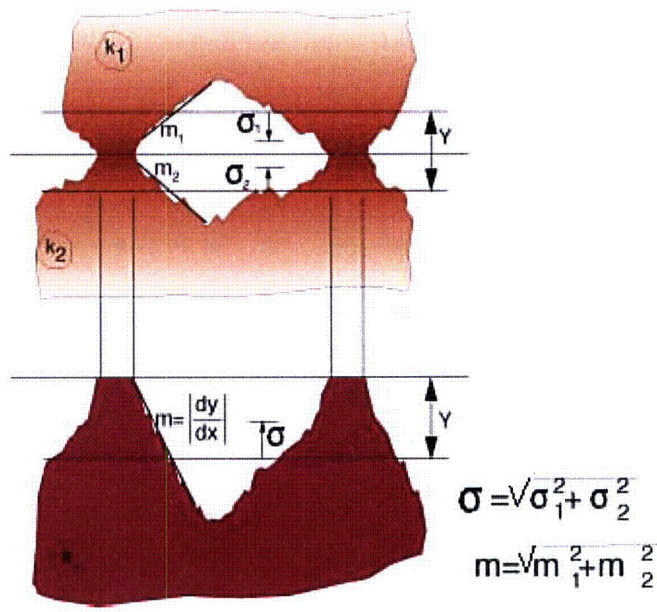

Figure B–2 Conforming Rough Surfaces [23]

APPENDIX C MESH SENSITIVITY ANALYSIS

C.1 Mesh Sensitivity for 69BTH DSC Model

The mesh sensitivity analysis for 69BTH DSC is performed based on a slice model of 69BTH DSC with Boral poison plates. The slice model is 26" long and is recreated by selecting the nodes and elements of the 69BTH DSC model form z=50.8" to z=76.8" (NUH69BTH_C run listed in Table 8-2). The length of the slice model is twice the length of the aluminum plates and the axial gaps between them. This model contains 124,968 elements and 137,423 nodes.

A fine mesh model for the same slice is recreated (NUH69BTH_F run listed in Table 8-3). The number of elements and nodes in the fine meshed model are almost tripled to 391,644 and 414,874, respectively. Fine and coarse meshed models for 69BTH DSC are shown in Figure C–1.

A fixed temperature of 400°F on the outer surface of the DSC shell and a decay heat of 26 kW with HLZC # 1 is selected as boundary conditions for the sensitivity analysis of 69BTH DSC. A peaking factor of 1.2 is considered to apply the heat generation rate on the homogenized fuel assemblies. The heat generation boundary conditions are applied using the same methodology as described in Section 5.2.

The maximum temperatures are retrieved from these models and listed in Table C–1 for comparison.

Table C–1 Maximum Temperatures for Fine and Coarse Mesh Models of 69BTH DSC

DSC type	69BTH DSC with 26 kW Heat Load		
Fuel Assembly Mesh Type	Fine	Coarse	
Run ID	NUH69BTH_F	NUH69BTH_C	
Component	T_{max} (°F)	T_{max} (°F)	Difference ($T_{Fine} - T_{Coarse}$) (°F)
DSC shell	400.0	400.0	0.0
Fuel Cladding	690.7	689.7	1.0
Basket (compartment)	678.6	677.6	1.0
Al / Poison Plate	678.3	677.3	1.0
Basket Rails	460.8	460.8	0.0

As seen in Table C–1, the differences between the maximum temperature for coarse and fine mesh models are approximately 1.0°F. It concludes that the 69BTH DSC model described in Section 5.2 is mesh insensitive and the results reported in Sections 6.0 and 5.3 are adequately accurate for evaluation.

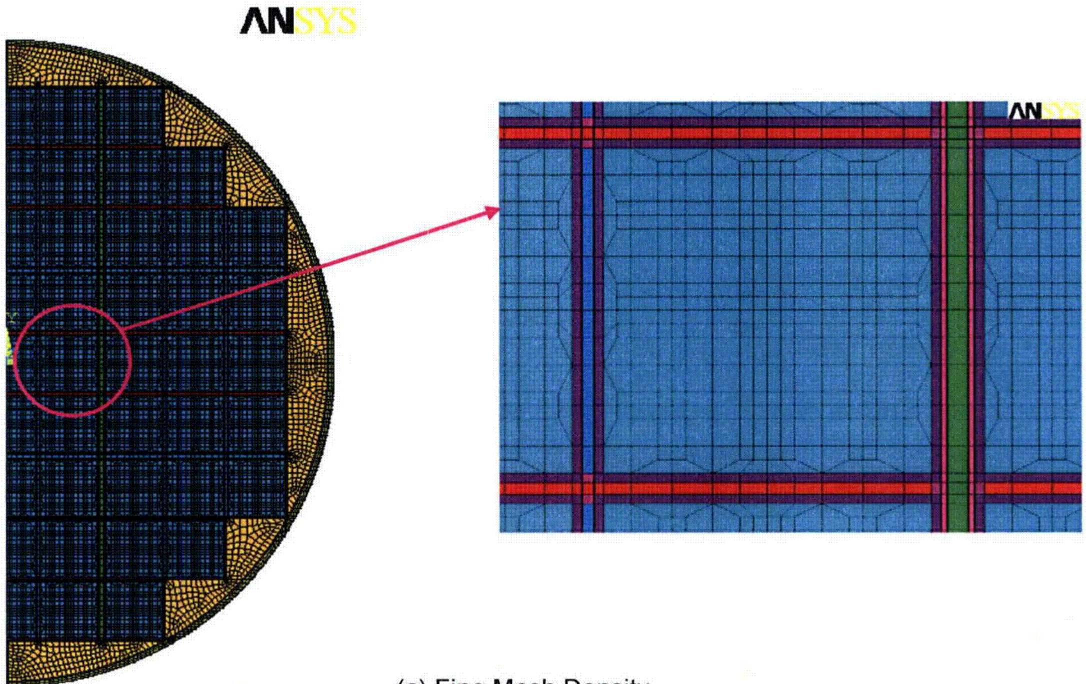

(a) Fine Mesh Density

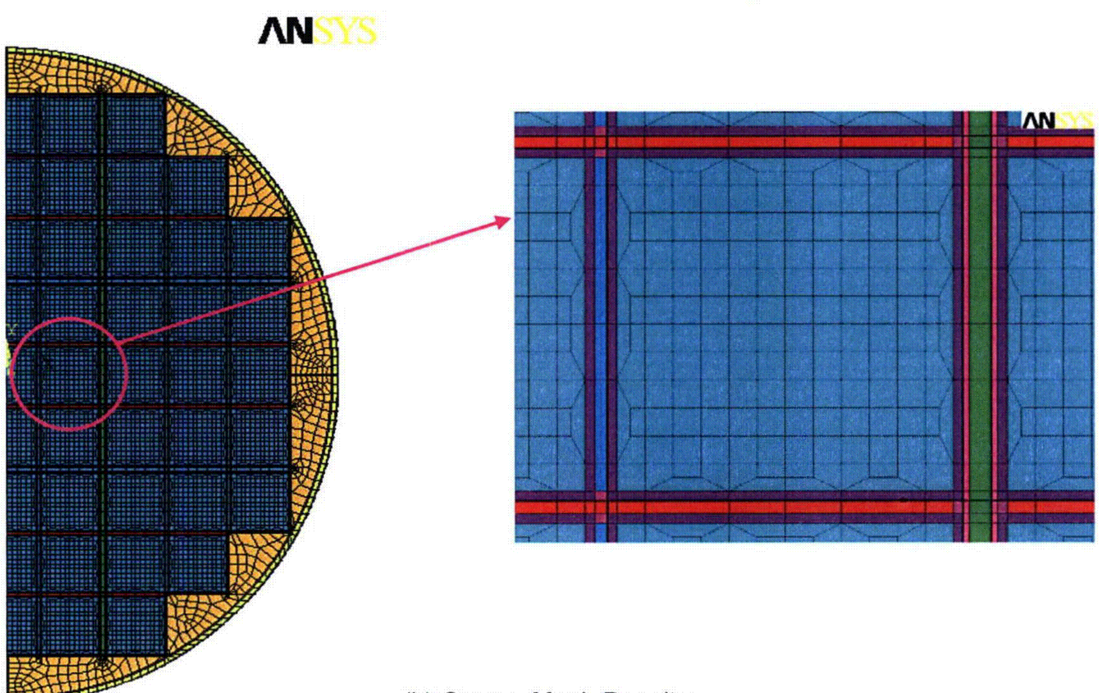

(b) Coarse Mesh Density

Figure C–1 69BTH DSC/Basket Model – Mesh Densities

C.2 Mesh Sensitivity for 37PTH DSC Model

The mesh density of each fuel assembly for the 37PTH DSC model described in Section 5.2 is modeled as 10x10 at the cross section with the largest mesh size of 0.95"×0.95" (37PTH_Model2 run listed in Table 8-2). This model contains 385,933 elements and 409,836 nodes.

A fine mesh model is created in which the fuel assembly mesh density is increased to 12x12 with the largest mesh size of 0.76" ×0.76" (37PTH_Model3 run listed in Table 8-2). The number of elements and nodes in the fine mesh model are increased to 508,605 and 536,592, respectively. Coarse and fine mesh densities for 37PTH DSC models are shown in Figure C–2.

The DSC shell temperature profile retrieved from MP197HB transport cask model for NCT at ambient temperature of 100°F with insolation and a decay heat of 22 kW are selected as boundary conditions for the sensitivity analysis of 37PTH DSC (Based on 0.075" Boral paired with 0.05" Aluminum plates).The boundary conditions are applied using the same methodology as described in Section 5.2. The maximum temperatures are retrieved from these models and listed in Table C–2 for comparison.

Table C–2 Maximum Temperatures for Fine and Coarse Mesh Models of 37PTH DSC

DSC type	37PTH DSC with 22 kW Heat Load		
Fuel Assembly Mesh Type	Fine	Coarse	
Run ID	37PTH_22_100CS3	37PTH_22_100CS	
Component	T_{max} (°F)	T_{max} (°F)	Difference ($T_{Fine} - T_{Coarse}$) (°F)
DSC shell	406.4	406.4	0.0
Fuel Cladding	660.6	659.5	1.1
Basket (compartment)	649.6	648.6	1.0
Al / Poison Plate	649.5	648.4	1.1
Basket Rails	442.6	442.6	0.0

As seen in Table C–2, the differences between the maximum temperature for coarse and fine mesh models are less than 1.5°F. It concludes that the 37PTH DSC model described in Section 5.2 is mesh insensitive and the results reported in Sections 6.0 and 5.3 are adequately accurate for evaluation.

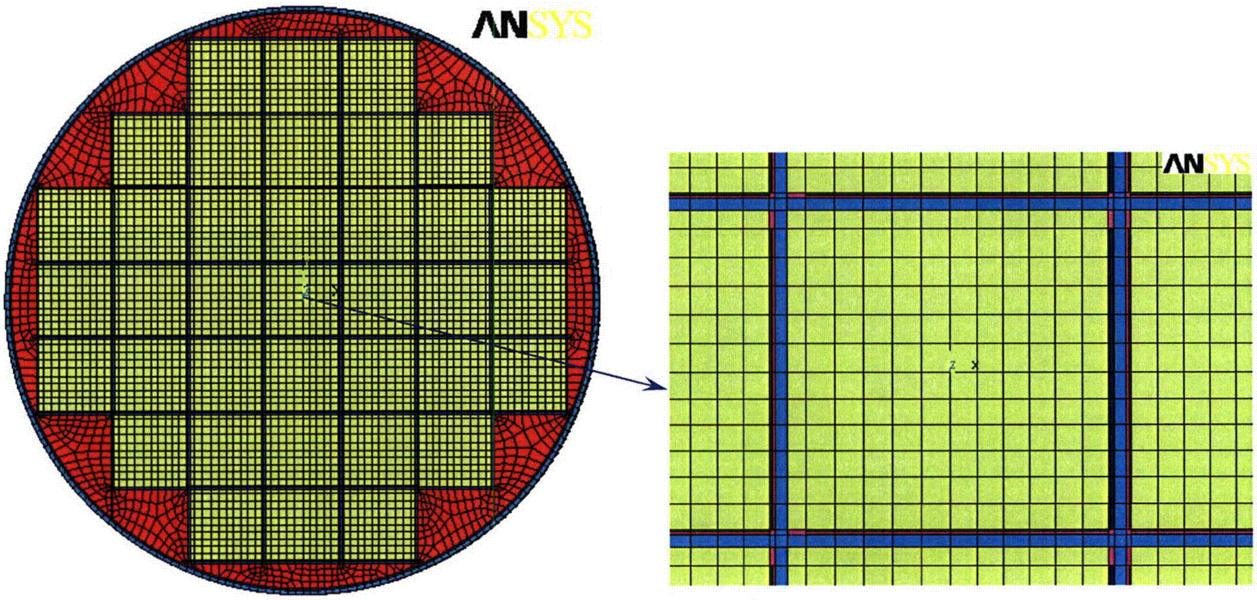

(a) Fine Mesh Density (12x12)

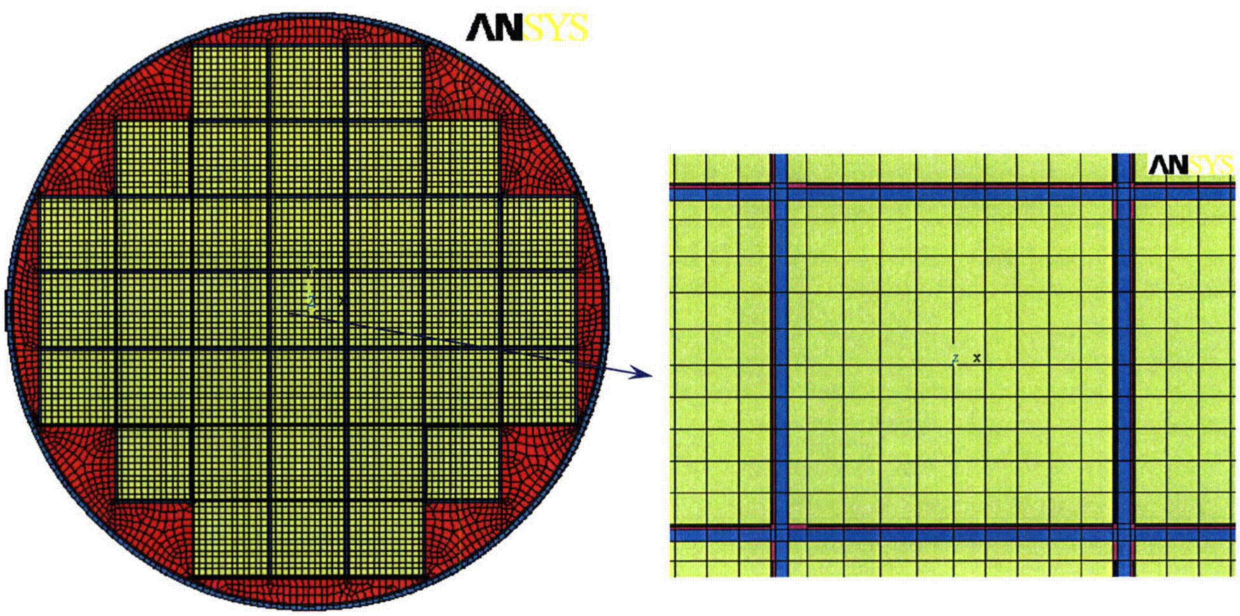

(b) Coarse Mesh Density (10x10)

Figure C–2 37PTH DSC/Basket Model – Mesh Densities

APPENDIX D 37PTH DSC WITH 23.2 KW HEAT LOAD FOR STRUCTURAL ANALYSIS

For the purpose of structural analysis a heat load of 23.3 kW is considered for the 37PTH DSC basket. The corresponding thermal runs for structural analysis are assigned as thermal-structural runs in this section.

The HLZC considered for 23.3 kW heat load is shown in Figure D–1.

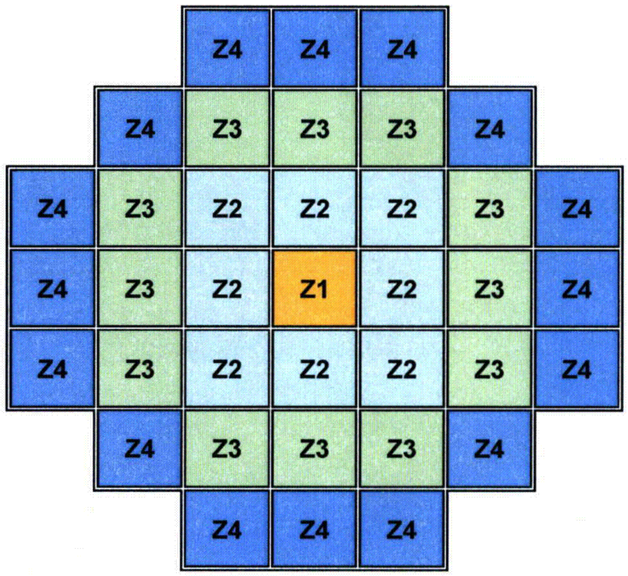

	Zone 1	Zone 2	Zone 3	Zone 4
Max. Decay Heat (kW/FA)	0.40	0.40	0.70	0.70
No. of Fuel Assemblies (1)	1	8	12	16
Max. Decay Heat per Zone (kW)	0.4	3.2	8.4	11.2
Max. Decay Heat per DSC (kW)	23.2 (2)			

Note: (1) Total number of fuel assemblies is 37 for this HLZC
(2) The HLZC for 37PTH is assigned as # 6 in input files

Figure D–1 HLZC in 37PTH Basket for Structural Analysis

As seen in Figure D–1, the heat loads per assembly in this HLZC bound those considered for 22.0 kW heat load shown in Figure 5-13. Since the total heat load and the heat load per assembly in the HLZC considered for the thermal-structural runs are higher than the design values, it is conservative to use the temperature profiles and the temperature gradients from the thermal-structural runs for structural evaluation.

The DSC shell temperatures for the thermal-structural runs are retrieved from the corresponding TC model runs discussed in [10] with 23.3 kW heat load.

Aluminum based neutron absorber with a thickness of 0.075" paired with Al-1100 plates with a thickness of 0.05" were considered in the basket model for the thermal-structural runs. The conductivity of the aluminum based neutron absorber is listed in Table D–1.

Table D–1 Conductivity of Aluminum Based Neutron Absorber

Aluminum Based Neutron Poison ([16], Table 4-1 and [1] Section M.4.3)		
Temperature (°F)	Conductivity (Btu/min-in-°F)	Conductivity (Btu/hr-in-°F)
68	0.120	7.20
212	0.144	8.64
482	0.148	8.88
572	0.148	8.88
774	0.148	8.88

The other material properties, assumptions, conservatism, and the methodology to apply the boundary conditions for the thermal-structural runs are the same as those discussed in Sections 3.0 through 5.0.

The maximum and the average component temperatures for the thermal-structural runs are listed in Table D–2 and Table D–3, respectively.

Table D–2 Maximum Temperatures for Thermal-Structural Runs of 37PTH DSC

Heat Load	23.2 kW	23.2 kW	23.2 kW
Conditions	NCT at 100°F with Insolation	NCT at -20° No Insolation	NCT at -40°F No Insolation
Component	T_{max} (°F)	T_{max} (°F)	T_{max} (°F)
Fuel Cladding	658	592	582
Basket (compartment)	648	580	569
Al / Poison Plate	647	580	569
Basket Rails	456	380	368
Top Shield Plug	319	224	208
Bottom Shield Plug	304	213	198

Table D–3 Average Temperatures for Thermal-Structural Runs of 37PTH DSC

Heat Load	23.2 kW
Conditions	NCT at 100°F with Insolation
Component	T_{avg} (°F)
Fuel Assembly	525
Helium in DSC Cavity	418
Large Rail @ 0° (1)	450
Small Rail @ 45°	447
Large Rail @ 90°	417
Small Rail @ 135°	407
Large Rail @ 180°	387

Note: (1) See the figure below Table 6-6 for orientation angles.

The computation files for the structural-thermal runs are listed in Table D-4.

Table D–4 List of Computation Files for Thermal-Structural Runs of 37PTH DSC

File Name (Input and Output)	Description	Required Files from [10]	Date / Time for Output File
TempMap_23CS	Transfer temp from TC to DSC/Basket model for 37PTH, 23.2 kW @ 100°F	TC_23kW_23CS.db TC_23kW_23CS.rth	08/27/08 10:17 AM
	Transfer temp from TC to DSC/Basket model for 37PTH, 23.2 kW @ -20°F	TC_23kW_20CS.db TC_23kW_20CS.rth	
	Transfer temp from TC to DSC/Basket model for 37PTH, 23.2 kW @ -40°F	TC_23kW_40CS.db TC_23kW_40CS.rth	
37PTH_23_100CS	37PTH basket, NCT, 23.2 kW, 100°F ambient	---	08/27/08 11:38 AM
37PTH_23_20CS	37PTH basket, NCT, 23.2 kW, -20°F ambient	---	08/28/08 10:58 AM
37PTH_23_40CS	37PTH basket, NTC, 23.2 kW, -40°F ambient	---	08/28/08 01:21 PM
37pthc6_23.hg	Heat generation for 37PTH, 23.3 kW	---	05/21/08 05:17 PM

APPENDIX E TEMPERATURE PLOTS FOR DSC SHELLS

The temperatures plots for DSC shell shown in Figure E–1 and Figure E–2 are resulted from analyses in [10] which were saved with the ANSYS computational files.

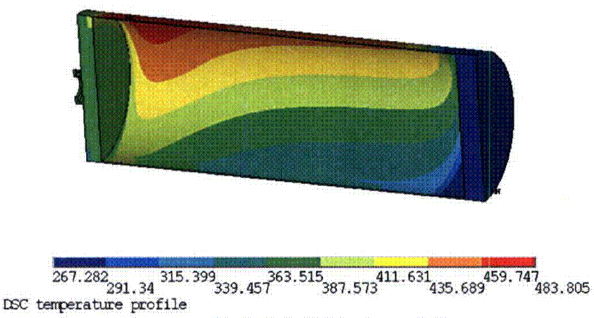

69BTH, 32 kW, NCT

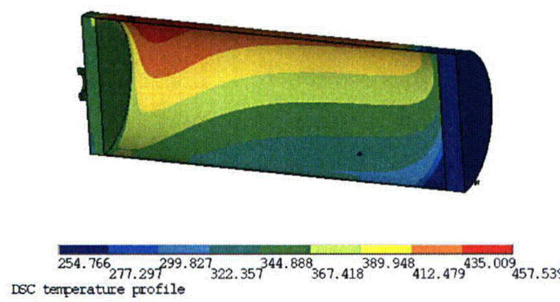

69BTH, 29.2 kW, NCT

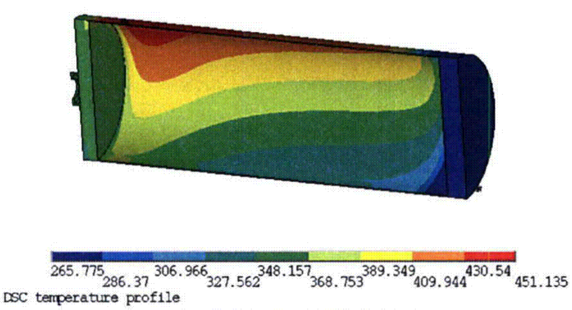

69BTH, 26 kW, NCT

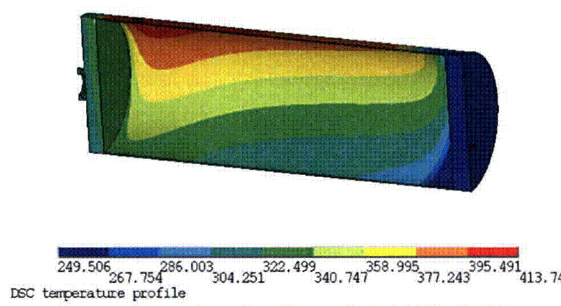

61BTH Type 1, 22 kW, NCT

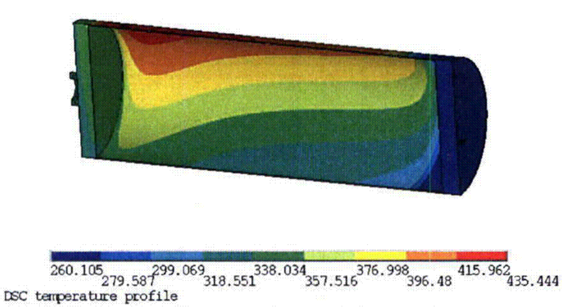

61BTH Type 2, 24 kW, NCT

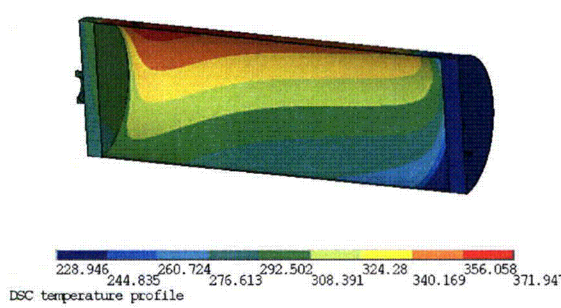

61BT, 18.3 kW, NCT

Figure E–1 DSC Temperature Plots, BWR DSC

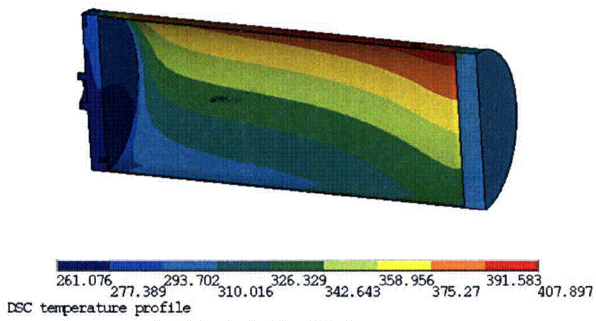

37PTH, 22kW, NCT

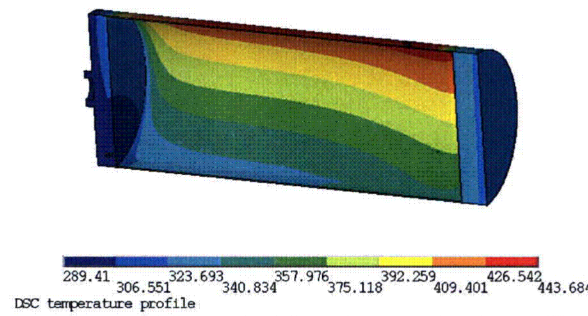

32PTH / 32PTH1 Type 1, 26 kW, NCT

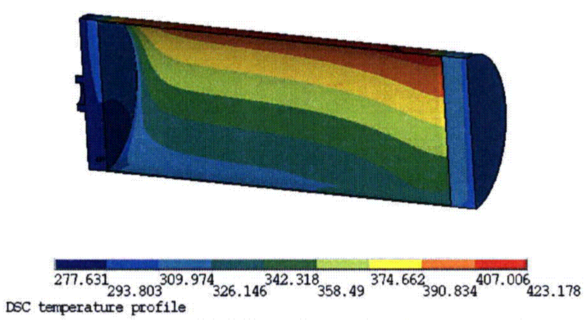

32PTH1 Type 2, 24 kW, NCT

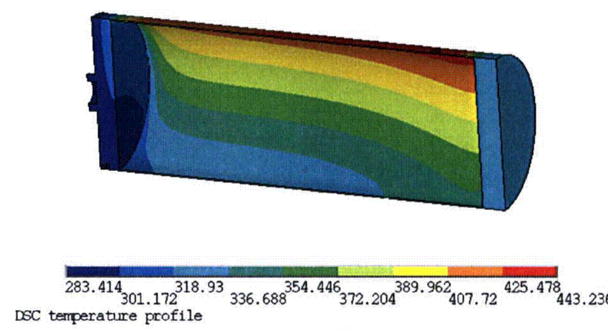

32PT, 24 kW, NCT

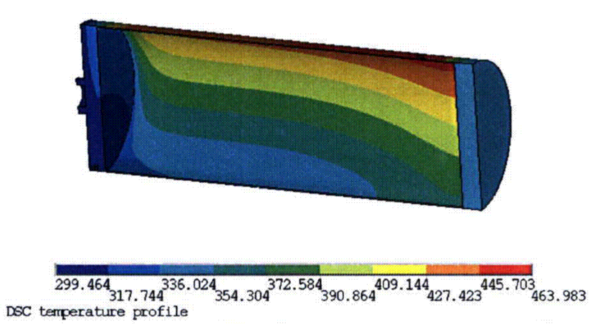

24PTH, Type 1 or 2, 26 kW, NCT

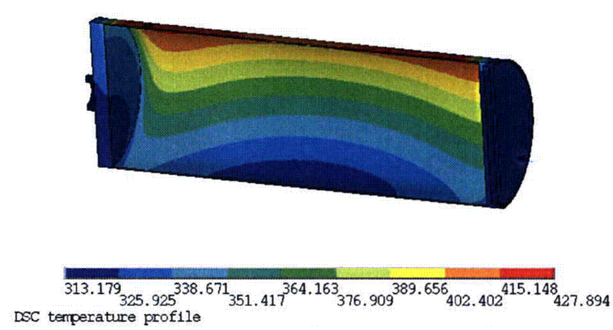

24PT4, 24 kW, NCT

Figure E–2 DSC Temperature Plots, PWR DSC

APPENDIX F THERMAL ANALYSIS RESULTS FOR MP197HB LOADED WITH DSC TYPE 24PTH-S AND 26KW HEAT LOAD

As discussed in Section 7.0, except for 69BTH and 37PTH DSCs, no additional thermal analysis is performed for all other DSCs (i.e., 61BTH, 61BT, 32PTH, 32PTH1, 32PT, 24PTH and 24PT4) that are previously evaluated under 10 CFR Part 72 conditions. As described in [10], Section 5.0, the maximum fuel cladding and basket temperatures for these DSCs in MP197HB cask are taken from 10 CFR Part 72 SARs by comparing the DSC shell temperature profile in MP197HB TC model with corresponding profile in the 10 CFR Part 72 SAR and represented as the bounding values for transport condition as listed in Table 7-1 and Table 7-2.

To justify the conservatism of the above methodology, 24PTH-S DSC (w/o Al inserts) under NCT is selected as the limiting case among the DSCs listed in Table 7-1 for thermal analysis since it has the smallest margin (19°F) for the maximum fuel cladding temperature under storage conditions and has the highest heat load for transportation conditions (26 kW).

Thermal analysis for 24PTH-S DSC (w/o Al inserts) for NCT is based on the same methodology and DSC model used previously for storage conditions in 10 CFR Part 72 SAR [1], Section P.4. The 24PTH DSC shell temperature profile under NCT calculated in MP197HB model [10] is mapped onto the 3D 24PTH-S DSC model from [9] using the macro "TempMap_24PTH.inp" listed in Table F-2Table F-2. Uniform heat load zone configuration with the maximum heat load of 26 kW is applied in the 24PTH-S DSC model.

Table F-1 presents a comparison of the maximum 24PTH-S DSC (w/o Al inserts) component temperatures between the bounding values listed in Table 7-1 and Table 7-2 from 10 CFR Part 72 SAR [1] and the results analyzed in this Appendix for NCT.

Table F-1 Maximum DSC Temperatures for NCT Thermal Evaluation

DSC Type	DSC Type 24PTH-S w/o Al inserts		
Operating Condition	Normal Transfer @ 31.2 kW	NCT @ 26 kW	
NCT Thermal Evaluation	Table 7-1 / Table 7-2	24PTH-S DSC Model	
Run ID	-	24PTH_26NCT (1)	
Heat Load Zone Configuration	Uniform (1.3 kW/FA)	Uniform (1.083 kW/FA)	Difference
Maximum Component Temperature	**T_{max} (°F)**	**T_{max} (°F)**	**ΔT (°F)**
Fuel Cladding	733	664 (=661+3)	+ 69
Fuel Compartment	682	616 (=612+4)	+ 66
Al/Poison	681	615 (=611+4)	+ 66
Basket Rail	576	490 (=486+4)	+ 86
DSC Shell	475 ([1],Table P.4-10)	463	+ 12

Note

(1) The bounding maximum temperature increases are 3°F for fuel cladding and 4°F for basket components to account for 2.375" steel band width as discussed in [9].

As seen from Table F-1Table F-1, the maximum fuel cladding and basket component temperatures for 24PTH-S DSC (w/o Al inserts) under NCT are 60°F lower than the bounding values listed in Table 7-1 and Table 7-2 from the applicable 10 CFR Part 72 SAR [1]. This large difference demonstrates that the comparison of the DSC shell temperatures as discussed above is a conservative approach to bound the maximum fuel cladding and basket component temperatures for transport conditions.

The computation files for the thermal analysis of 24PTH-S DSC (w/o Al inserts) in MP197HB cask are listed in Table F-2Table F-2. All the runs are performed using ANSYS version 10.0 [28] with operating system “Linux RedHat ES 5.1”, and CPU “Opteron 275 DC 2.2 GHz” / ”Xeon 5160 DC 3.0 GHz”.

Table F-2 List of Computation Files for Thermal Analysis Run of 24PTH-S DSC in MP197HB TC

File Name (Input and Output)	Description	Required Files from [10]	Date / Time for Output File
TempMap_24PTH [38]	Transfer temp from TC to DSC/Basket model for 24PTH, 26 kW @NCT, 100°F ambient	TC_24PTH_26CS.db TC_24PTH_26CS.rth	11/10/08 01:48 PM
24PTH_26NCT	24PTH-S basket, NCT, 26 kW, 100°F ambient	---	02/03/10 05:14 PM
HLC6.mac	Heat generation for 24PTH, 26 kW	---	01/06/10 00:20 PM
M3C5SD1.db	DSC Type 24PTH-S Model (w/o Al insert) from [9] Table 7-1.	---	06/04/03 08:08 AM
AllFuel.mp	Material properties for 24PTH basket from [9].	---	05/15/03 04:20 PM
Results_sen.mac	Post-processing macro for maximum 24PTH DSC component temperatures	---	01/06/10 02:21 PM
Macro.mac	Macro for maximum and minimum temperatures	---	11/05/08 04:00 PM

APPENDIX G SENSITIVITY ANALYSIS - GAPS BETWEEN BASKET PLATES

To justify the conservatism of the assumed gaps between basket plates used for the thermal evaluation for the MP197HB TC, 69BTH DSC with 32 kW heat load in MP197HB TC without external fins is selected as the limiting case for thermal sensitivity analysis since it has the highest maximum fuel cladding (674°F) [10, Table H-1] and has the highest heat loads for transportation conditions (32 kW) among all DSCs listed in Table 7-1.

The contact gaps between the basket plates are related only to the flatness and roughness tolerance of the plates. The micro gaps related to these tolerances are non-uniform and provide interference contact at some areas and gaps on the other areas. As justified in APPENDIX B, the assumed uniform gap of 0.01" between the basket plates is two times larger than the contact resistance between the plates and is thus conservative. As discussed in Section 3.1, additional gaps between basket plates in the 69BTH DSC model are summarized below:

69BTH-c) 0.01" gap between the sections of the paired aluminum and poison plates in axial direction as shown in Figure 5-9;

69BTH-d) 0.1" gap between the small aluminum rails in basket corners as shown in Figure 5-7;

69BTH-d) 0.1" gap between the two pieces of large aluminum rails at 0°-180° and 90°-270° orientations as shown in Figure 5-7.

A sensitivity analysis to determine the effect of these gaps on the thermal performance is based on MP197HB TC with no external fins loaded with 69BTH DSC and 32 kW heat load under NCT at 100°F ambient as discussed in [10], Appendix H. The DSC shell temperature profile retrieved from the MP197HB TC model described in [10] is applied as boundary conditions for the 69BTH DSC model, which is consistent with the approach described in Section 5.1. The results of this sensitivity analysis for doubling the sizes of these gaps in 69BTH DSC during NCT are summarized in Table G-1.

Table G-1 Maximum 69BTH DSC Temperatures for NCT Thermal Evaluation

	$T_{max, Fuel}$ (°F)	$T_{max, Comp}$ (°F)	$T_{max, Al/Poison}$ (°F)	$T_{max, Rail}$ (°F)
69BTH, 32kW from [10], Appendix H	674.3	638.3	621.8	534.3
69BTH, 32kW gap sizes 69BTH-c, -d, -e doubled	674.5	638.5	622.0	534.3
Difference (°F)	+ 0.2	+ 0.2	+ 0.2	0

As seen from Table G-1, doubling the size of the gaps listed above increases the maximum temperatures by less than 0.5°F. Therefore, the effect of these gaps on thermal performance is insignificant.

The computation file for the thermal sensitivity analysis run is listed in Table G-2. All the runs are performed using ANSYS version 10.0 [28] with operating system "Linux RedHat ES 5.1", and CPU "Opteron 275 DC 2.2 GHz" / "Xeon 5160 DC 3.0 GHz".

Table G-2 List of Computation Files for Thermal Sensitivity Analysis Run – Gap Effect

File Name (Input and Output)	Description	Date / Time for Output File
69BTH_32U_4G	69BTH basket in MP197HB without external fins, 32 kW @ NCT, 100°F ambient, gap sizes 69BTH-c, -d, -e doubled.	02/03/10 08:37 PM
TBCS_32U.inp [10], SBCS_32U.inp [10], BBCS_32U.inp [10]	DSC shell temperature input files for 69BTH DSC in MP197HB without external fins, 32 kW @ NCT, 100°F ambient	10/15/08 08:05 PM 10/15/08 08:06 PM 10/15/08 08:05 PM

APPENDIX H SENSITIVITY STUDY FOR EFFECTS OF HIGH BURNUP DAMAGED FUEL ASSEMBLIES

The cladding of high burnup damaged fuel assemblies (FAs) can experience further damages during NCT. To bound the effect of these damages, a sensitivity analysis is conducted considering the worst case condition, in which the high burnup damaged fuel assemblies become rubble. Following the rationale in NUREG/CR-6835 [39], it is assumed that the fuel rods do not shatter into very small pieces and the fuel rubble is not in a tightly compacted mass. Instead, the fuel rubble is assumed to be 50% void by volume. Since the end drop is the most critical condition under NCT and the end caps and the fuel compartment walls constrain the fuel assembly, the fuel rubble is assumed to be contained within the original active fuel volume, albeit in the lower portion of the original volume. Consistent with NUREG/CR-6835, the axial-burnup variation in the rubble is also assumed to be uniform.

The height of the fuel rubble with the assumption of 50% void by volume is determined based on the volume of fuel rods. The fuel rubble height for the BWR FAs listed in [6] is summarized in Table H-1.

Table H-1 Summary of Fuel Rubble Height for BWR FAs in MP197HB TC

Transnuclear ID	7x7-49/0	8x8-63/1	8x8-62/2	8x8-60/4	8x8-60/1	9x9-74/2	10x10-92/2	7x7- 49/0
Initial Design FA	GE1-GE3	GE4	GE5	GE8	GE9/10	GE11/13	GE12/14	ENC-IIIA
No. Fuel Rod	49	63	62	60	60	66	78	49
Active Fuel Length, in	150	146	150	150	150	146	150	144
Fuel Rod OD, in	0.563	0.493	0.483	0.483	0.483	0.44	0.404	0.57
$V_{UO2, Compact}$, in^3 (1)	2330	2236	2170	2100	2100	2005	2102	2292
V_{Rubble}, in^3 (50% Void Volume)	4659	4471	4339	4199	4199	4010	4203	4585
Fuel Rubble Length, in	129	124	121	117	117	111	117	127
Transnuclear ID	7x7-48/0	8x8-60/4	8x8-62/2	9x9-79/2	Siemens QFA	10x10-91/1	ABB-8x8	ABB-10x10
Initial Design FA	ENC-III	ENC Va/Vb	FANP 8x8-2	FANP 9x9-2	9x9	ATRIUM 10/10XM	SVEA-64	SVEA-100
No. Fuel Rod	48	60	62	79	72	83	64	96
Active Fuel Length, in	144	144	150	150	145.24	149.45	150.59	150.59
Fuel Rod OD, in	0.57	0.5015	0.484	0.424	0.433	0.3957	0.461	0.378
$V_{UO2, Compact}$, in^3 (1)	2246	2173	2179	2130	1961	2055	2048	2066
V_{Rubble}, in^3 (50% Void Volume)	4491	4346	4357	4261	3921	4110	4096	4131
Fuel Rubble Length, in	125	121	121	118	**109**	114	114	115

Note (1): Compact volume for fuel pellets estimated by $(\text{Fuel Rod OD})^2$ x (No. of Fuel Rods) x (Active Fuel Length).

The limiting case based on MP197HB TC loading with 69BTH DSC and 32 kW heat load without external fins is selected for thermal sensitivity analysis since it has the highest maximum fuel cladding (674°F) [10, Table H-1] and has the highest heat loads for transportation conditions (32 kW) among all DSC types listed in Table 7-1. In the sensitivity run, the heat generation rate corresponding to the damaged fuel assemblies is applied uniformly over the fuel rubble height of 108" concentrated at the bottom axial portion of the original active fuel volume with a peaking factor of one. The DSC shell temperature profile retrieved from the MP197HB cask model described in [10] is applied as boundary conditions for the 69BTH DSC model, which is consistent with the approach described in Section 5.1.

Considering the uncertainty of effective thermal conductivity for the fuel rubble region, two sensitivity runs are performed by the following assumptions for fuel rubble thermal conductivity:

1) 50% reduction of effective fuel conductivity for intact FA listed in Table 4-3;

2) helium conductivity listed in Table 4-9.

The maximum component temperatures resulting from the sensitivity analysis are compared to the corresponding values for the 69BTH DSC with intact fuel assemblies in Table H-2.

Table H-2 Maximum 69BTH DSC Temperatures for NCT Thermal Evaluation

	$T_{max, Fuel}$ (°F)	$T_{max, Comp}$ (°F)	$T_{max, Al/Poison}$ (°F)	$T_{max, Rail}$ (°F)
69BTH, 32kW from [10], Appendix H	674.3	638.3	621.8	534.3
69BTH, 32kW (fuel rubble based on 50% intact fuel conductivity)	679.3	643.9	627.6	537.0
69BTH, 32kW (fuel rubble based on helium conductivity)	679.6	644.3	628.0	537.1
Maximum Difference (°F)	+ 5.3	+ 6.0	+ 6.2	+ 2.8

As seen in the above table, the maximum fuel cladding temperature changes at most by 6°F. Considering the large margin of 78°F for the fuel cladding temperature, this small change does not have any significant effect on the thermal performance of the cask and DSC.

The computation files for the thermal sensitivity analysis runs are listed in Table H-3. All the runs are performed using ANSYS version 10.0 [28] with operating system "Linux RedHat ES 5.1", and CPU "Opteron 275 DC 2.2 GHz" / "Xeon 5160 DC 3.0 GHz".

Table H-3 List of Computation Files for Thermal Sensitivity Analysis Run – High Burnup Damaged FAs

File Name (Input and Output)	**Description**	**Date / Time for Output File**
69BTH_32U_4F108rb	69BTH basket in MP197HB without external fins, 32 kW @NCT, 100°F ambient – fuel rubble based on 50% intact fuel effective conductivity.	01/29/10 02:30 PM
69BTH_32U_4F108h	69BTH basket in MP197HB without external fins, 32 kW @NCT, 100°F ambient – fuel rubble based on helium conductivity.	01/29/10 04:42 PM
HeatGen_52bf108.inp	Heat generation for 69BTH, HLZC#4, with 108" Fuel Rubble Damaged FAs.	01/28/10 12:22 PM
TBCS_32U.inp [10], SBCS_32U.inp [10], BBCS_32U.inp [10]	DSC shell temperature input files for 69BTH DSC in MP197HB without external fins, 32 kW @ NCT, 100°F ambient	10/15/08 08:05 PM 10/15/08 08:06 PM 10/15/08 08:05 PM
Rubbled_Fuel.xls	Spreadsheet to calculate fuel rubble height for BWR FAs in MP197HB TC	02/04/10 04:26 PM

APPENDIX I JUSTIFICATION FOR POISON MATERIALS DENSITY AND SPECIFIC HEAT

Three different poison materials [43] as shown in Table 5-4 and listed below are used as neutron absorber materials for criticality control in the 69BTH basket depending on the HLZC:

1) BORAL® Composite - A precision hot-rolled composite plate material consisting of a core of mixed aluminum and boron carbide (B_4C) particles with an 1100 Series aluminum cladding on both external surfaces.

2) BORTEC® Metal Matrix Composite (MMC) - A composite of fine B_4C particles rolled or extruded in an aluminum or aluminum alloy matrix with B_4C contents up to 45% by volume.

3) Borated Aluminum (BAl)– An alloy material incorporating enriched Boron as a second phase in standard aluminum compositions.

The main components of poison materials are aluminum and B_4C or Boron. Poison material specific heat (c_p) and density (ρ) are assumed equal to those of Al 6061 for the calculation of 69BTH basket effective density and specific heat in Section 5.3.1 for use in transient HAC thermal evaluations.

The density (ρ) and specific heat (Cp) of Aluminum 6061 and boron carbide (B_4C) are calculated in the spreadsheet (Poison_Cp.xls) and listed in Table I-1.

Table I-1 Density and Specific Heat for Boron Carbide (B_4C) and Al 6061

	Al 6061 [6]		Boron Carbide (B_4C) [40]				
Temp	ρ	Cp	ρ (1)	ρ	Cp (2)	Cp	$(\rho x Cp)_{Al6061}/$
(°F)	(lbm/in^3)	(Btu/lbm-°F)	(gm/cm^3)	(lbm/in^3)	(kJ/kg-K)	(Btu/lbm-°F)	$(\rho x Cp)_{B_4C}$
70	0.098	0.213	2.500	0.090	0.991	0.237	0.98
100		0.215			1.013	0.242	0.96
150		0.218			1.051	0.251	0.94
200		0.221			1.088	0.260	0.92
250		0.223			1.124	0.269	0.90
300		0.226			1.161	0.277	0.88
350		0.228			1.196	0.286	0.87
400		0.230			1.231	0.294	0.85

Notes: (1) 100% theoretical density at 300K from [40], Section 8.4.3.

(2) Based on Eq. (8-3) from [40], Section 8.2.2.

As shown in Table I-1, specific heat and heat capacity (ρxCp) of Al 6061 are lower than those of B_4C. Therefore, incorporating B_4C into aluminum alloy has no adverse impact on overall heat capacity compared to aluminum alloy.

Samples of typical Borated Al, such as those proposed for use in the 69BTH basket, were tested for thermophysical properties in [42]. Table I- 2 summarizes the heat capacity results for Borated Al from [42] and Aluminum 6061.

Table I- 2 Density and Specific Heat for Poison Materials

	Al 6061 [6]		Borated Al [42]		
Temp (°F)	ρ (lbm/in³)	Cp (Btu/lbm-°F)	ρ ⁽¹⁾ (lbm/in³)	Cp ⁽²⁾ (Btu/lbm-°F)	$(\rho x Cp)_{Al6061}$ / $(\rho x Cp)_{BAl}$
70	0.098	0.213	0.097	0.207	**1.04**
100		0.215		0.212	**1.02**
150		0.218		0.220	1.00
200		0.221		0.225	0.99
250		0.223		0.229	0.98
300		0.226		0.233	0.98
350		0.228		0.236	0.97
400		0.230		0.239	0.97

Notes: (1) Based on density value of 2.693 gm/cm³ from test report PRL-801 [42].

(2) Interpolated values based on test report PRL-801 [42], Table 1.

As shown in Table I- 2, specific heat and heat capacity (ρxCp) for Al 6061 are lower than those of the Borated Aluminum samples for operating temperatures over 150°F. Since the poison material temperatures are over 150°F for all analyzed cases, assuming the specific heat and density of Al 6061 for poison materials is valid and has no adverse impact on the transient thermal evaluations.

Enclosure 35 to TN E-29128

A Survey of Strain-Rate Effects for Some Common Structural Materials Used in Radioactive Material Packaging and Transportation Systems, BMI-1954, associated with RAI 2-14

BMI-1954

A SURVEY OF STRAIN-RATE EFFECTS FOR SOME COMMON STRUCTURAL MATERIALS USED IN RADIOACTIVE MATERIAL PACKAGING AND TRANSPORTATION SYSTEMS

Topical Report

R. A. Robinson

A. A. Lawrence

BATTELLE
Columbus Laboratories
Columbus, Ohio

Report Date: August, 1976

PREPARED FOR THE
U. S. ENERGY RESEARCH AND DEVELOPMENT ADMINISTRATION
UNDER CONTRACT NO. W-7405-eng-92

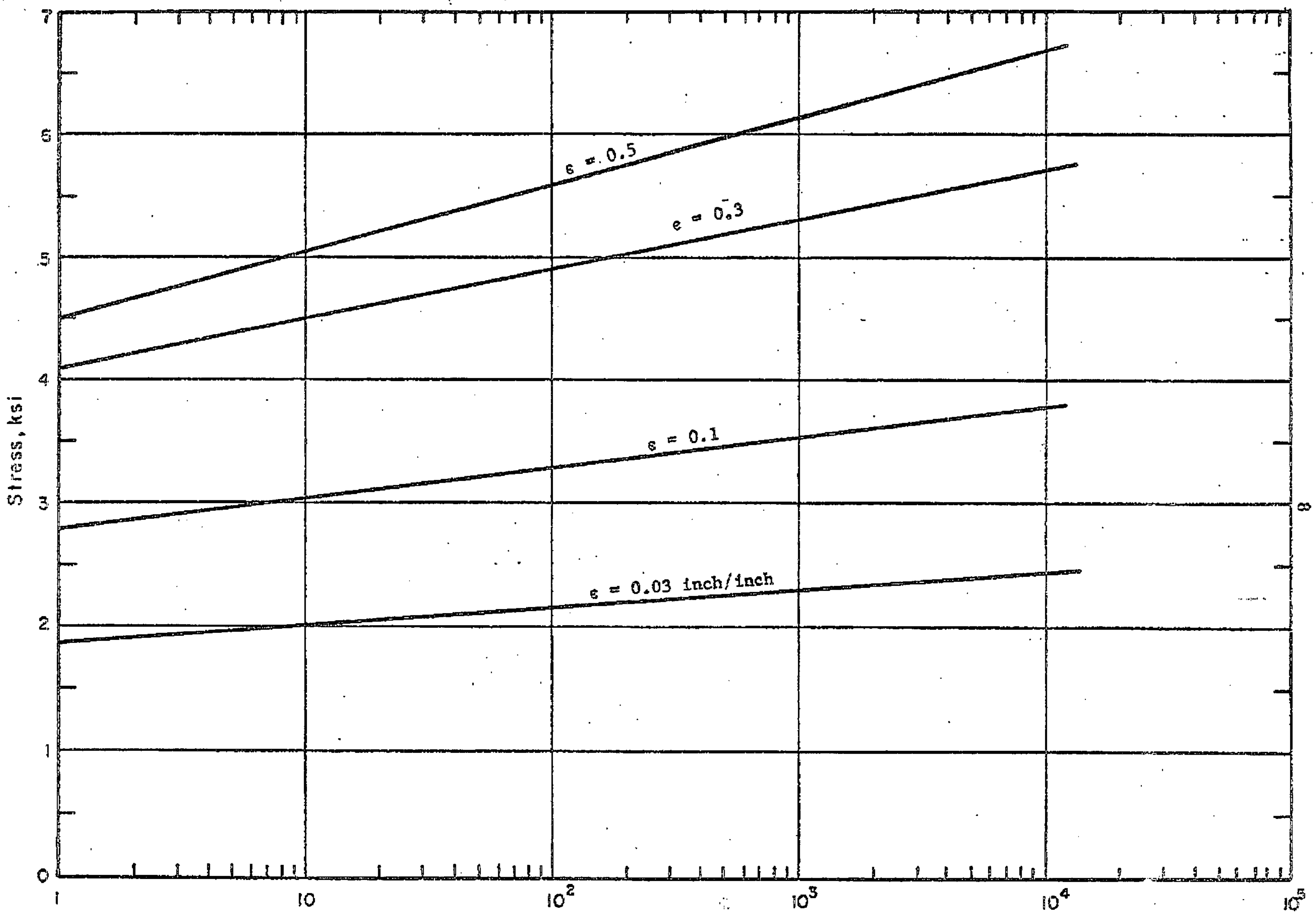
Stress, ksi
0
1
2
3
4
5
6
7
1
10
10^2
10^3
10^4
10^5
ε = 0.03 inch/inch
ε = 0.1
ε = 0.3
ε = 0.5

TABLE 1. LEAD PROPERTIES

Material Description		Static Strength, ksi		Dynamic Strength, ksi						Author: Bailey, J.A. and Singer, A.R.E.	
Alloy Code	Comp. w/o	Yield	Tensile	Yield	Tensile	Strain	Strain Rate in./in./sec	Impact Velocity, ft/sec.	Temperature, F	Comments	Ref. No.
Lead	99.98			5.0	-	2.0	0.4		RT	Logarithmic Cam Plastometer compression	5
Chem.	0.003Cu			6.0	-		9			Strain = natural strain	
Grade A	0.003Fe			6.5	-		101			Dynamic strength=true stress.	
	0.002Zn			7.0	-		311			Specimen:	
	0.002Ag									Width - 1 in.	
										Thick - 0.125 in.	
				1.7	2.5	2.0	0.4		230	Compression.	5
				2.6	3.3		9			Peak in dynamic tensile column at strain of	
				3.7	4.4		101			~ 0.3 to 0.4.	
				4.3	5.0		311				
				1.5	2.0	2.0	0.4		338	Compression.	5
				2.0	2.7		9			Peak in dynamic tensile column at strain of	
				3.0	3.6		101			~ 0.2 to 0.4.	
				3.5	4.4		311				
				0.4	0.8		0.4		500	Compression.	5
				1.1	1.5		9			Peak in dynamic tensile column at strain of	
				1.8	2.2		101			~ 0.2 to 0.4.	
				2.4	2.7		311				
				0.3	0.6		0.4		572	Compression.	5
				1.0	1.2		9			Peak in dynamic tensile column at strain of	
				1.7	1.9		101			~ 0.2 to 0.4.	
				2.2	2.4		311				
										All data interpolated from curves.	

List of Changed SAR Pages and Drawings, with Indication of the Reasons for Changes

SAR Page or Drawing Number	RAI #	Enclosure 31 Item	Notes
SAR Cover Page			Editorial - updated revision level
7-1	3-17		
7-3	3-17		
7-16		Item 1	Editorial
Appendix A Master TOC page 1			Shifted information
Appendix A Master TOC page 2			Update Table of Contents
Appendix A Master TOC page 3			Shifted information
Appendix A Master TOC page 4			Shifted information
Appendix A Master TOC page 5			Shifted information
Appendix A Master TOC page 6			Shifted information
Appendix A Master TOC page 7			Update Table of Contents
Appendix A Master TOC page 8			Shifted information
Appendix A Master TOC page 9			Update Table of Contents
Appendix A Master TOC page 10		Item 1	Update Table of Contents
Appendix A Master TOC page 11		Item 1	Update Table of Contents
Appendix A Master TOC page 12			Update Table of Contents
Appendix A Master TOC page 13			Update Table of Contents
Appendix A Master TOC page 14			Update Table of Contents
Appendix A Master TOC page 15			Update Table of Contents
Appendix A Master TOC page 16			Update Table of Contents
A.1-i			Update Table of Contents
A.1-1			Consistency
A.1-2	3-16		
A.1-3	2-6, 2-33		Consistency
A.1-4	2-6		Consistency
A.1-7	2-6		
A.1-8	2-6		Consistency
A.1-9			Consistency
A.1-10	3-16		
A.1-12			Consistency
A.1.4.1-1	2-5, 2-33		
A.1.4.1-6	2-7, 5-16		
A.1.4.1-9	2-7, 5-16		
A.1.4.1-10	2-7, 5-16		

List of Changed SAR Pages and Drawings, with Indication of the Reasons for Changes

SAR Page or Drawing Number	RAI #	Enclosure 31 Item	Notes
A.1.4.2-1	2-5		
A.1.4.2-3	2-33		
A.1.4.2-9	6-1		
A.1.4.2-10	6-1, P6-3		
A.1.4.2-11		Item 1	Editorial
A.1.4.3-i			Update Table of Contents
A.1.4.3-1	2-5		
A.1.4.3-2		Item 1	Consistency
A.1.4.3-3	2-2		
A.1.4.3-4	2-33		
A.1.4.3-6	2-7, 5-16, 6-5		
A.1.4.3-10	2-7, 5-16		
A.1.4.3-13	6-1		
A.1.4.3-14	6-1, P6-3		
A.1.4.3-14A	6-5		
A.1.4.3-14B	6-5, P6-3		
A.1.4.3-15	6-5		
A.1.4.4-i			Update Table of Contents
A.1.4.4-1	2-5		
A.1.4.4-2		Item 1	Consistency
A.1.4.4-4	2-33		
A.1.4.4-6	2-7, 5-16, 6-5		
A.1.4.4-10	6-5		
A.1.4.4-12	6-5		
A.1.4.4-13	6-1, P6-3		
A.1.4.4-14	6-5, P6-3		
A.1.4.5-i			Update Table of Contents
A.1.4.5-1	2-5		
A.1.4.5-2	2-2	Item 1	Consistency
A.1.4.5-4	2-33		
A.1.4.5-6	2-7, 5-16, 6-5		
A.1.4.5-10	6-5		
A.1.4.5-13	6-1		
A.1.4.5-14	6-1, P6-3		
A.1.4.5-15	6-5		
A.1.4.5-15A	6-5, P6-3		

List of Changed SAR Pages and Drawings, with Indication of the Reasons for Changes

SAR Page or Drawing Number	RAI #	Enclosure 31 Item	Notes
A.1.4.5-16	6-5		
A.1.4.6-i			Update Table of Contents
A.1.4.6-1	2-5		
A.1.4.6-2	2-2	Item 1	Consistency
A.1.4.6-4	2-33		
A.1.4.6-11	6-1, 6-5, P6-3		
A.1.4.6-12		Item 1	Editorial
A.1.4.6-13		Item 1	Editorial
A.1.4.7-i			Update Table of Contents
A.1.4.7-1	2-5, 2-33, 2-34		
A.1.4.7-2	1-1		
A.1.4.7-3	2-7, 5-16		
A.1.4.7-6	2-7, 5-16		
A.1.4.7-7	2-7, 5-16		
A.1.4.7-8	1-1		
A.1.4.8-1	2-5		
A.1.4.8-2		Item 1	Consistency
A.1.4.8-3	2-2		
A.1.4.8-4	2-33		
A.1.4.8-5		Item 1	Consistency
A.1.4.8-6	2-7, 5-16	Item 1	Consistency
A.1.4.8-12	2-7, 5-16		
A.1.4.8-13	2-7, 5-16		
A.1.4.9-1	2-33		
A.1.4.9-2	2-2		
A.1.4.9-3	2-7, 5-16		
A.1.4.9-5		Item 2	Fabrication Enhancement
A.1.4.9-7	2-7, 5-16		
A.1.4.9-8	2-7, 5-16		
A.1.4.9A-i	2-6		
A.1.4.9A-1	2-6		
A.1.4.9A-2	2-6		
A.1.4.9A-3	2-6		
A.1.4.9A-4	2-6		

List of Changed SAR Pages and Drawings, with Indication of the Reasons for Changes

SAR Page or Drawing Number	RAI #	Enclosure 31 Item	Notes
A.1.4.9A-5	2-6		
A.1.4.10-i			Update Table of Contents
A.1.4.10-1			Updated drawings MP197HB-71-1001, 1002, 1003, 1004, 1005, 1008 and 1009
A.1.4.10-2			Updated drawing NUH24PTH-71-1003
A.1.4.10-3			Updated drawings NUH32PTH-71-1001, -1002, -1015 and NUH32PTH TYPE 1-71-1001
A.1.4.10-4			Updated drawings NUH32PTH TYPE 1-71-1003 and -1004, NUH32PTH1-71-1003, NUH37PTH-71-1001, -1002, -1003, -1004, -1011, -1012, and -1015
A.1.4.10-5			Updated drawings NUH61BT-71-1001, NUH61BTH-71-1100, -1102 and -1106
A.1.4.10-6			Updated drawings NUH69BTH-71-1001, -1002, -1003, -1004, -1011, -1012, -1013, -1014 and -1015. Created drawings NUHRWC-71-1001, -1002 and -1003
MP197HB-71-1001 Rev 1 (sh 1-2)		Item 2	Fabrication Enhancement
MP197HB-71-1002 Rev 1 (sh 1-2)	4-3, 7-3	Item 7 (Sheet 2)	Fabrication Enhancement
MP197HB-71-1003 Rev 1 (sh 1)		Item 2	Fabrication Enhancement
MP197HB-71-1004 Rev 1 (sh 1)		Item 1 and Item 2	Fabrication Enhancement, Editorial
MP197HB-71-1005 Rev 1 (sh 1-3)		Item 2	Fabrication Enhancement
MP197HB-71-1008 Rev 1 (sh 1)	2-28, 2-32		
MP197HB-71-1009 Rev 1 (sh 1)	2-28, 2-32		
NUH24PTH-71-1003 Rev 1 (sh 1-8)		Item 2	Fabrication Enhancement
A.1.4.10-113			Updated page number
NUH32PTH-71-1001 Rev 1 (sh 1)	2-25		
NUH32PTH-71-1002 Rev 1 (sh1)	2-33		
NUH32PTH-71-1015 Rev 0 (sh 1)	2-3		
NUH32PTH TYPE 1-71-1001 Rev 1 (sh 1-4)		Item 1	Editorial
NUH32PTH TYPE 1-71-1003 Rev 1 (sh 1-7)	2-3		
NUH32PTH TYPE 1-71-1004 Rev 1 (sh 1-4)		Item 2	Fabrication Enhancement
A.1.4.10-159			Updated page number
NUH32PTH1-71-1003 Rev 1 (sh 1-8)	2-3		
A.1.4.10-194			Updated page number
NUH37PTH-71-1001 Rev 1 (sh 1-4)		Item 1 and Item 2	Fabrication Enhancement, Editorial
NUH37PTH-71-1002 Rev 1 (sh 1-5)		Item 1 and Item 2	Fabrication Enhancement, Editorial
NUH37PTH-71-1003 Rev 1 (sh 1-4)		Item 1 and Item 2	Fabrication Enhancement, Editorial
NUH37PTH-71-1004 Rev 1 (sh 1-6)		Item 1 and Item 2	Fabrication Enhancement, Editorial
NUH37PTH-71-1011 Rev 1 (sh 1-7)		Item 1 and Item 2	Fabrication Enhancement, Editorial

List of Changed SAR Pages and Drawings, with Indication of the Reasons for Changes

SAR Page or Drawing Number	RAI #	Enclosure 31 Item	Notes
NUH37PTH-71-1012 Rev 1 (sh 1-7)		Item 1 and Item 2	Fabrication Enhancement, Editorial
NUH37PTH-71-1015 Rev 0 (sh 1)	2-3		
NUH61BT-71-1001 Rev 1 (sh 1)		Item 1	Consistency with Calculation
NUH61BTH-71-1102 Rev 1 (sh 1-8)		Item 1	Consistency with Calculation
NUH61BTH-71-1106 Rev 1 (sh 1)		Item 2	Fabrication Enhancement
NUH61BTH-71-1100 Rev 1 (sh 1-7)	2-33		
NUH69BTH-71-1001 Rev 1 (sh 1-4)	2-33	Item 1 and Item 2	Fabrication Enhancement, Editorial
NUH69BTH-71-1002 Rev 1 (sh 1-4)		Item 1 and Item 2	Fabrication Enhancement, Editorial
NUH69BTH-71-1003 Rev 1 (sh 1-4)		Item 2	Fabrication Enhancement
NUH69BTH-71-1004 Rev 1 (sh 1-6)	2-33	Item 1 and Item 2	Fabrication Enhancement, Editorial
NUH69BTH-71-1011 Rev 1 (sh 1-5)		Item 1 and Item 2	Fabrication Enhancement, Editorial
NUH69BTH-71-1012 Rev 1 (sh 1-6)		Item 1 and Item 2	Fabrication Enhancement, Editorial
NUH69BTH-71-1013 Rev 1 (sh 1-2)		Item 2	Fabrication Enhancement
NUH69BTH-71-1014 Rev 1 (sh 1)		Item 2	Fabrication Enhancement
NUH69BTH-71-1015 Rev 1 (sh 1)		Item 2	Fabrication Enhancement
A.1.4.10-308			Updated page number
NUHRWC-71-1001 Rev 0 (sh 1-5)	2-6		
NUHRWC-71-1002 Rev 0 (sh 1-3)	2-6		
NUHRWC-71-1003 Rev 0 (sh 1-4)	2-6		
A.2-4		Item 1	Editorial Correction
A.2-5		Item 2	Fabrication Enhancement
A.2-6		Item 1	Editorial Correction
A.2-9	2-14		
A.2-28		Item 2	Fabrication Enhancement
A.2-29			Shifted information
A.2-34	2-17		
A.2-36		Item 2	Fabrication Enhancement
A.2-37		Item 1	Editorial Correction
A.2-38	2-14		
A.2-42	2-18		
A.2-44	2-14		
A.2.13.1-2	2-14		
A.2.13.1-4	2-28		
A.2.13.1-27	2-14		
A.2.13.2-2		Item 2 and Item 6	Fabrication Enhancement
A.2.13.2-3		Item 2 and Item 6	Fabrication Enhancement

List of Changed SAR Pages and Drawings, with Indication of the Reasons for Changes

SAR Page or Drawing Number	RAI #	Enclosure 31 Item	Notes
A.2.13.2-14		Item 2 and Item 6	Fabrication Enhancement
A.2.13.2-27		Item 2	Fabrication Enhancement
A.2.13.2-29		Item 2	Fabrication Enhancement
A.2.13.2-32		Item 2 and Item 6	Fabrication Enhancement
A.2.13.2-33		Item 2 and Item 6	Fabrication Enhancement
A.2.13.2-38		Item 2 and Item 6	Fabrication Enhancement
A.2.13.2-39		Item 2 and Item 6	Fabrication Enhancement
A.2.13.7-7	2-14		
A.2.13.7-49	2-14		
A.2.13.7-52	2-14		
A.2.13.8-3	2-35		
A.2.13.8-37	2-27		
A.2.13.8-38	2-27		
A.2.13.8-44	2-27		
A.2.13.8-49	2-27		
A.2.13.8-54	2-27		
A.2.13.8-55	2-27		
A.2.13.8-61	2-27		
A.2.13.8-65	2-27		
A.2.13.9-7	2-28		
A.2.13.11-i	2-7,2-30,2-38		
A.2.13.11-ii	2-7,2-30,2-38		
A.2.13.11-4		Item 1	Editorial Correction
A.2.13.11-8	2-30, 2-38		
A.2.13.11-9	2-30, 2-38		
A.2.13.11-10	2-30, 2-38		
A.2.13.11-11	2-30, 2-38		
A.2.13.11-12	2-30, 2-38		
A.2.13.11-13	2-30, 2-38		
A.2.23.11-14	2-7, 2-30, 2-38		
A.2.23.11-15	2-7		
A.2.23.11-16	2-7		
A.2.23.11-17	2-7		
A.2.13.11-21	2-7, 2-30, 2-38		
A.2.13.11-22	2-7, 2-30, 2-38		

List of Changed SAR Pages and Drawings, with Indication of the Reasons for Changes

SAR Page or Drawing Number	RAI #	Enclosure 31 Item	Notes
A.2.13.11-25	2-30, 2-38		
A.2.13.11-26	2-30, 2-38		
A.2.13.11-27	2-30, 2-38		
A.2.13.11-36	2-30, 2-38		
A.2.13.11-37	2-30, 2-38		
A.2.13.11-38	2-30, 2-38		
A.2.13.11-39	2-30, 2-38		
A.2.13.11-48	2-30, 2-38		
A.2.13.11-49	2-30, 2-38		
A.2.13.11-50	2-30, 2-38		
A.2.13.11-51	2-30, 2-38		
A.2.13.11-52	2-30, 2-38		
A.2.13.11-53	2-30, 2-38		
A.2.13.11-54	2-7		
A.2.13.11-55	2-7		
A.2.13.11-56	2-7		
A.2.13.11-57	2-7		
A.2.13.11-58	2-7		
A.2.13.11-59	2-7		
A.2.13.11-60	2-7		
A.2.13.11-61	2-7		
A.2.13.11-62	2-7		
A.2.13.11-63	2-30, 2-38		
A.2.13.11-64	2-30, 2-38		
A.2.13.12-ii		Item 1	Editorial Correction
A.2.13.12-iii	2-28, 2-37	Item 1	Editorial Correction
A.2.13.12-2	2-28		
A.2.13.12-3	2-17		
A.2.13.12-5	2-17, 2-18, 2-28		
A.2.13.12-6	2-17, 2-28		
A.2.13.12-7	2-36, 2-37		
A.2.13.12-9	2-17, 2-28	Item 1	Editorial
A.2.13.12-10	2-17, 2-18		
A.2.13.12-11	2-17, 2-28		
A.2.13.12-12			Shifted information
A.2.13.12-13	2-28	Item 1	Editorial
A.2.13.12-14	2-28	Item 1	Editorial
A.2.13.12-18	2-28		

List of Changed SAR Pages and Drawings, with Indication of the Reasons for Changes

SAR Page or Drawing Number	RAI #	Enclosure 31 Item	Notes
A.2.13.12-19	2-28		
A.2.13.12-29	2-28		
A.2.13.12-30	2-28		
A.2.13.12-31	2-28		
A.2.13.12-32	2-28		
A.2.13.12-33	2-28		
A.2.13.12-40	2-28		
A.2.13.12-41	2-28		
A.2.13.12-42	2-28		
A.2.13.12-43	2-28		
A.2.13.12-44	2-28		
A.2.13.12-47	2-28		
A.2.13.12-50	2-28		
A.2.13.12-51	2-28		
A.2.13.12-54	2-28		
A.2.13.12-55	2-28		
A.2.13.12-56	2-28		
A.2.13.12-57	2-28		
A.2.13.12-58	2-28		
A.2.13.12-59	2-28		
A.2.13.12-60	2-28		
A.2.13.12-61	2-28		
A.2.13.12-62	2-28		
A.2.13.12-63	2-28		
A.2.13.12-64	2-28		
A.2.13.12-65	2-28		
A.2.13.12-66	2-28		
A.2.13.12-67	2-28		
A.2.13.12-68	2-28		
A.2.13.12-69	2-28		
A.2.13.12-70	2-28		
A.2.13.12-71	2-28		
A.2.13.12-72	2-28		
A.2.13.12-73	2-28		
A.2.13.12-74	2-28		
A.2.13.12-75	2-28		
A.2.13.12-76	2-28		
A.2.13.12-77	2-28		
A.2.13.12-78	2-28		

List of Changed SAR Pages and Drawings, with Indication of the Reasons for Changes

SAR Page or Drawing Number	RAI #	Enclosure 31 Item	Notes
A.2.13.12-79	2-28		
A.2.13.12-80	2-28		
A.2.13.12-81	2-28		
A.2.13.12-83	2-28		
A.2.13.12-84	2-28		
A.2.13.12-85	2-28		
A.2.13.12-86	2-28		
A.2.13.12-87	2-28		
A.2.13.12-88	2-28		
A.2.13.12-91	2-37		
A.2.13.12-92	2-28		
A.2.13.12-93	2-28		
A.2.13.12-94	2-28		
A.2.13.12-95	2-28		
A.2.13.12-96	2-28		
A.2.13.12-97	2-28		
A.2.13.12-98	2-28		
A.2.13.12-99	2-28		
A.2.13.12-100	2-28		
A.2.13.12-101	2-28		
A.2.13.13-2		Item 2	Fabrication Enhancement
A.2.13.13-3		Item 2	Fabrication Enhancement
A.2.13.13-3A		Item 2	Fabrication Enhancement
A.3-i			Update Table of Contents
A.3-iv			Update Table of Contents
A.3-4		Item 1	Editorial
A.3-8	3-13		
A.3-9	2-11		
A.3-10	2-11		
A.3-12	3-1		
A.3-13	2-10		
A.3-19	2-11		
A.3-28	3-3	Item 1	Editorial
A.3-38	3-4		
A.3-40	3-4		
A.3-40a	3-4		
A.3-40b	3-4		

List of Changed SAR Pages and Drawings, with Indication of the Reasons for Changes

SAR Page or Drawing Number	RAI #	Enclosure 31 Item	Notes
A.3-40c	3-4		
A.3-40d	3-4		
A.3-40e	3-4		
A.3-47	2-7		
A.3-48	3-7		
A.3-48a	3-7		
A.3-68		Item 1	Correction to make data consistent with SAR, Section A.3.1.3 (page A.3-7) and Section A.3.3.1.2 (page A.3-40)
A.3-75	3-13		
A.3-78	3-13		
A.3-79	3-8	Item 1	An editorial correction is also considered in this page
A.3-80	3-8		
A.3-82		Item 1	Editorial
A.3-92	3-13		
A.3-93		Item 1	Corrections to reflect the latest version of the referenced documents
A.3-95			New references used in Chapter A.3 are added to the reference list
A.3-104a	3-6		
A.3-105	3-6		
A.3-120		Item 1	Editorial
A.3-127	2-20		
A.3-128	2-14	Item 1	An editorial correction is also considered in this page
A.3-139c	2-7		
A.3-139d	3-9, 3-12		
A.3-139e	3-9, 3-12		
A.3-139f	3-9, 3-12		
A.3-140		Item 1	Editorial
A.3-149		Item 4	
A.3-150		Item 4	
A.3-157		Item 4	
A.3-161	3-13		
A.3-162	3-13		
A.3-216	3-9, 3-12		
A.3-217	3-9, 3-12		
A.3-218	3-9, 3-12		
A.4-1	4-4		

List of Changed SAR Pages and Drawings, with Indication of the Reasons for Changes

SAR Page or Drawing Number	RAI #	Enclosure 31 Item	Notes
A.4-3	4-3		
A.4-5	4-3		
A.4-6			Consistency
A.5-i			Update Table of Contents
A.5-ii			Update Table of Contents
A.5-iii			Update Table of Contents
A.5-1	2-6		
A.5-3	5-3		
A.5-4	2-7, 5-16		
A.5-4a	2-7, 5-16		
A.5-4b	2-6		
A.5-4c	5-7, 5-10		
A.5-6	5-8		
A.5-7	5-8, 5-9		
A.5-7a	5-9, 2-7, 5-16		
A.5-9	2-7, 5-16		
A.5-10	2-7, 5-16	Item 1	Editorial
A.5-11	2-7, 5-16		
A.5-12	2-7, 5-16, 5-13		
A.5-13	2-6, 2-7, 5-16		
A.5-14	5-15		
A.5-14a	2-7, 5-16		
A.5-16	5-9		
A.5-19	2-7, 5-16		
A.5-20	5-17		
A.5-21	5-10		
A.5-21a	2-7, 5-16		
A.5-23	2-6		
A.5-33	5-19		
A.5-34	5-19		
A.5-34a	5-18		
A.5-34b	5-8		
A.5-34c		Item 1	Editorial
A.5-106		Item 1	Editorial
A.5-106a	2-7, 5-16		
A.5-106b	2-7, 5-16	Item 1	Editorial
A.5-108	2-7, 5-16		
A.5-111	5-12		

List of Changed SAR Pages and Drawings, with Indication of the Reasons for Changes

SAR Page or Drawing Number	RAI #	Enclosure 31 Item	Notes
A.5-115a	2-7, 5-16		
A.5-119	5-9		
A.5-120	5-9		
A.5-128	5-17		
A.5-131	5-17		
A.5-133	5-17		
A.5-133a	5-19		
A.5-133b	5-19		
A.5-133c	5-19		
A.5-133d	5-18		
A.5-139a	2-7, 5-16		
A.5-139b	2-7, 5-16		
A.5-139c	2-7, 5-16		
A.5-149	5-17		
A.6-i			Update Table of Contents
A.6-ii			Update Table of Contents
A.6-1	2-6		
A.6-2	2-6, 6-1, 6-5		
A.6-5	6-1, 6-5		
A.6-7	P6-5		
A.6-9	P6-3		
A.6-10		Item 3	
A.6-11	6-1, 6-5		
A.6-12	6-1, 6-5		
A.6-12a	P6-4		
A.6-12b	P6-4, P6-3		
A.6-12c	P6-3, 6-8		
A.6-12d	P6-5	Item 3	
A.6-12e		Item 3	
A.6-14	P6-7		
A.6-15	P6-7, 6-9		
A.6-16	6-4		
A.6-17	6-8, P6-6		
A.6-19	P6-8		
A.6-20a	P6-8		
A.6-21	P6-7, P6-8		
A.6-23	P6-8		
A.6-24	P6-8		

List of Changed SAR Pages and Drawings, with Indication of the Reasons for Changes

SAR Page or Drawing Number	RAI #	Enclosure 31 Item	Notes
A.6-27	P6-2		
A.6-28	P6-1		
A.6-29	P6-1		
A.6-29a	P6-1		
A.6-29b			Shifted information
A.6-30		Item 1	Editorial
A.6-31	P6-8	Item 3	
A.6-42	6-1, 6-5		
A.6-47	P6-6		
A.6-65	P6-8		
A.6-66	P6-8		
A.6-67	P6-8		
A.6-68	P6-8		
A.6-69		Item 1 and Item 3	Editorial
A.6-87	P6-1		
A.6-88	P6-1		
A.6-89	P6-1		
A.6-90	P6-1		
A.6-91	P6-4		
A.6-92	P6-3, P6-4		
A.6-93	6-8		
A.6-94	P6-5	Item 3	
A.6-95			Shifted information
A.6-96	6-4		
A.6-97	6-4		
A.6-98	6-4		
A.6-99	6-4		
A.6-100	6-4		
A.6-101	6-4		
A.6-102	6-4		
A.6-103	6-4		
A.6-104	6-4		
A.6-105	6-4		
A.6-106	6-4		
A.6-107	6-4		
A.6-108	6-4		
A.6-109	6-4		
A.6-110	6-8		
A.6-111	6-8		

List of Changed SAR Pages and Drawings, with Indication of the Reasons for Changes

SAR Page or Drawing Number	RAI #	Enclosure 31 Item	Notes
A.6-112	6-8		
A.6-113			Shifted information
A.6-114			Shifted information
A.6-115			Shifted information
A.6.5.1-i			Update Table of Contents
A.6.5.1-1		Item 1	Consistency
A.6.5.1-7		Item 1	Editorial
A.6.5.1-28		Item 1	Consistency
A.6.5.2-ii			Table of contents
A.6.5.2-3		Item 2	Fabrication Enhancement
A.6.5.2-4		Item 2	Fabrication Enhancement
A.6.5.2-5		Item 1 and Item 2	Fabrication Enhancement, Editorial
A.6.5.2-6		Item 1	Editorial
A.6.5.2-7		Item 2	Fabrication Enhancement
A.6.5.2-8		Item 2	Fabrication Enhancement
A.6.5.2-11		Item 2	Fabrication Enhancement
A.6.5.2-12		Item 2	Fabrication Enhancement
A.6.5.2-14		Item 1	Consistency
A.6.5.2-15		Item 2	Fabrication Enhancement
A.6.5.2-16		Item 2	Fabrication Enhancement
A.6.5.2-17		Item 2	Fabrication Enhancement
A.6.5.2-18		Item 2	Fabrication Enhancement
A.6.5.2-19		Item 1	Consistency
A.6.5.2-20		Item 2	Fabrication Enhancement
A.6.5.2-21		Item 1	Consistency
A.6.5.2-22~A.6.5.2-63	6-2	Item 2 and Item 5	Fabrication Enhancement
A.6.5.2-64		Item 2	Fabrication Enhancement
A.6.5.2-70		Item 1	Consistency
A.6.5.2-72		Item 2	Fabrication Enhancement
A.6.5.2-76		Item 2	Fabrication Enhancement
A.6.5.2-77		Item 2	Fabrication Enhancement
A.6.5.2-78		Item 2	Fabrication Enhancement
A.6.5.2-79		Item 2	Fabrication Enhancement
A.6.5.2-80		Item 2	Fabrication Enhancement
A.6.5.2-81		Item 2	Fabrication Enhancement
A.6.5.2-82		Item 2	Fabrication Enhancement
A.6.5.2-83		Item 2	Fabrication Enhancement

List of Changed SAR Pages and Drawings, with Indication of the Reasons for Changes

SAR Page or Drawing Number	RAI #	Enclosure 31 Item	Notes
A.6.5.2-84		Item 2	Fabrication Enhancement
A.6.5.2-85		Item 2	Fabrication Enhancement
A.6.5.2-90		Item 2	Fabrication Enhancement
A.6.5.2-96		Item 2	Fabrication Enhancement
A.6.5.2-97		Item 2	Fabrication Enhancement
A.6.5.2-98		Item 2	Fabrication Enhancement
A.6.5.2-99		Item 2	Fabrication Enhancement
A.6.5.2-103		Item 2	Fabrication Enhancement
A.6.5.2-105		Item 2	Fabrication Enhancement
A.6.5.2-108		Item 1	Consistency
A.6.5.2-109		Item 1	Consistency
A.6.5.2-113		Item 2	Fabrication Enhancement
A.6.5.2-114		Item 1	Consistency
A.6.5.2-115		Item 1	Consistency
A.6.5.2-124		Item 2	Fabrication Enhancement
A.6.5.2-125		Item 2	Fabrication Enhancement
A.6.5.2-126		Item 2	Fabrication Enhancement
A.6.5.3-i			Update Table of Contents
A.6.5.3-9	6-2		
A.6.5.3-24	6-2		
A.6.5.3-24a~A.6.5.3-24ll	6-2		
A.6.5.4-i			Update Table of Contents
A.6.5.4-ii			Update Table of Contents
A.6.5.4-2	6-1, 6-5, P6-4		
A.6.5.4-5	6-1, 6-5, P6-4		
A.6.5.4-6	6-1, 6-5, P6-4		
A.6.5.4-7	6-1, 6-5, P6-4		
A.6.5.4-8	6-6		
A.6.5.4-10	6-1, 6-5, P6-4		
A.6.5.4-11	6-1, 6-5, P6-4		
A.6.5.4-12	6-1, 6-5, P6-4		
A.6.5.4-13	6-1, 6-5, P6-4		
A.6.5.4-14	6-1, 6-5, P6-4		
A.6.5.4-15	6-1, 6-5, P6-4, P6-8		
A.6.5.4-16	6-1, 6-5, P6-4, P6-8		
A.6.5.4-17		Item 1	Consistency
A.6.5.4-18~32	6-1		

List of Changed SAR Pages and Drawings, with Indication of the Reasons for Changes

SAR Page or Drawing Number	RAI #	Enclosure 31 Item	Notes
A.6.5.4-32a~A.6.5.4-32u	6-5		
A.6.5.4-39	6-1, 6-5, P6-4		
A.6.5.4-42	6-5		
A.6.5.4-48	6-1		
A.6.5.4-49	6-1		
A.6.5.4-50	6-5		
A.6.5.4-51	6-5		
A.6.5.4-52	6-1		
A.6.5.4-53	6-1		
A.6.5.4-54	6-1		
A.6.5.4-55	6-1		
A.6.5.4-56	6-1		
A.6.5.4-57	6-1		
A.6.5.4-58	6-1		
A.6.5.4-59	6-1		
A.6.5.4-60	6-1		
A.6.5.4-61	6-5		
A.6.5.4-62	6-5		
A.6.5.4-63	6-5		
A.6.5.4-64	6-5		
A.6.5.4-65	6-5		
A.6.5.4-65a	6-5		
A.6.5.4-65b	6-5		
A.6.5.4-65c	6-5		
A.6.5.4-68		Item 1	Consistency
A.6.5.4-69		Item 1	Editorial
A.6.5.4-71		Item 1	Consistency
A.6.5.4-73	6-1		
A.6.5.4-74	6-5		
A.6.5.5-i			Update Table of Contents
A.6.5.5-ii			Update Table of Contents
A.6.5.5-1		Item 1	Consistency
A.6.5.5-2	6-1, 6-5, P6-4		
A.6.5.5-5	6-1, 6-5, P6-4		
A.6.5.5-6	6-1, 6-5, P6-4		
A.6.5.5-7	6-1, 6-5, P6-4		
A.6.5.5-8	6-6		
A.6.5.5-10	6-1, 6-5, P6-4		

List of Changed SAR Pages and Drawings, with Indication of the Reasons for Changes

SAR Page or Drawing Number	RAI #	Enclosure 31 Item	Notes
A.6.5.5-11	6-1, 6-5, P6-4		
A.6.5.5-12	6-1, 6-5, P6-4		
A.6.5.5-13	6-1, 6-5, P6-4		
A.6.5.5-14	6-1, 6-5, P6-4, P6-8		
A.6.5.5-15	6-1, 6-5, P6-4, P6-8		
A.6.5.5-16		Item 1	Editorial
A.6.5.5-17		Item 1	Consistency
A.6.5.5-18~34	6-1		
A.6.5.5-34a~A.6.5.5-34ff	6-5		
A.6.5.5-35		Item 1	Consistency
A.6.5.5-38	6-1, 6-5, P6-4		
A.6.5.5-43	6-1		
A.6.5.5-44	6-5		
A.6.5.5-45	6-1		
A.6.5.5-46	6-1		
A.6.5.5-47	6-1		
A.6.5.5-48	6-1		
A.6.5.5-49	6-5		
A.6.5.5-50	6-5		
A.6.5.5-51	6-5		
A.6.5.5-52	6-5		
A.6.5.5-56		Item 1	Consistency
A.6.5.5-57		Item 1	Editorial
A.6.5.5-60		Item 1	Consistency
A.6.5.5-62	6-1		
A.6.5.5-63		Item 1	Editorial
A.6.5.6-i			Update Table of Contents
A.6.5.6-ii			Update Table of Contents
A.6.5.6-2	6-1, P6-4		
A.6.5.6-5		Item 1	Consistency
A.6.5.6-6	6-1, P6-4		
A.6.5.6-7	6-1, P6-4		
A.6.5.6-8	6-6		
A.6.5.6-9	6-1, P6-4		
A.6.5.6-10			Shifted information
A.6.5.6-11	6-1, P6-4, 6-7		
A.6.5.6-12	6-1, P6-4, 6-7, P6-8		
A.6.5.6-13	6-1, P6-4, 6-7, P6-8		

List of Changed SAR Pages and Drawings, with Indication of the Reasons for Changes

SAR Page or Drawing Number	RAI #	Enclosure 31 Item	Notes
A.6.5.6-14		Item 1	Consistency
A.6.5.6-15~A.6.5.6-24	6-1		
A.6.5.6-24a	6-1		
A.6.5.6-27	6-1, P6-4, 6-7		
A.6.5.6-30	6-1		
A.6.5.6-32	6-1, 6-7		
A.6.5.6-33	6-1, 6-7		
A.6.5.6-34		Item 1	Editorial
A.6.5.6-35	6-1, 6-7		
A.6.5.6-36	6-1, 6-7		
A.6.5.6-37	6-1		
A.6.5.6-38	6-1		
A.6.5.6-39	6-1		
A.6.5.6-40	6-1		
A.6.5.6-41	6-1, 6-7		
A.6.5.6-42	6-1, 6-7		
A.6.5.6-43	6-1, 6-7		
A.6.5.6-44	6-1		
A.6.5.6-45	6-1		
A.6.5.6-46		Item 1	Editorial
A.6.5.6-62		Item 1	Consistency
A.6.5.6-63		Item 1	Editorial
A.6.5.6-67		Item 1	Consistency
A.6.5.6-70	6-1		
A.6.5.6-71		Item 1	Editorial
A.6.5.7-i			Update Table of Contents
A.6.5.7-ii			Update Table of Contents
A.6.5.7-iii			Update Table of Contents
A.6.5.7-2	6-1, 6-5, P6-4		
A.6.5.7-4	6-1, 6-5, P6-4		
A.6.5.7-5	6-1, 6-5, P6-4		
A.6.5.7-6	6-1, 6-5, P6-4		
A.6.5.7-7	6-1, 6-5, P6-4, 6-6		
A.6.5.7-8	6-6		
A.6.5.7-9	P6-4		
A.6.5.7-10	P6-4		
A.6.5.7-11	6-1, 6-5, P6-4		
A.6.5.7-12	6-1, 6-5, P6-4		

List of Changed SAR Pages and Drawings, with Indication of the Reasons for Changes

SAR Page or Drawing Number	RAI #	Enclosure 31 Item	Notes
A.6.5.7-13	6-1, 6-5, P6-4		
A.6.5.7-14	6-1, 6-5, P6-4, P6-8		
A.6.5.7-15	6-1, 6-5, P6-4, P6-8		
A.6.5.7-16		Item 1	Consistency
A.6.5.7-17~A.6.5.7-28	6-1		
A.6.5.7-28a~A.6.5.7-28w	6-1, 6-5		
A.6.5.7-30	6-1, 6-5	Item 2	Fabrication Enhancement
A.6.5.7-31	6-1, 6-5, P6-4		
A.6.5.7-37	6-1, 6-5		
A.6.5.7-38	6-1		
A.6.5.7-40	6-1		
A.6.5.7-41		Item 1	Editorial
A.6.5.7-42	6-1		
A.6.5.7-43	6-1, 6-5		
A.6.5.7-44		Item 1	Editorial
A.6.5.7-47		Item 1	Editorial
A.6.5.7-48		Item 1	Consistency
A.6.5.7-53	6-1		
A.6.5.7-54		Item 1	Editorial
A.7-i			Update Table of Contents
A.7-1	3-17	Item 1	Consistency, editorial
A.7-2	3-19, P6-1	Item 1	Consistency, editorial
A.7-3	3-19, 7-3, P6-1	Item 1	Consistency
A.7-4	3-18	Item 1	Consistency
A.7-5	7-1	Item 1	Consistency
A.7-6	7-3	Item 1	Consistency
A.7-7	2-9, 3-20, 7-1		
A.7-8	3-18	Item 1	Consistency
A.7-9	7-3, 7-4	Item 1	Consistency
A.7-10	3-16, 7-4	Item 1	Consistency
A.7-11	7-3	Item 1	Consistency
A.7-12	3-17, 7-1	Item 1	Consistency
A.7-13		Item 1	Consistency
A.7-14		Item 1	Consistency
A.7-15		Item 1	Consistency
A.7-16		Item 1	Consistency
A.7-17		Item 1	Consistency
A.7-18		Item 1	Consistency

List of Changed SAR Pages and Drawings, with Indication of the Reasons for Changes

SAR Page or Drawing Number	RAI #	Enclosure 31 Item	Notes
A.7-19	7-1		
A.7-20	7-1		
A.7-21	7-1		
A.7-22			Shifted information
A.7-23		Item 1	Consistency
A.7.7.1-i	7-1		
A.7.7.1-1	7-1		
A.7.7.1-2	7-1		
A.7.7.1-3	7-1		
A.7.7.1-4	7-1		
A.7.7.1-5	7-1		
A.7.7.1-6	7-1		
A.7.7.1-7	7-1		
A.7.7.1-8	7-1		
A.7.7.2-i	7-1		
A.7.7.2-1	7-1, P6-2		
A.7.7.2-2	7-1, P6-2		
A.7.7.2-3	7-1		
A.7.7.2-4	7-1		
A.7.7.2-5	7-1		
A.7.7.2-6	7-1		
A.7.7.2-7	7-1		
A.7.7.2-8	7-1		
A.7.7.3-i	7-1		
A.7.7.3-1	7-1, P6-2		
A.7.7.3-2	7-1, P6-2		
A.7.7.3-3	7-1		
A.7.7.3-4	7-1		
A.7.7.3-5	7-1		
A.7.7.3-6	7-1		
A.7.7.3-7	7-1		
A.7.7.3-8	7-1		
A.7.7.3-9	7-1		
A.7.7.4-i	7-1		

List of Changed SAR Pages and Drawings, with Indication of the Reasons for Changes

SAR Page or Drawing Number	RAI #	Enclosure 31 Item	Notes
A.7.7.4-1	7-1, P6-2		
A.7.7.4-2	7-1, P6-2		
A.7.7.4-3	7-1		
A.7.7.4-4	7-1		
A.7.7.4-5	7-1		
A.7.7.4-6	7-1		
A.7.7.4-7	7-1		
A.7.7.4-8	7-1		
A.7.7.4-9	7-1		
A.7.7.5-i	7-1		
A.7.7.5-1	7-1, P6-2		
A.7.7.5-2	7-1, P6-2		
A.7.7.5-3	7-1		
A.7.7.5-4	7-1		
A.7.7.5-5	7-1		
A.7.7.5-6	7-1		
A.7.7.5-7	7-1		
A.7.7.5-8	7-1		
A.7.7.5-9	7-1		
A.7.7.6-i	7-1		
A.7.7.6-1	7-1, P6-2		
A.7.7.6-2	7-1, P6-2		
A.7.7.6-3	7-1		
A.7.7.6-4	7-1		
A.7.7.6-5	7-1		
A.7.7.6-6	7-1		
A.7.7.6-7	7-1		
A.7.7.6-8	7-1		
A.7.7.6-9	7-1		
A.7.7.7-i	7-1		
A.7.7.7-1	7-1		
A.7.7.7-2	7-1		
A.7.7.7-3	7-1		
A.7.7.7-4	7-1		
A.7.7.7-5	7-1		
A.7.7.7-6	7-1		

List of Changed SAR Pages and Drawings, with Indication of the Reasons for Changes

SAR Page or Drawing Number	RAI #	Enclosure 31 Item	Notes
A.7.7.7-7	7-1		
A.7.7.7-8	7-1		
A.7.7.8-i	7-1		
A.7.7.8-1	7-1		
A.7.7.8-2	7-1		
A.7.7.8-3	7-1		
A.7.7.8-4	7-1		
A.7.7.8-5	7-1		
A.7.7.8-6	7-1		
A.7.7.8-7	7-1		
A.7.7.8-8	7-1		
A.7.7.8-9	7-1		
A.7.7.9-i	7-1		
A.7.7.9-1	7-1		
A.7.7.9-2	7-1		
A.7.7.9-3	7-1		
A.7.7.9-4	7-1		
A.7.7.9-5	7-1		
A.7.7.9-6	7-1		
A.7.7.9-7	7-1		
A.7.7.9-8	7-1		
A.7.7.10-i	7-1, 2-6		
A.7.7.10-1	7-1, 2-6		
A.7.7.10-2	7-1, 7-2, 2-6		
A.7.7.10-3	7-2		
A.8-i			Update Table of Contents
A.8-2		Item 1	Editorial
A.8-3		Item 1 and Item 2	Editorial and Fabrication Enhancement
A.8-4	2-13	Item 1 and Item 2	Editorial and Fabrication Enhancement
A.8-5	2-13, 8-1	Item 1	Editorial
A.8-6	2-4, 8-1		
A.8-7	2-4		
A.8-8	2-4		
A.8-9	2-4		
A.8-10	2-4		

List of Changed SAR Pages and Drawings, with Indication of the Reasons for Changes

SAR Page or Drawing Number	RAI #	Enclosure 31 Item	Notes
A.8-11	2-4		
A.8-12	2-4		
A.8-13	2-4		
A.8-14	2-4, 3-15		
A.8-15	3-15	Item 1	Editorial
A.8-16		Item 1	Editorial
A.8-17		Item 1	Editorial
A.8-18	2-4	Item 1	Editorial